Assessing Brain Pathology Based on Large-Scale Interaction Patterns of Spontaneous Brain Activity

Dissertation

der Mathematisch-Naturwissenschaftlichen Fakultät

der Eberhard Karls Universität Tübingen

zur Erlangung des Grades eines

Doktors der Naturwissenschaften

(Dr. rer. nat.)

vorgelegt von

David Johannes Hawellek

aus Hagen

Tübingen

2012

Tag der mündlichen Qualifikation:	Mittwoch, 22. August 2012
Dekan:	Prof. Dr. Wolfgang Rosenstiel
1. Berichterstatter:	Prof. Dr. Andreas K. Engel
2. Berichterstatter:	Prof. Dr. Hanspeter A. Mallot

Table of contents

Acknowledgements

This work would not have been possible without the outstanding support of several people who need to be mentioned at the very first place.

I would like to thank Prof. Engel and Prof. Mallot for enabling me to carry out this project spanning Germany in its entirety. It was an environment with both substantial freedom for pursuing ideas but also dedicated support and structure. I appreciate this as unique chance to make an own step into research.

I am deeply grateful to Jörg Hipp for his commitment in supervising and guiding me. All scientific aspects described here took their form from the close interaction with Jörg. Your ambition and demand in doing research will remain as a guiding model for me.

The most fundamental support however came from my beloved ones and friends. Thank you for shaping my decisions, sharing my worries and bearing my moods. This may have been the most important prerequisite for letting this happen.

Abstract

This thesis introduces two methodological advances in studying the large-scale organization of spontaneous activity of the human brain and in addition provides a translation of these methods to the clinical realm.

First, a generic, data-driven framework for identifying alterations in brain wide functional connectivity is presented and tested in a patient population suffering from multiple sclerosis. A correlation between fMRI derived measures of functional connectivity and behavior is established. In the face of a strong cognitive decline and the severe disintegration of the central white matter, specific networks increased their functional connectivity. This observation challenges the prevailing view on how functional connectivity indicates the integrity of brain networks and holds important implications for resting state fMRI investigations of brain diseases as well as theoretical and modeling studies of large-scale cortical dynamics. In addition, the observed correlation between behavior and connectivity has a high relevance for medical settings as it may potentially serve as an objective proxy and biomarker for the degree of impact of multiple sclerosis on functional processing and brain network organization.

Second, a novel method for measuring functional connectivity based on noninvasive electrophysiological data (M/EEG) is established. The method overcomes a fundamental problem for deriving measures of interaction from noninvasive electrophysiological data by a novel technique of phase orthogonalized power correlation. By applying the method to MEG recordings of spontaneous brain activity in a large cohort of healthy participants, a characterization of the large-scale organization of spontaneous neuronal oscillatory activity could be provided. Spontaneous fluctuations of oscillatory activity are spatially organized into frequency dependent and functionally specific correlation structures. Thus, the method provides a new tool for understanding large-scale brain organization based on neuronal oscillatory activity.

The combined application of both methods to MEG recordings of spontaneous brain activity of a group of congenitally blind participants further highlights the strong potential of the approaches by demonstrating specific alterations in the organization of spontaneous oscillatory neuronal activity in the blind. Occipital areas of the blind are found to exhibit known oscillatory signatures of active functional processing. The

phase of slow oscillatory processes (delta range ~2 Hz) predicted the amplitude of faster rhythms (gamma range ~90 Hz). In addition the formerly visual areas of the blind exhibited frequency specific connectivity (beta range ~25 Hz) with prefrontal sites. These findings suggest that formerly visual areas serve non-visual processing during unconstrained mental activity in the blind and that a specific occipito-prefrontal pathway may underlie the reintegration of the occipital processing resources into cortical networks.

Overall, the application of the two novel methods to clinical populations demonstrates the unique access that spontaneous brain activity provides to pathophysiological principles of brain organization. The advances described in this thesis bridge methodological and conceptual gaps in the study of spontaneous activity of the human brain.

Introduction

Some of the most considerable advances in cognitive neuroscience and especially in the field of systems level neurophysiology arose from the use of specific sensory stimulation paradigms (Hubel and Wiesel, 1962). Treating the brain as a passive device while controlling external parameters of sensory stimulation allowed studying the functional response properties of neurons and their networks and, thus, establishing a link between physical parameters of the environment and neural activity. With the advent of modern neuro-imaging methods such as functional magnetic resonance imaging (fMRI), this powerful approach has been extended and refined to include increasingly complex cognitive manipulations that now are invaluable for mapping higher cognitive functioning on to human brain structure (Friston et al., 2007).

For a long time, the tacit assumption behind the use of stimulation and cognitive task paradigms has been that the variability in the evoked neural responses as well as the activity, which is present in neural networks without any external input, is mere noise and does not represent a meaningful component of brain activity (Raichle, 2010). Accordingly, inference about neural processing and the dynamics of networks has only been made after extensive averaging across repeated presentations of the stimulation. This procedure aimed to even out any nuisance variability not associated

to the question of interest and effectively eliminated the impact of ongoing activity fluctuations.

A conceptually younger approach considers spontaneously occurring fluctuations of brain activity as an important contributor to neural processing and brain functioning (Arieli et al., 1996). This view posits brainwork to involve constantly active and ongoing processes, which compose a core feature of neural processing by predicting and modulating sensory input and evoked activity (Engel et al., 2001). Driven by such a framework of an active brain and backed by the insight that the brain is indeed given a major portion of the body's energy resources for maintaining ongoing processes and activity (Shulman et al., 2004), the study of spontaneous brain activity has risen to unprecedented heights within the past decade. One of the key observations in neuro-imaging has hereby been that the spontaneous fluctuations of the blood oxygen level dependent (BOLD) signal are correlated between left and right somatomotor and medial premotor structures while subjects lay silently and awake (in a resting state) in the MRI scanner (Biswal et al., 1995). This finding showed that spontaneous activity levels that are accessible noninvasively are not random noise but are actually organized in a functionally specific manner. This seminal work unlocked a new and fruitful road of neuro-imaging investigations by providing a measure of functional connectivity (correlated brain activity) based on the brain's intrinsic activity. The approach of measuring correlations in spontaneous brain activity (functional connectivity MRI, fcMRI) allowed for unveiling the large-scale organization of the brain into constituent functional networks and for imaging entire brain networks without the bias of specific task paradigms and their associated processing demands (Fox and Raichle, 2007).

With modern neuro-imaging methods spontaneous brain activity can readily be obtained even in severely compromised patient populations. In addition, investigating changes in functional connectivity allows for studying the network organization in contrast to isolated brain regions in response to pathological processes. Thus, the resting state dynamics of the brain holds an outstanding promise for potential biomarkers of diseases and possibly represents a key level of description for characterizing pathophysiological processes (He et al., 2007; Greicius, 2008; Zhang and Raichle, 2010). However, approaches for measuring and analyzing human brain network organization from spontaneous brain activity are still in their infancy and

unequivocal ways of translating the methods to clinical populations are not yet realized.

One of the main hurdles in identifying disease related alterations of brain wide intrinsic functional connectivity as measured with fMRI arises from the huge search space. A common fMRI volume contains about 65,000 brain voxels (3 mm^3 isotropic), resulting in more than 2 billion pair wise connections. When no strong a priori hypotheses about the functional networks that are involved can be made, substantial challenges are presented by analyzing the entire search space in a computationally efficient manner while perusing sensitivity for physiological changes and a conservative segregation of spurious effects (Fox and Greicius, 2010). This is further highlighted by the fact that even when strong a priori assumptions are justified, the specificity of detected changes cannot be assessed. Any effect may arise in the context of or even be secondary to other far more important alterations that simply are out of the focus of analysis. Thus, generic frameworks for analyzing global changes of functional connectivity are of outstanding interest but have not yet been established.

Another area of growing interest for investigating brain organization and pathology based on spontaneous brain activity results from the fact the major developments in the field have been limited to fMRI and, thus, an indirect, hemodynamic measure of mass brain activity. Despite its indisputable relevance and superior spatial resolution, the relation between the BOLD signal and true neuronal activity is complex and generally ambiguous (Logothetis, 2008). Approaches for the study of ongoing activity patterns based on noninvasive electrophysiological measurements of neuronal activity, such as magneto- and electroencephalography (M/EEG) are largely lacking. To date the large-scale organization of spontaneous neuronal activity is virtually unknown. The major hindrance for such advances is represented by the limited spatial resolution of the noninvasive electrophysiological measurement techniques. Separating true neuronal interactions (such as correlations in activity) from trivial correlations that result from the identical signal component contributing to several sensors or sources is the major challenge for neuroelectric imaging of brain networks (Schoffelen and Gross, 2009; Brookes et al., 2011; Hipp et al., 2011). Thus, approaches that tackle these problems and provide a handle on the spatial structuring of spontaneous brain activity as measured by noninvasive

electrophysiological measurement techniques would represent a highly significant advance.

Overall, it can well be said that the study of spontaneous brain activity has transformed into one of the most promising avenues of neuro-imaging investigation. However, important methodological advances and conceptual steps are still needed to further build on and unfold this potentially invaluable access to human brain organization and function.

The scope of this thesis

The work described in this thesis aims at creating new approaches for studying intrinsic functional connectivity, which address important shortcomings of the current state of the art. The overarching goal is to achieve a translation of these methods to patient populations and to hereby take significant steps towards uncovering and understanding pathophysiological processes.

Specifically, two methodological advances are introduced. First, a generic analysis framework is presented, which offers a powerful, data-driven procedure for studying brain wide alterations of functional connectivity. Second, a novel method that allows for imaging functional connectivity and brain networks based on noninvasive electrophysiological measurements of neuronal activity (M/EEG) is established. The application of these methods to patient populations (multiple sclerosis, congenital blindness) shows the potential of these approaches and demonstrates that spontaneous brain activity provides unique insight into brain organization and pathology.

The thesis comprises three manuscripts. The first manuscript (*M1*) describes the data driven procedure for studying global alterations in functional connectivity along with its application to a patient population suffering from multiple sclerosis. The second manuscript (*M2*) describes the novel method for imaging intrinsic functional connectivity based on M/EEG. The third manuscript (*M3*) constitutes the synthesis of the two approaches and describes the combined application of both methods to a group of subjects suffering from congenital blindness.

An important aspect of this thesis is that beyond the ambition to provide methodological innovations, each part, in its core, aims at revealing physiological or pathophysiological principles by means of these innovations.

Summary of publications

M1: Increased functional connectivity indicates the severity of cognitive impairment in multiple sclerosis

Multiple sclerosis is a chronic, inflammatory and neurodegenerative disease of the central nervous system (CNS) and a main cause of neurological impairment (such as motor, autonomic, cognitive, neuropsychiatric) in young adulthood. Despite the high prevalence of the disease and the profound socioeconomic burden, there is still little known about how these behavioral impairments, which occur commonly and early in the disease course, relate to structural and functional alterations of the brain. This study investigated the relationship between the severity of cognitive impairment and brain wide alterations of anatomical and intrinsic functional connectivity.

Sixteen patients suffering from early stages of multiple sclerosis and 16 individually matched healthy control participants were included in the study. The analyses comprised three steps. First, the structure of the prevailing cognitive impairment was characterized and subsequently the accompanying structural and functional alterations of the CNS as measured by magnetic resonance imaging were investigated. A new, data-driven procedure to study alterations of brain wide functional connectivity hereby built the centerpiece of the analyses.

The patients exhibited a salient pattern of cognitive impairment taking the form of a general factor. This indicated that, instead of individual and heterogeneous patterns of impairment, the patients mainly differed in the general bandwidth of cognitive processes and suggested a widespread and broad impact of the disease on brain networks. Congruent with these observations, the analysis of the structural parameters that are associated with this type of cognitive decline revealed that the level of this strong cognitive impairment was highly correlated with a loss of integrity of the central white matter in a widespread and diffuse manner. In order to study the changes in intrinsic functional connectivity associated with the cognitive impairment a new, data-driven procedure was applied to resting state fMRI data. For each voxel the amount of correlations with the strong cognitive impairment within its global intrinsic functional connectivity was quantified and statistically tested against an empirical distribution of the hypothesis of no effect, which was obtained by a random permutation procedure. This approach identified a distributed set of cortical regions

to exhibit significant modulation of their connectivity. A post hoc analysis of the involved functional networks and type of modulation revealed that the strong cognitive impairment was correlated with increased functional connectivity within distinct networks, including the default mode network as a central target of these modulations. Thus, despite the strong behavioral decline and a marked disintegration of the central white matter, networks increased their functional connectivity.

These results seemingly contradict the common view on the association of functional connectivity with both the processing capacity of networks as well as their structural integrity. Increased functional connectivity is usually taken as a direct proxy for improved functioning and behavior. Thus, these findings challenge the prevailing view and suggest a complex and diverging relation of functional and structural connectivity in regard to behavior in early multiple sclerosis. Overall this study provides a new, generic framework for analyzing alterations in functional connectivity. Beyond this, it holds important conceptual implications for investigations of intrinsic functional connectivity in brain diseases as well as theoretical and modeling studies of large-scale cortical dynamics.

M2: Large-scale cortical correlation structure of spontaneous oscillatory activity

The brain's wiring represents a key puzzle for understanding neural processing. The analysis of the spontaneous covariance of the BOLD signal as a measure of large-scale functional connectivity has provided unprecedented access to important organizing principles of connectivity in the CNS. However, the BOLD signal is an indirect measure of neuronal mass activity and the large-scale organization of spontaneous neuronal activity is largely unknown. A major problem in deriving true connectivity from noninvasive electrophysiological data (M/EEG) is the limited spatial resolution of the measurement techniques, leading to spurious connectivity due to identical signal components contributing to several sites.

This study describes a new method for deriving functional connectivity from M/EEG data based on the correlation of band limited signal power. Importantly, a novel technique of phase orthogonalization tackles the overwhelming problem of spuriously correlated source estimates and allows for deriving a well-defined measure of

interaction that is insensitive to these noise interactions. Based on MEG recordings in 43 healthy subjects this study observed highly structured, frequency dependent, large-scale correlation patterns in spontaneous oscillatory neuronal activity. Distinct hub structures dominating the global connectivity emerged in the theta (4-8 Hz) and alpha to beta (8-32 Hz) as well as low gamma (~45 Hz) range in medial temporal lobe structures, lateral parietal and somatomotor cortices. Beyond these globally dominating patterns, functionally specific correlation structures were found that reflected known patterns of functional networks as seen in task activations, such as interhemispheric connectivity patterns between sensory homologue areas or extended fronto-parietal networks. Thus, spontaneous, neuronal, oscillatory activity is spatially organized in a functionally specific and frequency dependent manner across the human brain.

This study provides a major methodological improvement and important empirical advances for understanding the large-scale organizational principles of the human brain. These steps open up a new road for investigating healthy and diseased human brain connectivity based on noninvasive electrophysiological data.

M3: Intrinsic local and long-range couplings in oscillatory activity of blind visual cortex

Congenital blindness represents a condition of severe sensory deprivation during CNS development. Strikingly, the computational resources offered by occipital areas get reintegrated into cortical networks and serve non-visual processing in the blind. The blind visual cortex exhibits activations upon stimulation of other sensory modalities as well as cognitive demands and is thought to contribute to a range of higher cognitive processes. The associated changes in the structural and functional architecture of the CNS represent a remarkable example of cortical plasticity.

This study investigated the reorganization of spontaneous oscillatory neuronal activity in a group of 11 congenitally blind participants and individually matched controls. Based on recordings of resting state MEG, the changes of spontaneous oscillatory neuronal activity were studied using the novel method for imaging MEG power correlations as a measure of functional connectivity, as presented in manuscript *M2*. Changes in spontaneous oscillatory activity were investigated on two

levels of analysis: a local, visual as well as global, whole brain level. For the latter the data-driven procedure to identify alterations of global connectivity, presented in manuscript *M1,* was applied.

Visual areas exhibited power correlations in the delta (~2 Hz) and gamma (~90 Hz) range that were absent in sighted controls. The phase of the delta oscillation predicted the amplitude of the gamma oscillation. Visual areas of sighted controls exhibited an entirely different pattern of oscillatory activity in which alpha (~10 Hz) range processes dominated. Here, a 10 Hz oscillation predicted the amplitude of a low gamma (~40 Hz) oscillation. Interestingly, the absolute level of visual alpha activity (10 Hz signal power) was strongly reduced in the blind, while the visual alpha connectivity (power correlations) was on a comparable level to the sighted. In addition, the increased delta and gamma range connectivity in blind visual cortex was not reflected in an increased signal power over occipital sites. Thus, signal power and power correlations showed a double dissociation, suggesting the two measures to capture complementary, non-redundant information about the organization of oscillatory neuronal activity. Alpha range activity has been associated to processes of functional inhibition, while delta and gamma range processes and specifically their interaction have been identified as signatures of active processing in visual cortex of the sighted. Thus, the change from alpha dominated processes to an oscillatory profile in which delta and gamma processes prevail is consistent with an elevated level of functional processing in occipital cortex during rest in the blind.

For studying the changes of spontaneous oscillatory activity in the blind on a whole brain level the data driven procedure for identifying alterations in functional connectivity was applied. For a grid of ~3,000 voxels the amount of global connectivity differences between the sighted and blind was quantified and statistically tested against an empirical distribution of the hypothesis of no difference, which was obtained by a random permutation procedure. By repeating the procedure for a range of different carrier frequencies this procedure revealed which frequencies contain information about the groups in their global connectivity structure. This identified the beta (~25 Hz) range to exhibit global power correlation patterns, which dissociated the blind from the sighted. A post hoc analysis revealed that an extended network of frontal regions had increased beta connectivity with visual areas in the blind. Beta range oscillations are thought to especially underlie integrative processes. Thus, these findings may suggest specific frontal to visual beta range connectivity to

underlie the reintegration of the occipital resources into the functionally intact but reorganized cortical processing networks in the blind.

Overall this study finds specific alterations of spontaneous oscillatory neuronal activity in the blind on a local visual as well as whole brain level. Blind visual areas exhibited oscillatory signatures that are known to occur in the sighted during processing demands, suggesting that blind visual areas have an elevated level of functional processing during rest and may thus contribute to unconstrained mental activity. In addition a specific frontal pathway emerged in the beta range that may indicate that visual areas get integrated into a larger network in the blind to contribute their computational resources to cortical processing. The methodological innovations introduced in the manuscripts *M1/M2* were central for arriving at these findings.

Discussion

Within the past decades spontaneous brain activity has been the subject of intense investigations with a broad range of neuroscientific tools and across a likewise broad range of spatial levels of investigation (Arieli et al., 1996; Tsodyks et al., 1999; Fox and Raichle, 2007; Plenz and Thiagarajan, 2007). With the advent of resting state functional connectivity MRI (Biswal et al., 1995), which uses correlations in spontaneous fluctuations of the BOLD signal as a measure of functional connectivity, the noninvasive neuro-imaging approach to spontaneous brain activity has become an especially fruitful road for understanding the large-scale functional organization of the human brain. The recording conditions are well replicable and put minimal demands on subjects: the most widely used protocol for recording such data simply requires the subjects to silently fixate their view on a visually presented cross and stay awake. Next to the potential clinical relevance implied by these circumstances (He et al., 2007; Zhang and Raichle, 2010), the ease of recording and power behind analyzing spontaneous brain activity even resulted in the promising vista that functional connectivity MRI may even lead to the first discovery science of human brain function. Here, the analysis of large datasets shared across research institutes may result in unprecedented and novel insight into healthy and diseased human brain function (Biswal et al., 2010).

Despite these highly promising prospects there are however still several methodological as well as conceptual shortcomings of the current state of the art.

This thesis provided two methodological innovations that bridge existing gaps and described the translation of these methods to clinical populations. In what follows the novelty of each of the two methods will first be described before the conceptual impact of their application is highlighted.

First, a generic approach for identifying alterations of functional connectivity estimated from neuro-imaging data such as fMRI or M/EEG is presented (*M1/M3*). The core advance of the method is that it allows for identifying functional networks, which are associated with a certain property of interest (such as a behavioral parameter or experimental groups of subjects), in a data-driven way. When studying alterations in functional connectivity the data driven assessment of the complete, global regime is indeed of special importance for several reasons. Common approaches so far often either preselect a few sites (seeds) or specific functional networks identified by analysis approaches such as independent component analysis (ICA) for then further investigating modulations of functional connectivity (Fox and Greicius, 2010). This introduces strong hypotheses about the networks and brain regions that are involved and often renders interpretations of the presence or absence of modulations in connectivity difficult. Any effect could be unspecific and secondary to other effects that are not detected by this reduction of the analysis onto a small fraction of the entire covariance structure. By the same token, the changes in functional connectivity within isolated networks - be it increases or decreases - is often marginally interpretable as more complex effects involving across network interactions or effects that are common to several functional networks are not taken into consideration. This is an unfortunate shortcoming as these more distributed properties of network behavior likely play a pivotal role in the pathophysiology of brain networks (Corbetta, 2010). Thus, the simultaneous assessment of the global correlation structure is important when trying to understand modulations in functional connectivity in terms of specificity and true extent. The procedures described in this thesis provide a way of identifying connectivity effects in global connectivity graphs (containing all pairwise connections between spatial locations such as voxels, sensors, source locations).

Based on fMRI resting state data a correlation between cognitive decline due to multiple sclerosis and functional network behavior could be established demonstrating the power of the approach (*M1*). Surprisingly, specific networks increased their functional connectivity despite a strong reduction of the structural

integrity of the interconnecting white matter and a severe cognitive decline. These observations challenge the prevailing view on how the structural integrity of cortical networks and their processing capacity is reflected in spontaneous couplings of activity and suggest a complex relation between structural and functional connectivity. Further, these findings underline the importance of understanding how structural connectivity relates to correlations in activity of distant brain regions when making inferences about the association of functional connectivity and behavior.

In another step the method was applied to MEG derived connectivity graphs of a group of congenitally blind subjects (*M3*). As MEG has a high temporal resolution, the approach was extended to incorporate a mapping of global connectivity structures that are informative about the difference between the blind and sighted onto the underlying frequency range of the neuronal dynamics. Two frequency ranges emerged in which the whole brain connectivity showed high discriminative power between the blind and sighted: the delta (~2 Hz) and beta range (~25 Hz). While the delta range was specifically predictive about the groups for occipital brain regions, the beta range also incorporated a highly structured and extended network of prefrontal brain regions. Together these results highlight the generic nature of the analysis method, being sensitive to alterations in functional connectivity estimated from distinct imaging modalities such as fMRI and MEG.

Second, a new technique for deriving estimates of functional connectivity from noninvasive electrophysiological data such as M/EEG was presented. This technique uses correlations in spontaneous fluctuations of source reconstructed, frequency resolved signal power of neuronal population activity as a measure of functional connectivity. The major advance of the novel technique is that it allows for deriving estimates of functional connectivity that are not confounded by the trivial correlations, which result from the limited spatial resolution of the measurement techniques (Schoffelen and Gross, 2009). Before correlating the power time courses between two regions, the signals are orthogonalized, removing any signal part that is identical in phase (and thus likely confounded due to the quasi instantaneous propagation of electromagnetic fields) between the two timecourses. Using this technique to derive frequency resolved estimates of functional connectivity within a grid covering the whole brain, a characterization of the large-scale spatial structuring of spontaneous oscillatory neuronal activity was provided. The main finding of the study (*M2*) was that oscillatory neuronal activity exhibits a functionally specific, frequency dependent

correlation structure. Next to the application of the method to a large cohort of healthy subjects, the method was also applied to MEG recordings of a group of congenitally blind subjects (*M3*). Here, characteristic differences in oscillatory activity between the blind and sighted were found. Interestingly, a double dissociation between power and power correlation effects was found. While alpha (~10 Hz) power was strongly reduced over occipital sites in the blind, alpha connectivity within visual areas was on comparable levels in the blind and sighted. Vice versa, the blind visual areas exhibited connectivity in the delta (~2 Hz) and gamma (~90 Hz) range, which was not mirrored in increased signal power for these frequencies. These findings indicate that the bivariate measure resolves additional and complementary information about the organization of spontaneous oscillatory activity, not present in the plain strength of oscillatory activity.

Overall, the results obtained with the new method for imaging functional connectivity from M/EEG, demonstrate that spontaneous electrophysiological signal fluctuations exhibit a rich and frequency dependent spatial structure that is sensitive to pathological alterations of brain organization. This method thus opens up a novel road for investigating human brain connectivity in health as well as diseases.

In sum, this thesis described two new approaches for studying human brain connectivity based on spontaneous brain activity and provided evidence for their potential in studying pathological cases of 'rewiring' in multiple sclerosis and congential blindness.

Conclusion

Spontaneous brain activity has the potential for providing invaluable access to the organization and functioning of the healthy and diseased human brain. The developments and findings provided in this thesis constitute significant steps for unfolding this potential by bridging methodological and conceptual gaps in the current state of the art.

References

Arieli A, Sterkin A, Grinvald A, Aertsen A (1996) Dynamics of ongoing activity: explanation of the large variability in evoked cortical responses. Science 273:1868–1871.

Biswal B, Yetkin FZ, Haughton VM, Hyde JS (1995) Functional connectivity in the motor cortex of resting human brain using echo-planar MRI. Magn Reson Med 34:537–541.

Biswal BB et al. (2010) Toward discovery science of human brain function. Proc Natl Acad Sci USA 107:4734–4739.

Brookes MJ, Woolrich M, Luckhoo H, Price D, Hale JR, Stephenson MC, Barnes GR, Smith SM, Morris PG (2011) Investigating the electrophysiological basis of resting state networks using magnetoencephalography. Proc Natl Acad Sci USA 108:16783–16788.

Corbetta M (2010) Functional connectivity and neurological recovery. Dev Psychobiol Available at: http://www.ncbi.nlm.nih.gov/pubmed/21086510

Engel AK, Fries P, Singer W (2001) Dynamic predictions: oscillations and synchrony in top-down processing. Nat Rev Neurosci 2:704–716.

Fox MD, Greicius M (2010) Clinical applications of resting state functional connectivity. Front Syst Neurosci 4:19.

Fox MD, Raichle ME (2007) Spontaneous fluctuations in brain activity observed with functional magnetic resonance imaging. Nat Rev Neurosci 8:700–711.

Friston KJ, Ashburner JT, Kiebel S, Nichols T, Penny WD (2007) Statistical Parametric Mapping: The Analysis of Functional Brain Images, 1st ed. Academic Press.

Greicius M (2008) Resting-state functional connectivity in neuropsychiatric disorders. Curr Opin Neurol 21:424–430.

He BJ, Shulman GL, Snyder AZ, Corbetta M (2007) The role of impaired neuronal communication in neurological disorders. Curr Opin Neurol 20:655–660.

Hipp JF, Engel AK, Siegel M (2011) Oscillatory synchronization in large-scale cortical networks predicts perception. Neuron 69:387–396.

Hubel DH, Wiesel TN (1962) Receptive fields, binocular interaction and functional architecture in the cat's visual cortex. J Physiol (Lond) 160:106–154.

Logothetis NK (2008) What we can do and what we cannot do with fMRI. Nature 453:869–878.

Plenz D, Thiagarajan TC (2007) The organizing principles of neuronal avalanches: cell assemblies in the cortex? Trends Neurosci 30:101–110.

Raichle ME (2010) Two views of brain function. Trends Cogn Sci (Regul Ed) 14:180–190.

Schoffelen J-M, Gross J (2009) Source connectivity analysis with MEG and EEG. Hum Brain Mapp 30:1857–1865.

Shulman RG, Rothman DL, Behar KL, Hyder F (2004) Energetic basis of brain activity: implications for neuroimaging. Trends Neurosci 27:489–495.

Tsodyks M, Kenet T, Grinvald A, Arieli A (1999) Linking spontaneous activity of single cortical neurons and the underlying functional architecture. Science 286:1943–1946.

Zhang D, Raichle ME (2010) Disease and the brain's dark energy. Nat Rev Neurol 6:15–28.

Abstract in German (Zusammenfassung)

Diese Thesis führt zwei methodische Fortschritte für die Erforschung der hirnweiten Organisation neuronaler Spontanaktivität im Menschen ein und leistet eine Übertragung dieser Methoden in den klinischen Bereich.

Zunächst wird ein generisches, datengetriebenes Prozedere zur Identifizierung von Veränderungen hirnweiter intrinsischer funktioneller Konnektivität vorgestellt und in einer Patientenpopulation mit Multipler Sklerose getestet. Mit Hilfe der neuen Technik konnte eine Korrelation zwischen fMRT-basierten Maßen der funktionellen Konnektivität und Verhalten etabliert werden. Trotz starker kognitiver Beeinträchtigungen und der schwerwiegenden Zersetzung der zentralnervösen weißen Substanz, erhöhten spezifische Netzwerke ihre funktionelle Konnektivität. Diese Beobachtung hinterfragt die vorherrschende Ansicht, wie funktionelle Konnektivität die Integrität von Hirnnetzwerken anzeigt und hat wichtige Implikationen für Ruhe-fMRT Untersuchungen von Hirnerkrankungen sowie für theoretische und Modellierungsstudien kortikaler Aktivitätsdynamik. Darüber hinaus hat die beobachtete Korrelation zwischen Verhalten und Konnektivität eine hohe Relevanz für den medizinischen Bereich, da diese möglicherweise als Biomarker für den Grad der Auswirkungen der Multiplen Sklerose auf die funktionelle Verarbeitung und Netzwerk-Organisation im Gehirn dienen kann.

Des Weiteren wird eine neuartige Methode zur Messung funktioneller Konnektivität basierend auf nicht-invasiven, elektrophysiologischen Daten wie Magneto - Elektroenzephalographie (M/EEG) eingeführt. Kernfortschritt der Methode ist die Überwindung eines fundamentalen Problems für das Messen echter Hirninteraktionen von M/EEG Daten durch eine neue Technik der Phasenorthogonalisierung. Durch die Anwendung dieser Methode auf MEG-Aufnahmen von Spontanaktivität einer großen Kohorte von gesunden Probanden wurde eine Charakterisierung der hirnweiten Organisation spontaner, neuronaler Oszillationen erreicht. Spontane Fluktuationen oszillatorischer Aktivität sind räumlich in frequenzabhängige und funktional spezifische Korrelationsstrukturen organisiert. Diese Methode stellt ein neues Werkzeug dar, das ein Verständnis der hirnweiten Organisation neuronaler oszillatorischer Aktivität erlaubt.

Zuletzt untermauert die kombinierte Anwendung der beiden Methoden auf MEG-Aufnahmen spontaner Hirnaktivität einer Gruppe geburtsblinder Teilnehmer das

Potenzial der Ansätze durch den Nachweis spezifischer Veränderungen in der Organisation von spontaner oszillatorischer Aktivität der Blinden. Okzipitale Hirnbereiche der Blinden besaßen bekannte oszillatorische Signaturen aktiver funktioneller Verarbeitung bei denen die Phase langsamer oszillatorischer Prozesse (delta Bereich ~2 Hz) die Amplitude schnellerer Rhythmen (gamma Bereich ~90 Hz) bestimmte. Zusätzlich besaßen diese eigentlich visuell arbeitenden Gehirnbereiche frequenzspezifische Konnektivität (beta Bereich ~25 Hz) mit prefrontalen Arealen. Diese Befunde legen nahe, dass normalerweise visuell arbeitende Gehirnbereiche in den Blinden freier mentaler Aktivität dienen könnten und spezifische occipito-frontale Konnektivität der Reintegration dieser Resourcen in kortikale Netzwerke unterliegt.
Insgesamt demonstriert die Anwendung der zwei neuen Methoden auf Daten von klinischen Populationen, dass spontane Hirnaktivität einen einzigartigen Zugriff auf pathophysiologische Prinzipien der Hirnorganisation zulässt. Die Fortschritte, welche in dieser Thesis beschrieben sind überbrücken methodische und konzeptionelle Lücken im Studium der Spontanaktivität des menschlichen Gehirns.

Contributions

1. Contributed scientific ideas
2. Generated data
3. Analyzed and interpreted the data
4. Wrote the paper
* Contributed equally

M1:
Hawellek DJ, Hipp JF, Lewis CM, Corbetta M, Engel AK (2011) Increased functional connectivity indicates the severity of cognitive impairment in multiple sclerosis, Proc. Natl. Acad. Sci. U.S.A. 108:19066-19071.

Hawellek DJ: 1,2,3,4
Hipp JF: 1,3,4
Lewis CM: 3
Corbetta M: 1,4
Engel AK: 1,4

M2:
Hipp JF, **Hawellek DJ**, Corbetta M, Siegel M, Engel AK, (2012) Large-scale cortical correlation structure of spontaneous oscillatory activity. Nature Neuroscience Available at: *http://www.nature.com/neuro/journal/vaop/ncurrent/abs/nn.3101.html*

Hipp JF: 1,2,3,4,conceived the technique of phase orthogonalized power correlations
Hawellek DJ: 1,2,3,4
Corbetta M: 1,4
Siegel M: 1,4
Engel AK: 1,4

M3:
Hawellek DJ, Schepers IM, Engel AK, Siegel M, Hipp, JF (ready for submission) Intrinsic local and long-range couplings in oscillatory activity of blind visual cortex

Hawellek DJ: 1,2,3,4
Schepers IM: 1,2,4
Engel AK: 1,4
Siegel M: 1,3,4,*
Hipp JF: 1,3,4,*

Appended manuscripts

Increased functional connectivity indicates the severity of cognitive impairment in multiple sclerosis

David J. Hawellek[a,1], Joerg F. Hipp[a,b], Christopher M. Lewis[c,d,e], Maurizio Corbetta[d,e,f], and Andreas K. Engel[a]

[a]Department of Neurophysiology and Pathophysiology, University Medical Center Hamburg-Eppendorf, 20246 Hamburg, Germany; [b]Centre for Integrative Neuroscience, University of Tübingen, 72076 Tübingen, Germany; [c]Ernst Stüngmann Institute in cooperation with The Max Planck Society, 60528 Frankfurt, Germany; [d]Department of Clinical Sciences and Bioimaging and [e]Institute for Advanced Biomedical Technologies, G. D'Annunzio University, 66100 Chieti, Italy; and [f]Departments of Neurology, Radiology, Anatomy and Neurobiology, Washington University School of Medicine, St. Louis, MO 63110

Edited by Marcus E. Raichle, Washington University, St. Louis, MO, and approved October 19, 2011 (received for review June 22, 2011)

Correlations in spontaneous brain activity provide powerful access to large-scale organizational principles of the CNS. However, making inferences about cognitive processes requires a detailed understanding of the link between these couplings and the structural integrity of the CNS. We studied the impact of multiple sclerosis, which leads to the severe disintegration of the central white matter, on functional connectivity patterns in spontaneous cortical activity. Using a data driven approach based on the strength of a salient pattern of cognitive pathology, we identified distinct networks that exhibit increases in functional connectivity despite the presence of strong and diffuse reductions of the central white-matter integrity. The default mode network emerged as a core target of these connectivity modulations, showing enhanced functional coupling in bilateral inferior parietal cortex, posterior cingulate, and medial prefrontal cortex. These findings imply a complex and diverging relation of anatomical and functional connectivity in early multiple sclerosis and, thus, add an important observation for understanding how cognitive abilities and CNS integrity may be reflected in the intrinsic covariance of functional signals.

resting state | BOLD fMRI | diffusion tensor imaging | fractional anisotropy | neurological

Understanding how disease processes affect functional interactions in the CNS is a core challenge of neuroscience research. fMRI connectivity has become an important tool for revealing large-scale network interactions by analyzing correlations in intrinsic fluctuations of the BOLD signal (1). This method is sensitive to plastic as well as developmental changes of the functional architecture (2–5), and has successfully linked specific cognitive syndromes to the pathology of distinct functional systems (e.g., spatial neglect after stroke, different forms of dementias, and healthy aging) (6–8). The structural wiring of the brain plays an essential role in shaping the spatial patterns of functional interactions (9, 10). However, the activity correlations are not fully determined by the anatomical connections and, thus, provide complementary information about network organization (11). Especially in the context of neurological damage, the functional covariance structure may document pathological effects well beyond focal damage, indicating the complex changes of interactions that occur in distributed networks (12–14). Commonly, the coupling strength of spontaneous brain activity is thought to be a direct proxy for the functioning of brain networks, with stronger interactions also reflecting a stronger computational capacity (15, 16).

In this study we have investigated how cognitive pathology due to neurological damage in multiple sclerosis (MS) is reflected in changes of structural and functional connectivity. Compared with other CNS pathologies, MS stands out due to the prominent involvement of the central white matter. During the disease process, the immune system exerts inflammatory insults to neuronal myelination and axonal integrity (17). These processes may lead to the loss of functional cofluctuations (18), especially in late and severe stages of the disease (19), reminiscent of a scenario of complete disconnection as in the extreme case of corpus callosotomy (20). Surprisingly, however, recent studies also report increased functional connectivity in earlier stages of the disease (21–23). This raises the question of how cognitive impairment that occurs as an early and prominent consequence of MS (24) may relate to changes of functional connectivity. A challenging aspect of the cognitive decline is the weak association between specific lesion parameters, such as the location of T2-visible plaques and circumscribed cognitive abilities (25, 26). It is becoming increasingly clear that subtle, nonfocal white matter damage (as assessed by, e.g., diffusion-weighted imaging) plays a crucial role in determining the presence and extent of cognitive impairment (27–30). Thus, the manner in which the disease affects cognition is likely not a collection of random and focal disturbances, but has widespread structural and functional consequences as an important pathological element (31).

In a group of early stage patients, we found the cognitive pathology to exhibit a salient multivariate pattern, a general factor. Further, we found this pattern of impairment to be related to the widespread integrity of the central white matter. Finally, by means of a data driven approach, we identified the default mode network to be central to strong modulations of functional connectivity by the severity of the cognitive pathology. Strikingly, the reduction in cognitive ability and widespread anatomical connectivity was associated with increased functional connectivity. These results reveal a dissociation of changes in functional and anatomical connectivity in relation to cognitive ability and add an important empirical observation for understanding how fMRI connectivity may index the integrity of cortical circuits. Our findings hold significant implications for resting state investigations of brain diseases as well as theoretical and modeling studies of large-scale cortical dynamics.

Results

Cognitive Efficiency. To assess the presence and structure of cognitive impairment, we quantified the performance of 16 patients in the early stages of MS (Table S1) and individually matched controls in a set of neuropsychological tests. All tests were standard tools used in clinical and research settings and together probed a broad range of different sensory, cognitive, and output modalities. Fig. 1*A* summarizes the test results for all patients, sorted such that the patient with the worst performance appears at the top and the test accumulating the most negative performance appears to the left. Three important features of the overall

Author contributions: D.J.H., J.F.H., M.C., and A.K.E. designed research; D.J.H. performed research; D.J.H., J.F.H., and C.M.L. analyzed data; and D.J.H., J.F.H., M.C., and A.K.E. wrote the paper.

The authors declare no conflict of interest.

This article is a PNAS Direct Submission.

Freely available online through the PNAS open access option.

[1]To whom correspondence should be addressed. E-mail: d.hawellek@uke.de.

This article contains supporting information online at www.pnas.org/lookup/suppl/doi:10.1073/pnas.1110024108/-/DCSupplemental.

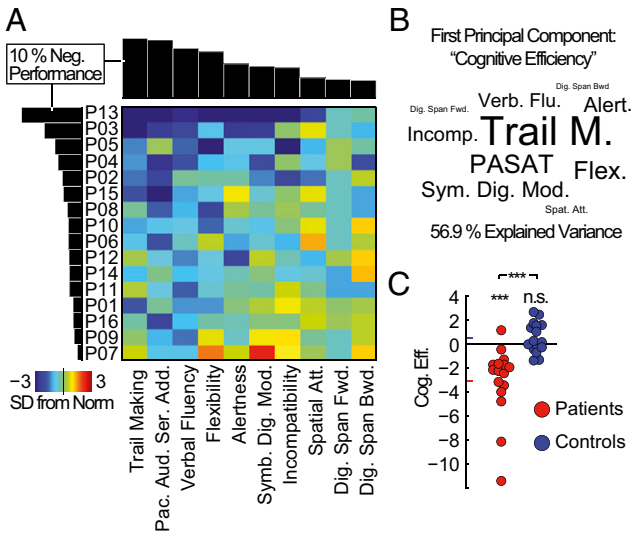

Fig. 1. Cognitive pathology is dominated by a general factor of cognitive functioning. (*A*) Neuropsychological test results for all patients (see Fig. S1 for the combined patient and control data set). The color code indicates deviations from the age and education norm in SDs. Both axes have been sorted by the percentage of overall negative performance, as shown in the margins. (*B*) Test name sizes scaled by the loadings of the first principal component for the combined patient and control dataset (spatial positioning is arbitrary). This component explained 56.9% of the overall variance in test performance and is referred to as cognitive efficiency in all subsequent analyses. (*C*) Component scores of the first principal component for all study participants. Group means are indicated by the colored bars at the ordinate.

pattern of cognitive pathology in the sample emerged. First, the cognitive impairment exhibited a considerable variability, with some patients showing only mild deficits and other patients being more severely affected. Second, some tests were particularly sensitive in uncovering negative performance early, suggesting that they tap into functions, which are especially prone to the disease process. And third, with increasing severity of the pathology, the impairment appeared to broaden across tests, successively spanning a wider range of tested modalities. Thus, instead of multiple, more-specific patterns of impairment, the patients mainly differed in the general bandwidth of cognitive processes, leading to the emergence of a general factor of cognitive pathology. To quantify and further analyze this pattern, we applied principal component analysis (PCA) to the behavioral performance of patients and healthy controls.

The first principal component of the test battery explained >50% of the total behavioral variance observed; it was the only pattern discernible from Gaussian noise ($P < 10^{-16}$), and robust to overfitting effects (Fig. S1 *B* and *C*). Importantly, all weights of the component had the same sign, again indicating the main feature of a general factor, i.e., the positive correlation of test performance across subjects. To give an idea of how each of the tests contributed to the component, Fig. 1*B* shows the test names scaled by the first component's eigenvector (loadings). The tests with a high impact (trail making, paced auditory serial addition test, and verbal fluency) had an emphasis on executive functions, speed of processing, and cognitive flexibility, and presumably require the dynamic integration of information in large-scale networks (32). The level of this general factor, hereafter referred to as cognitive efficiency, separated the patient and control group (Fig. 1*C*). The patient group showed a significant decrease in cognitive efficiency (difference from zero: *t* test, $P = 9.63 \times 10^{-4}$; group difference: paired *t* test, $P = 9.24 \times 10^{-4}$). The healthy control group did not differ from the norm level of cognitive efficiency (*t* test, $P = 0.101$). A classification into patients and controls based on cognitive efficiency yielded a sensitivity of up to 81% while maintaining full specificity (Fig. S1*D*). Fatigue or depression could be excluded to confound the results, as none of the patients was found to show symptoms of depression (Table S1). and the level of cognitive efficiency was unrelated to any metric of the Modified Fatigue Impact Scale (33) (Fig. S1*E*).

Taken together, we find cognitive impairment to be a prevailing feature in early stages of MS. The impairment exhibited a salient pattern across patients in the form of a general factor, suggestive of widespread network dysfunctions. In the following we investigated how this behavioral decline manifested itself in structural and functional changes of the CNS.

Structural Damage. To evaluate the structural damage that underlies the observed behavioral impairment, we quantified the relation of cognitive efficiency to several anatomical parameters. For each participant we obtained estimates of the volume of the peripheral gray matter and ventricular cerebrospinal fluid from the structural scans. The volumes of these structures are sensitive markers of atrophy processes. Additionally, we derived maps of fractional anisotropy and mean diffusivity from the diffusion-weighted imaging data. These diffusion parameters indicate the integrity of highly organized tissue, such as the white matter, and allow for an assessment of even subtle disturbances. The strongest association was found within the diffusion parameters. Cognitive efficiency strongly correlated with a distributed pattern of fractional anisotropy (Fig. 2*A*) in the corpus callosum and immediately surrounding structures (see Fig. S2 for mean diffusivity). The atrophy markers did show a considerably weaker relation (Fig. 2*B*). Indeed, the diffusion tensor parameters kept significant predictive power on the level of cognitive efficiency,

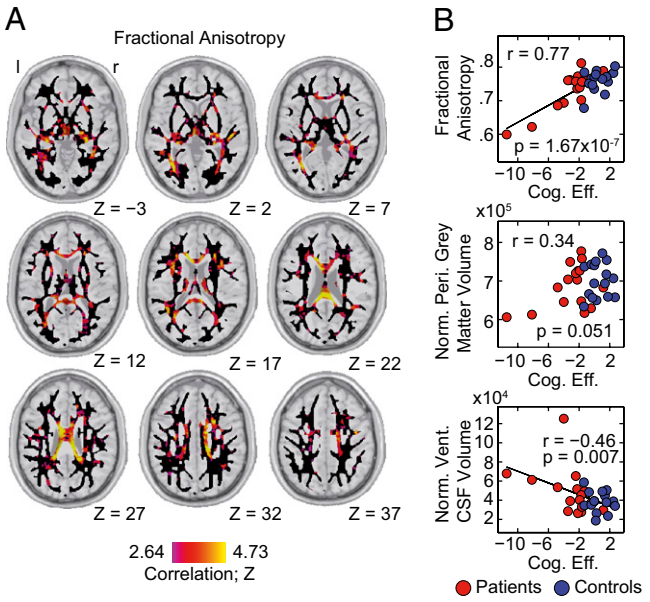

Fig. 2. The loss of cognitive efficiency relates to widespread structural damage. (*A*) Group-level correlation of cognitive efficiency with voxel-wise fractional anisotropy. The analysis was performed within a standard-space white matter mask shown as a black underlay. Correlations are shown as corresponding z-scores and have been thresholded at $P = 0.05$, FDR corrected. No negative correlations passing this threshold were observed. (*B*) The relation of cognitive efficiency to three anatomical parameters: (*Top*) mean fractional anisotropy within a corpus callosum mask, (*Middle*) volume of the peripheral gray matter normalized for individual head size, and (*Bottom*) normalized volume of the ventricular cerebrospinal fluid. Patients are shown as red dots; healthy controls are shown as blue dots.

NEUROSCIENCE

even when removing the most extreme patients from the analysis or performing the analysis only within the patient group (Fig. S2). These results suggest the level of cognitive efficiency to strongly relate to structural damage as reflected in a broadly distributed pattern of reduced white matter integrity.

Functional Connectivity Modulations. We studied the changes in functional connectivity that are related to cognitive efficiency with a data-driven procedure (Fig. 3*A* and *Materials and Methods*). First, we derived measures of connectivity based on the covariation of BOLD time series between ~40,000 voxels that span the cortex for each participant. Then, we quantified the behavioral modulation of functional connectivity by correlating the strength of each connection with cognitive efficiency across participants. We used random permutation statistics to identify voxels that had a modulation in connectivity (see Fig. 3*A*, Fig. S3, and *SI Materials and Methods* for a detailed description of the method). This procedure identified distributed sets of voxels [$n = 447$, $P < 0.05$, false discovery rate (FDR) corrected] that exhibited significant modulation (Fig. 3*B*). The largest clusters of behavioral modulation localized to bilateral inferior parietal cortices as well as to midline structures in the posterior cingulate and medial frontal cortex (Table S2). Importantly, the procedure did not make any assumptions about specific functional networks or whether connectivity increases or decreases contribute to the modulation. In other words, these regions changed their connectivity, but the spatial patterns of these connectivity changes, as well as the direction in which the connectivity was changed (increase or decrease), remained unresolved by this first analysis step.

The spatial patterns underlying the behavioral modulation can be revealed from the individual modulation profiles of each of the identified voxels. The modulation profile contains the global increases and decreases of connectivity with cognitive efficiency. First, we analyzed whether the 447 modulation profiles exhibited similarity across voxels. Indeed, the similarity matrix revealed a strong dominance by one underlying pattern (Fig. 4*A*). Two groups of voxels emerged that were characterized by a highly similar modulation profile within the group and an inverted pattern between the groups. We then derived the underlying dominant spatial pattern of modulation as the first principal component of the modulation profiles (Fig. 4*B*). This dominant spatial pattern explained 40.4% of the total modulation variance and comprised two functional networks: (*i*) the default mode network (DMN; negative values) and (*ii*) areas implicated in the deployment of attention and cognitive control, hereafter referred to as the control network (CN; positive values) (34). The networks' opposite sign indicated that the major connectivity modulation was a concurrent increase of connectivity to one network and a decrease of connectivity to the other. We then further analyzed the strength with which each of the 447 voxels expressed this dominant pattern of modulation (Fig. 4*C*). Rendering the loadings of the dominant modulation pattern on the cortical surface again revealed the two groups of voxels, which exhibited the pattern in an inverted way. The larger group was located in the bilateral parietal cortices, posterior cingulate cortex, and medial prefrontal cortex. These structures spatially overlapped with core parts of the DMN. The positive loadings of these regions showed them to exhibit the modulation pattern as depicted in Fig. 4*B*. Connectivity was shifted toward the DMN in cognitively less-efficient participants (anticorrelation), whereas it was shifted toward the CN in cognitively efficient participants (positive correlation). The smaller cluster exhibited the same pattern of modulation, but connectivity was shifted in the opposite way between the networks (negative loadings). These structures, spatially corresponding to parts of the CN, showed a connectivity shift toward the CN in cognitively less-efficient participants, and a connectivity shift toward the DMN in cognitively efficient participants. Thus, the spatially distributed modulations of functional connectivity involved two major functional networks, the DMN and CN. The nature of the modulations was a shift of connectivity toward the spatially corresponding network in cognitively less-efficient participants and, at the same time, away from the other network.

An increase in BOLD time-course correlations (connectivity) could reflect a change from moderately positive to highly positive correlation values in the patients, but also a change from strong anticorrelation toward less anticorrelation. The important difference between these scenarios cannot be revealed from the modulation alone. In a last step, we thus went back to the first level of analysis and mapped the actual range of connectivity that was underlying the modulations. To this end we constructed a connectivity graph between the two groups of identified regions (Fig. 4*C*) and the two networks of the dominant spatial modulation pattern (Fig. 4*B* and *SI Materials and Methods*). We then derived the average within- and across-network connectivity. The within-network connectivity increased toward more positive correlation values in the patients (Fig. 4 *D* and *E*). For both groups the average within-network connectivity was significantly positive (DMN: patient group, *t* test, $P = 8.5 \times 10^{-5}$, control group, *t* test, $P = 7 \times 10^{-7}$; CN: patient group, *t* test, $P = 2.6 \times 10^{-6}$, control group, *t* test, $P < 1 \times 10^{-7}$), with the patient group showing a higher connectivity (DMN: paired *t* test, $P = 0.035$; CN: paired *t* test, $P = 0.022$). The finding that the control group exhibited positive connectivity suggested that the identified regions were loosely associated with the networks in the healthy condition and became integrated more strongly in the patient group.

The two networks involved in these modulations have previously been shown to exhibit an intrinsically anticorrelated relationship during rest (35) as well as in task situations (36). In agreement with these findings, for both networks the increased connectivity was accompanied by a more marked anticorrelation with the other network. The average across-network correlations were negative for both groups (Fig. 4*F*; patient group *t* test, $P = 0.0017$, control group *t* test, $P = 7 \times 10^{-4}$), with the patients exhibiting stronger anticorrelations (paired *t* test, $P = 0.037$).

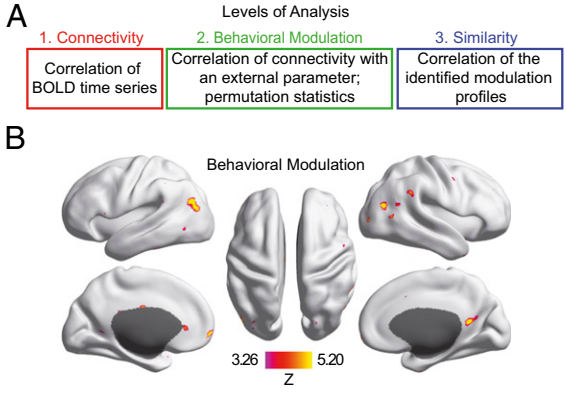

Fig. 3. Functional connectivity is modulated by the level of cognitive efficiency. (*A*) Three levels of the fMRI data analysis stream build upon each other. The colored frames correspond with the more detailed depiction in Fig. S3. Based on the global connectivity between all voxel pairs, we calculated the correlation of all connections with cognitive efficiency across participants. This calculation resulted in a global modulation matrix in which each row (modulation profile) represented the increases and decreases of connectivity that occurred in association with the level of cognitive efficiency for a given voxel. We assessed the statistical significance of the modulation by permutation statistics (*SI Materials and Methods* and Fig. S3). To further investigate the effect, we calculated the similarity matrix of the identified modulation profiles (Fig. 4*A*) in subsequent analyses. This matrix represents the cross-correlations of all of the identified modulation profiles. (*B*) Cortical regions, which exhibit significant modulation by cognitive efficiency. The map has been thresholded at $P = 0.05$, one-tailed, FDR corrected.

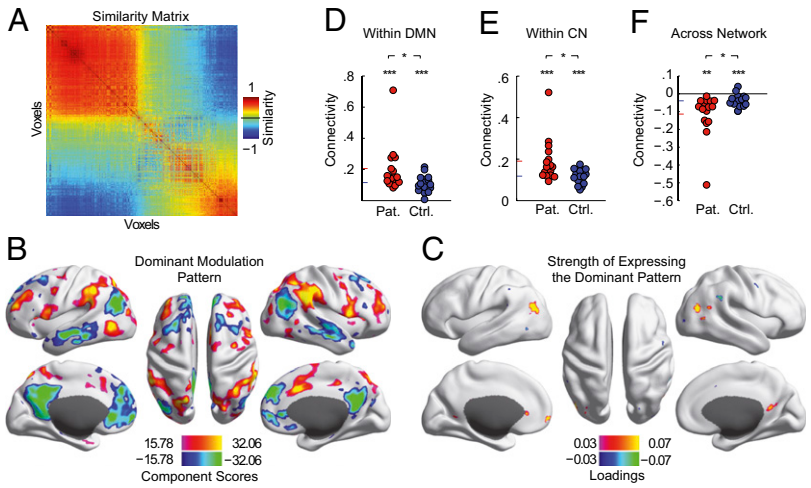

Fig. 4. Increased functional connectivity marks the severity of the cognitive pathology. (*A*) Similarity matrix of the modulation profiles (n = 447; cf. Fig. 3*B*). (*B*) The dominant spatial pattern of connectivity modulations explaining 40.4% of the overall connectivity modulation variance. The color range is set to show the top 25% of absolute values. (*C*) Voxel-wise principal PCA loadings indicating how strongly and with which sign each of the identified regions expressed the spatial pattern of connectivity modulations shown in *B*. The color range is set to show the top 75% of absolute values. (*D–F*) Average cross-connectivity between the two clusters of identified regions and the two networks of the dominant spatial modulation pattern (*SI Materials and Methods*). Group means are indicated by colored bars at the ordinate.

Note that the statistics shown in Fig. 4 *D–F* are not independent from the procedure, which identified the effect. The existence of group differences in the connectivity data underscores the robustness of the effect but had to be expected from the nature of the behavioral parameter. The focus of analysis here was the range of actual connectivity that is spanned by the modulations. To control whether the two most extreme cases in the patient group could have driven these results alone, we performed control analyses without them (Fig. S4*C*). Both the association of connectivity with behavior as well as the group differences were present when omitting these patients. Additional control analyses regarding the preprocessing of the fMRI data and head movement levels are detailed in *SI Materials and Methods*.

Taken together, the pathological loss of cognitive efficiency was associated with a gain of functional connectivity among core parts of the default mode network as well as a control network. These effects distinguished the groups and got stronger as the cognitive impairment and thus structural damage worsened.

Discussion

We have investigated the relation of a salient, pathological pattern in behavior to the covariance structure of spontaneous brain activity in patients with early stage MS. At the heart of our observations lies the divergent role of anatomical and functional connectivity measures in indexing the level of cognitive ability. Functional connectivity within two networks increased in the face of a concomitant reduction of anatomical connectivity and a decline in cognitive efficiency. This finding seemingly contradicts the predominant view of how functional connectivity indexes the integrity of the underlying circuits. A gain in shared variance of the BOLD fluctuations is often interpreted as a gain in functional interactions between the brain regions. Conversely, a pathological loss of function is thought to be reflected in a loss of cofluctuations in dedicated brain systems. This view has been supported by numerous studies across diverse neurological conditions, such as stroke (6, 37), traumatic brain injury (38), Alzheimer's disease (39), vegetative state and coma (40), callosotomy (20), and the decline in healthy aging (8), raising the question of what may be different in the case of MS.

Several of our observations suggest that a main distinct feature of the pathology may be the diffuse and distributed impact MS has on white matter integrity and CNS networks. First, the behavioral parameter, which was used to identify the connectivity modulations, exhibited a notable multivariate structure. The appearance of a general factor suggests a loss of resources, which are required to support a sufficient bandwidth of cognitive processes, conjointly affecting otherwise more distinct cognitive domains (Fig. S1*F*). Second, we find the strongest association between the level of cognitive efficiency and structural measures in a spatially widespread pattern of white matter integrity. And third, the increased connectivity was present in networks implied in different cognitive functions, such as cognitive control of external (41, 42) and internal information (34, 36, 43–45). These networks are commonly recruited across a wide variety of cognitive tasks, and require the coordinated flow of information across a wide expanse of cortex, supported by long-range fiber tracts. Thus, all aspects of our analyses coherently point to a diffuse and widespread impact of the disease on CNS functioning.

With these considerations in mind, there may be two major lines of argument for assigning physiological significance to the increased functional connectivity. First, cortical plasticity processes may be central to our results. A well-replicated finding in task activation studies is that patients in various stages of the disease will show an enhanced recruitment of task-relevant areas (46–49). These effects specifically involve an extension of the activation patterns to additional and functionally related brain areas. Such results are commonly interpreted as indicating an increased neural effort in cortical computation due to the presence of structural damage. Our observations could thus reflect the traces of these repetitive and increased coactivations, with the functional connectivity tracking the statistical history of coactivation in cortical circuits. A number of recent studies in healthy subjects have documented the strengthening of functional connectivity with training-induced improvement in functions in multiple domains, including the motor (2), visual (3), and mnemonic system (4). Thus, increased functional connectivity could provide a compensatory mechanism that, through Hebbian plasticity, limits the consequences of neurological damage and helps to maintain a viable level of computational capacity. However, this putative compensatory function does not agree well with the negative relationship between functional connectivity and cognitive abilities as reported here. Enhanced plasticity

might, in principle, also be maladaptive and directly contribute to the worsening of cognitive functions.

An alternative explanation would be that the reduction in white matter integrity may have led to a loss of diversity in large-scale cortical dynamics. The finding of widespread structural disturbances suggests that the pathological process may have strongly reduced the anatomical basis for functional interactions in a diffuse manner. Instead of specific connectivity being lost completely, the identified regions of modulation might hereby have lost flexibility in their functional interactions. With progressing severity, the regions would be unable to gear up to more variable states and thus more frequently participate in prevalent global patterns of activity (DMN, CN), which would result in stronger apparent connectivity on long time-scales resulting from the more rigid and less-differentiated patterns of functional connectivity. Such a loss-of-diversity account also fits well with reduced cognitive efficiency as the major neuropsychological consequence, suggesting that less-diverse patterns of functional connectivity may be a correlate of the reduced bandwidth of cognitive processes. These arguments share conceptual similarity with the process of dedifferentiation during aging, in which cognitive representations such as receptive fields get gradually less specific and more broadly tuned (50, 51). Increased functional connectivity reflecting a loss of diversity in interactions may indeed be a phenomenon common to pathologies in which a diffuse reduction, but not the absence, of anatomical connectivity is a prevalent feature. Recent converging lines of theoretical work further support this view. Here the functional dynamics are seen as an exploration of possible states upon a static structural scaffold (52). The hypothesis of a loss of possible interactions within this scaffold naturally reconciles the seemingly divergent role of anatomical and functional connectivity in indexing the level of cognitive ability. However, given the available data, these considerations so far remain hypothetical. Our observations call for theoretical studies addressing the effects of gradual and diffuse, instead of complete and focal, ablations in the cortical connectivity regime on the organization of the unfolding functional dynamics.

Overall, our findings show an association of increased functional connectivity in distinct systems with decreased cognitive ability in MS. These observations were made without assumptions regarding specific brain systems and by means of a careful consideration of the prevailing cognitive impairment. The functional connectivity analysis was entirely data driven and based on the hypothesis that the behavioral parameter derived from the neuropsychological testing is informative about individual CNS integrity. Our approach took advantage of the strong pathological variability in the patient data, which may render mean-based approaches such as group comparisons insensitive, and thus represents a valuable procedure in revealing pathophysiological principles in functional imaging data. Our findings extend recent observations, which have been made using independent component analysis, of spontaneous brain activity in MS. These studies have reported on increased synchronization measures of network patterns in different stages of the disease (21–23), but the exact relation to individual behavioral status had remained unclear. Changes of functional networks and their large-scale dynamics may provide a key level of description for understanding how MS affects the CNS. Future studies will be needed to characterize the stage of white matter disintegration that marks the transition from increased functional connectivity to reductions in coupling and the eventual complete absence of cofluctuations (18–23). Our findings suggest that incorporating subtle estimates of the individual behavioral state in addition to contrasts between clinically defined groups is an important element when investigating the impact of MS on brain networks.

Materials and Methods

A detailed description of the applied methods is given in *SI Materials and Methods*. In the following we give a brief account of our procedures.

Study Design. Sixteen early stage MS patients and 16 healthy controls matched for age, sex, and education participated in the experiments (*SI Materials and Methods* and Table S1). Each participant completed three experimental stages within 1–4 successive days: (*i*) neuropsychological examination with a battery of self-evaluation and cognitive measures; (*ii*) 20-min recording of magnetencephalography (275-channel CTF MEG System) during silent fixation; and (*iii*) MRI session, with a recording of ~20 min BOLD signal during silent fixation and high-resolution anatomical as well as diffusion-weighted images. The local ethics committee approved the study, and each study participant gave informed consent before taking part in the experiments. All experiments were conducted according to the Declaration of Helsinki.

Data Analysis. The analysis of the behavioral data was performed on 10 cognitive measures, which were extracted from the more demanding parts of the tests. The raw scores were normalized with the appropriate normative data of a healthy population, matching the individual participants in age and education. The behavioral parameter "cognitive efficiency" was then estimated as the first principal component of the resulting performance matrix containing all normalized test results of all participants. The analysis of the structural damage was done using FSL (http://www.fmrib.ox.ac.uk/fsl/) (53). The diffusion tensor parameters were estimated with the diffusion-weighted imaging tools as documented in the initial steps of TBSS (http://www.fmrib.ox.ac.uk/fsl/tbss/index.html) (54). Statistical analyses were performed within a standard-space white matter mask (FMRIB58_FA skeleton thresholded at 0.2), shown as a black underlay in Fig. 2*A* and Fig. S2*A*. The tissue volumes (normalized for individual head size) were calculated using SIENAX (55). The global modulation of functional connectivity by the level of cognitive efficiency was calculated after standard preprocessing procedures of the functional data. In short, for each voxel, the behavioral modulation of functional connectivity was calculated as the number of significant ($P = 0.01$, uncorrected) group-level correlations that occurred between its global connectivity pattern and the level of cognitive efficiency. For assessing the statistical significance of the modulations, the procedure was repeated 100× while randomly permuting the behavioral parameter. A normal distribution was fitted to these resamples to derive an empirical distribution for the null hypothesis of no connectivity modulation with cognitive efficiency. This distribution was used to derive z-scores (subtraction of mean and division by the SD) and *P* values. We corrected for multiple statistical testing by controlling for the FDR (56).

ACKNOWLEDGMENTS. We thank all patients who participated in these experiments. We also thank Roland Martin, Sven Schippling, and the team of the Institute for Neuroimmunology and Clinical MS Research at the Department of Neurology of the University Medical Center Hamburg-Eppendorf for support. This work was supported by European Union Grant HEALTH-F2-2008-200728, BrainSync.

1. Fox MD, Raichle ME (2007) Spontaneous fluctuations in brain activity observed with functional magnetic resonance imaging. *Nat Rev Neurosci* 8:700–711.
2. Albert NB, Robertson EM, Miall RC (2009) The resting human brain and motor learning. *Curr Biol* 19:1023–1027.
3. Lewis CM, Baldassarre A, Committeri G, Romani GL, Corbetta M (2009) Learning sculpts the spontaneous activity of the resting human brain. *Proc Natl Acad Sci USA* 106:17558–17563.
4. Tambini A, Ketz N, Davachi L (2010) Enhanced brain correlations during rest are related to memory for recent experiences. *Neuron* 65:280–290.
5. Dosenbach NUF, et al. (2010) Prediction of individual brain maturity using fMRI. *Science* 329:1358–1361.
6. He BJ, et al. (2007) Breakdown of functional connectivity in frontoparietal networks underlies behavioral deficits in spatial neglect. *Neuron* 53:905–918.
7. Seeley WW, Crawford RK, Zhou J, Miller BL, Greicius MD (2009) Neurodegenerative diseases target large-scale human brain networks. *Neuron* 62(1): 42–52.
8. Damoiseaux JS, et al. (2008) Reduced resting-state brain activity in the "default network" in normal aging. *Cereb Cortex* 18:1856–1864.
9. Hagmann P, et al. (2008) Mapping the structural core of human cerebral cortex. *PLoS Biol* 6:e159.
10. Skudlarski P, et al. (2008) Measuring brain connectivity: Diffusion tensor imaging validates resting state temporal correlations. *Neuroimage* 43:554–561.

11. Honey CJ, et al. (2009) Predicting human resting-state functional connectivity from structural connectivity. *Proc Natl Acad Sci USA* 106:2035–2040.
12. Alstott J, Breakspear M, Hagmann P, Cammoun L, Sporns O (2009) Modeling the impact of lesions in the human brain. *PLOS Comput Biol* 5:e1000408.
13. Honey CJ, Sporns O (2008) Dynamical consequences of lesions in cortical networks. *Hum Brain Mapp* 29:802–809.
14. Corbetta M (2010) Functional connectivity and neurological recovery. *Dev Psychobiol*, 10.1002/dev.20507.
15. Honey CJ, Thivierge J-P, Sporns O (2010) Can structure predict function in the human brain? *Neuroimage* 52:766–776.
16. Zhang D, Raichle ME (2010) Disease and the brain's dark energy. *Nat Rev Neurol* 6(1): 15–28.
17. Compston A, Coles A (2008) Multiple sclerosis. *Lancet* 372:1502–1517.
18. Lowe MJ, et al. (2002) Multiple sclerosis: Low-frequency temporal blood oxygen level-dependent fluctuations indicate reduced functional connectivity initial results. *Radiology* 224(1):184–192.
19. Rocca MA, et al. (2010) Default-mode network dysfunction and cognitive impairment in progressive MS. *Neurology* 74:1252–1259.
20. Johnston JM, et al. (2008) Loss of resting interhemispheric functional connectivity after complete section of the corpus callosum. *J Neurosci* 28:6453–6458.
21. Roosendaal SD, et al. (2010) Resting state networks change in clinically isolated syndrome. *Brain* 133:1612–1621.
22. Valsasina P, et al. (2011) A multicentre study of motor functional connectivity changes in patients with multiple sclerosis. *Eur J Neurosci* 33:1256–1263.
23. Bonavita S, et al. (2011) Distributed changes in default-mode resting-state connectivity in multiple sclerosis. *Mult Scler* 17:411–422.
24. Chiaravalloti ND, DeLuca J (2008) Cognitive impairment in multiple sclerosis. *Lancet Neurol* 7:1139–1151.
25. Filippi M, et al. (2010) The contribution of MRI in assessing cognitive impairment in multiple sclerosis. *Neurology* 75:2121–2128.
26. Barkhof F (2002) The clinico-radiological paradox in multiple sclerosis revisited. *Curr Opin Neurol* 15:239–245.
27. Filippi M, et al. (2000) Changes in the normal appearing brain tissue and cognitive impairment in multiple sclerosis. *J Neurol Neurosurg Psychiatry* 68(2):157–161.
28. Dineen RA, et al. (2009) Disconnection as a mechanism for cognitive dysfunction in multiple sclerosis. *Brain* 132:239–249.
29. Mesaros S, et al. (2009) Corpus callosum damage and cognitive dysfunction in benign MS. *Hum Brain Mapp* 30:2656–2666.
30. Roosendaal SD, et al. (2009) Regional DTI differences in multiple sclerosis patients. *Neuroimage* 44:1397–1403.
31. Filippi M, Rocca MA (2005) MRI evidence for multiple sclerosis as a diffuse disease of the central nervous system. *J Neurol* 252(Suppl 5):v16–v24.
32. Duncan J (2010) The multiple-demand (MD) system of the primate brain: Mental programs for intelligent behaviour. *Trends Cogn Sci* 14(4):172–179.
33. Zimmermann C, Hohlfeld R (1999) "Fatigue" in multiple sclerosis (Translated from German). *Nervenarzt* 70:566–574.
34. Raichle ME (2010) Two views of brain function. *Trends Cogn Sci* 14(4):180–190.
35. Fox MD, et al. (2005) The human brain is intrinsically organized into dynamic, anti-correlated functional networks. *Proc Natl Acad Sci USA* 102:9673–9678.
36. Sestieri C, Shulman GL, Corbetta M (2010) Attention to memory and the environment: Functional specialization and dynamic competition in human posterior parietal cortex. *J Neurosci* 30:8445–8456.
37. Carter AR, et al. (2010) Resting interhemispheric functional magnetic resonance imaging connectivity predicts performance after stroke. *Ann Neurol* 67:365–375.
38. MacDonald CL, et al. (2008) Verbal memory deficit following traumatic brain injury: Assessment using advanced MRI methods. *Neurology* 71:1199–1201.
39. Greicius MD, Srivastava G, Reiss AL, Menon V (2004) Default-mode network activity distinguishes Alzheimer's disease from healthy aging: Evidence from functional MRI. *Proc Natl Acad Sci USA* 101:4637–4642.
40. Vanhaudenhuyse A, et al. (2010) Default network connectivity reflects the level of consciousness in non-communicative brain-damaged patients. *Brain* 133(Pt 1): 161–171.
41. Corbetta M, Shulman GL (2002) Control of goal-directed and stimulus-driven attention in the brain. *Nat Rev Neurosci* 3:201–215.
42. Dosenbach NU, Fair DA, Cohen AL, Schlaggar BL, Petersen SE (2008) A dual-networks architecture of top-down control. *Trends Cogn Sci* 12(3):99–105.
43. Buckner RL, Andrews-Hanna JR, Schacter DL (2008) The brain's default network: Anatomy, function, and relevance to disease. *Ann N Y Acad Sci* 1124:1–38.
44. Shulman GL, et al. (1997) Common blood flow changes across visual tasks: II. Decreases in cerebral cortex. *J Cogn Neurosci* 9:648–663.
45. Raichle ME, et al. (2001) A default mode of brain function. *Proc Natl Acad Sci USA* 98: 676–682.
46. Audoin B, et al. (2003) Compensatory cortical activation observed by fMRI during a cognitive task at the earliest stage of MS. *Hum Brain Mapp* 20(2):51–58.
47. Pantano P, et al. (2002) Cortical motor reorganization after a single clinical attack of multiple sclerosis. *Brain* 125:1607–1615.
48. Rocca MA, et al. (2005) Cortical adaptation in patients with MS: A cross-sectional functional MRI study of disease phenotypes. *Lancet Neurol* 4:618–626.
49. Loitfelder M, et al. (2011) Reorganization in cognitive networks with progression of multiple sclerosis: Insights from fMRI. *Neurology* 76:526–533.
50. Park DC, et al. (2004) Aging reduces neural specialization in ventral visual cortex. *Proc Natl Acad Sci USA* 101:13091–13095.
51. Goh JOS (2011) Functional dedifferentiation and altered connectivity in older adults: Neural accounts of cognitive aging. *Aging Dis* 2(1):30–48.
52. Deco G, Jirsa VK, McIntosh AR (2011) Emerging concepts for the dynamical organization of resting-state activity in the brain. *Nat Rev Neurosci* 12(1):43–56.
53. Smith SM, et al. (2004) Advances in functional and structural MR image analysis and implementation as FSL. *Neuroimage* 23(Suppl 1):S208–S219.
54. Smith SM, et al. (2006) Tract-based spatial statistics: Voxelwise analysis of multi-subject diffusion data. *Neuroimage* 31:1487–1505.
55. Smith SM, De Stefano N, Jenkinson M, Matthews PM (2001) Normalized accurate measurement of longitudinal brain change. *J Comput Assist Tomogr* 25:466–475.
56. Benjamini Y, Hochberg Y (1995) Controlling the false discovery rate: A practical and powerful approach to multiple testing. *J R Stat Soc B* 57:289–300.

Supporting Information

Hawellek et al. 10.1073/pnas.1110024108

SI Materials and Methods

Study Participants. Sixteen patients (13 female and 3 male, 23–46 y old, mean age: 35.3) and 16 healthy controls (13 female, 3 male, 23–49 y old, mean age: 33.6) participated in the experiments. Inclusion criteria for the patients were the diagnosis of either a clinically isolated syndrome suggestive of multiple sclerosis (MS) or definite MS (1), an Expanded Disability Status Scale (EDSS) (2) score <4 (excluding motor disabilities), and <4 y of disease duration. All patients were relapse-free and had ceased relapse-related cortisone treatment at least 3 mo before the start of the experiments. All control participants were matched to the patients individually for sex, age, and school education. Table S1 provides a list with further demographic and clinical information for all patients.

Neuropsychological Examination. All neuropsychological examinations were carefully conducted according to published guidelines, using an identical setup and procedure for each participant in a soundproofed room. Each examination began with questionnaires and self-evaluation measures: Demographic Information Questionnaire, Edinburgh Handedness Inventory (3), Modified Fatigue Impact Scale (4), and Hospital Anxiety and Depression Scale (HADS) (5). Subsequently, each participant performed a set of neuropsychological tests, probing a range of different cognitive modalities: Paced Auditory Serial Addition Test (6, 7), Symbol Digit Modalities Test (8), Trail Making Test (9), Digitspan (10), Verbal Intelligence Test "Mehrfachwortschatztest-B" (11), Controlled Oral Word Association Test with the letters B, A, S, N, and the word category "supermarket." Additionally, each participant performed on the following subtests of the test battery of attentional performance (12): alertness, covert shifts of attention, cross modal integration, flexibility and incompatibility. These tests represent reaction time-based measurements of cognitive functioning, including several classic task-paradigm components, such as spatial attention cueing, set shifting, and the Simon effect.

MRI. All scans were done on a 3T Siemens MAGNETOM Trio Scanner. Functional images were acquired using an echo planar imaging sequence in the axial plane [repetition time (TR) = 2 s, echo time (TE) = 25 ms, flip angle (FA) = 80°, voxel size = $4 \times 4 \times 4$ mm^3, matrix = 64×52, field of view = 256×208 mm^2, 36 slices for whole-brain coverage]. These resting-state runs included 606 frames corresponding to ~20 min in which the participants were told to silently fixate their view on a visually presented cross and stay awake. The following additional sequences were recorded: (*i*) T1-weighted image, using a coronal magnetization-prepared rapid gradient echo sequence (MPRAGE; TR = 2.3 s, TE = 2.98 ms, FA = 9°, inversion time (TI) = 1,100 ms, voxel size = $1 \times 1 \times 1$ mm^3); (*ii*) T2-weighted image, using a fast-spin echo sequence in the axial plane (TR = 6 s, TE = 91 ms, FA = 120°, slice thickness = 4 mm, field of view = 220 mm, 0.7×0.7 mm in-plane resolution, 25 slices); (*iii*) diffusion-weighted echo planar imaging sequence (TR = 17,200 ms, TE = 115 ms, FA= 90°, TI = 2,400 ms, b = 1,000 mm^2/s, 24 noncolinear directions, three averages, 45 slices, voxel size = $2 \times 2 \times 2$ mm^3).

Software and Visualization. If not indicated otherwise, data analyses were done in MATLAB (MathWorks) using custom-written software. The diffusion tensor parameters were displayed on mosaic slices of the atlas brain (MNI152) with the mask used for statistical analyses as a black underlay. For visualizing the fMRI results, we projected the data on the inflated surface of the Population-Average, Landmark-, and Surface-Based (PALS) atlas (13).

Behavioral Analysis. The analysis of the behavioral data was confined to a subset of 10 neuropsychological test measures, including the cognitively more challenging subpart of each test. The abbreviations used to index the test names in the figures refer to the following test metrics: Trail Making, Trail Making Test Part B; Pac. Aud. Ser. Add, Paced Auditory Serial Addition Test in the 2-s version; verbal fluency, average performance on the letters B, A, S, and N of the Controlled Oral Word Association Test; flexibility, reaction time on a set shifting task [flexibility, subtest of the Test Battery of Attentional Performance (TAP)]; alertness, reaction time on a target detection task (alertness, subtest of the TAP); Symb. Dig. Mod., Symbol Digit Modalities Test; incompatibility, reaction time in a Simon task on incompatible trials (incompatibility, subtest of the TAP); spat. att., reaction time in a Posner paradigm on invalid cue trials (covert shifts of attention, subtest of the TAP); dig. span. fwd., longest digit span forward; dig. span bwd., longest digit span backward.

Before further analysis, the raw test results were transformed into deviations from the corresponding age and education norm of each test for each participant. The behavioral parameter cognitive efficiency was then estimated as the first principle component of the test performance covariance matrix. To control for possible overfitting effects within the small data set, we made several analyses using a leave-one-out cross-validation (LOOCV) procedure (Fig. S1 *B* and *C*). Here, the principal component analysis (PCA) was repeated once for each participant. In each round, one dataset (test data set) was left out of the analysis, deriving the components' eigenvector (weights) only from the remaining data (training data set). Afterward, the left-out data were projected onto the derived weights. This procedure resulted in one estimate of the components' explained variance per participant, without the specific data of any participant directly contributing to the components' structure. Fig. S1 *B* and *C* report the average LOOCV estimates of the components' values across participants. Sensitivity and specificity were evaluated for a binary classification into patients and controls based on the level of cognitive efficiency (Fig. S1*D*). Sensitivity reflects the true positive rate (fraction of correctly identified patients), whereas specificity reflects the true negative rate (fraction of correctly identified healthy controls).

fMRI Preprocessing. The functional data were realigned within scanning runs to correct for head motion using an eight-parameter (rigid body plus in-plane stretch) cross-modal registration. Differences in the acquisition time of each slice within a frame were compensated for by sync interpolation. A whole-brain normalization factor was applied to correct for changes in signal intensity between runs (mode of 1,000). For each subject, an atlas transformation was computed on the basis of the first frame of each functional run, the T2-weighted and MPRAGE structural images to the atlas representative target using a 12-parameter general affine transformation. Functional data were interpolated to 3-mm^3 voxels in atlas space. The atlas representative MPRAGE target brain (711-2C) was produced by mutual coregistration (12-parameter affine transformations) of images obtained in six young and six older subjects. In preparation for functional connectivity analysis, data were passed through several additional preprocessing steps: (*i*) spatial smoothing (6-mm FWHM Gaussian

blur); (*ii*) temporal filtering retaining frequencies in the 0.009- to 0.08-Hz band; and (*iii*) removal of several sources of spurious variance unlikely to reflect spatially specific functional correlations through linear regression: (*a*) six parameters obtained by rigid-body correction of head motion, (*b*) the whole-brain signal averaged over a fixed region in atlas space, (*c*) the signal from a ventricular region of interest, (*d*) the signal from a region centered in the white matter ; and (*e*) the first derivatives of all regressors. These additional preprocessing steps help to separate true from spurious sources of signal variance and have been shown to result in a substantial improvement in the accessibility of functional networks in resting-state fMRI data (14, 15). All preprocessing steps were performed using in-house software. Before the actual analysis, the first five frames of the functional data were removed to allow settlement of the signal. For one control subject (C03), only the first 330 frames (11 min) of the functional data could be used for analysis due to excessive movement artifacts toward the end of the recording.

Control Analyses. To assess whether the preprocessing of the functional data or movement levels might have had confounding effects on the results, we carried out several control analyses. The removal of a global signal influences the presence of anti-correlations in the data (15) and calls into question the physiological origin of the across networks effect. We thus repeated the connectivity analysis without regression of the global signal and found all connectivity effects to still persist (correlation with cognitive efficiency, DMN connectivity: $r = -0.65$, $P = 4 \times 10^{-5}$; CN connectivity: $r = -0.66$, $P = 4 \times 10^{-5}$; across-network connectivity: $r = 0.58$, 4.9×10^{-4}). To further assess whether the removal of any of the noise regressors' variance might have had a confounding effect for our analyses, we tested whether the amount of variance that each regressor removed from the BOLD data of each participant was associated with either cognitive efficiency or the connectivity across subjects. There were no significant correlations (Pearson's r, all $P > 0.1$).

We assessed the levels of head movement during the resting-state recordings by calculating the peak-to-peak excursion (PE) and rms for each of six head-movement parameters (three translational, three rotational) (16). Before calculating the metrics, the rotational head-movement levels were transformed from degrees into the most conservative worst-case millimeter rotational movements by multiplying with 72.6 mm, the geometric mean of the maximal extents of the standard space's brain mask. The maximal movement components across the six parameters within each subject are reported here. The movement levels were 2.03 ± 1.03 mm (PE) and 0.45 ± 0.24 mm (rms) for the patients and 1.72 ± 0.92 mm (PE) and 0.47 ± 0.31 mm (rms) for the healthy controls, not significantly differing between the groups (t tests, PE: $P = 0.38$, rms: $P = 0.85$). None of the movement parameters were correlated with cognitive efficiency (all $P > 0.17$). Thus, neither the preprocessing nor differences in the levels of gross head movement had confounding effects on the results.

Modulation of Functional Connectivity. We restricted the analyses to voxels within a standard-space brain mask, which resided within 6 mm Euclidian distance of the standard-space target brain's cortical surface (13). In a first step, the global connectivity matrix of these voxels was calculated for each participant. In this matrix each entry represents the correlation of two voxels' BOLD time series. Before passing these matrices to further analysis, all values were Fisher's z-transformed. To quantify the modulation of connectivity by the level of cognitive efficiency, the group-level correlation of the connectivity strength between any two voxels with cognitive efficiency was calculated. This calculation resulted in a matrix of global connectivity modulations with each row representing the modulation profile (increases and decreases in functional connectivity) of a given voxel. We derived the raw modulation for each voxel as the sum across all columns (or rows) of this modulation matrix after statistical thresholding. All results were obtained with a threshold that corresponded to an uncorrected α-level of $P = 0.01$. Changing this threshold within reasonable ranges ($P = 0.05$ to $P = 0.001$) yielded highly similar results. We then performed permutation statistics on the raw modulation by repeating the entire procedure 100× while randomly permuting the behavioral parameter on each round. A normal distribution was fitted to these resamples to derive an empirical distribution for the null hypothesis of no connectivity modulation with cognitive efficiency. This distribution was used to derive z-scores (subtraction of mean and division by the SD) and P values.

We extracted the dominant pattern of the connectivity modulations (Fig. 4*B*) as the first principal component of all modulation profiles identified in the procedure described above. To map the actual range of connectivity that was indicated by the modulations (Fig. 4 *D–F* and Fig. S4*C*), we constructed for each participant a connectivity graph based on these PCA results. The graph contained the voxels belonging to the top 5% of negative (DMN) or positive values (CN) of the dominant modulation pattern (Fig. S4 *A* and *B*) as well as those voxels whose loadings of this pattern ranked within the top 50% of negative or positive values. Thus, the resulting graph contained four voxel groups: the two networks of the dominant spatial pattern of modulations (DMN, CN) and the two voxel clusters, which exhibited this pattern of modulation in an inverted way (Fig. 4*C*). We excluded any voxel that occurred in more than one of these groups. First, the graphs were Fisher's z-transformed, then we derived the within- and across-network connectivity as the average connectivity between the corresponding voxel groups for each participant.

1. McDonald WI, et al. (2001) Recommended diagnostic criteria for multiple sclerosis: Guidelines from the International Panel on the Diagnosis of Multiple Sclerosis. *Ann Neurol* 50(1):121–127.
2. Kurtzke JF (1983) Rating neurologic impairment in multiple sclerosis: An Expanded Disability Status Scale (EDSS). *Neurology* 33:1444–1452.
3. Oldfield RC (1971) The assessment and analysis of handedness: The Edinburgh Inventory. *Neuropsychologia* 9(1):97–113.
4. Zimmermann C, Hohlfeld R (1999) "Fatigue" in multiple sclerosis (Translated from German). *Nervenarzt* 70:566–574.
5. Snaith P, Zigmond AS (1988) Anxiety and depression in general medical settings. *BMJ* 297:1544.
6. Rao SM, Leo GJ, Haughton VM, St Aubin-Faubert P, Bernardin L (1989) Correlation of magnetic resonance imaging with neuropsychological testing in multiple sclerosis. *Neurology* 39(2 Pt 1):161–166.
7. Gronwall DM (1977) Paced auditory serial-addition task: A measure of recovery from concussion. *Percept Mot Skills* 44:367–373.
8. Parmenter BA, Weinstock-Guttman B, Garg N, Munschauer F, Benedict RHB (2007) Screening for cognitive impairment in multiple sclerosis using the Symbol Digit Modalities Test. *Mult Scler* 13(1):52–57.
9. Tombaugh TN (2004) Trail Making Test A and B: Normative data stratified by age and education. *Arch Clin Neuropsychol* 19:203–214.
10. Kaufman AS, Lichtenberger EO (2006) *Assessing Adolescent and Adult Intelligence* (Wiley, New York).
11. Lehrl S (1991) *Mehrfachwahl-Wortschatz-Intelligenztest (MWT-B)* (Straube, Erlangen, Germany), 2nd Ed.
12. Zimmermann P, Fimm B (2002) A test battery for attentional performance (Chapter 4). *Applied Neuropsychology of Attention: Theory, Diagnosis and Rehabilitation*, eds Leclercq M, Zimmermann P (Psychology Press, London), pp 110–151.
13. Van Essen DC (2005) A Population-Average, Landmark- and Surface-based (PALS) atlas of human cerebral cortex. *Neuroimage* 28:635–662.
14. Fox MD, et al. (2005) The human brain is intrinsically organized into dynamic, anticorrelated functional networks. *Proc Natl Acad Sci USA* 102:9673–9678.
15. Fox MD, Zhang D, Snyder AZ, Raichle ME (2009) The global signal and observed anticorrelated resting state brain networks. *J Neurophysiol* 101:3270–3283.
16. Thomason ME, Glover GH (2008) Controlled inspiration depth reduces variance in breath-holding-induced BOLD signal. *Neuroimage* 39:206–214.

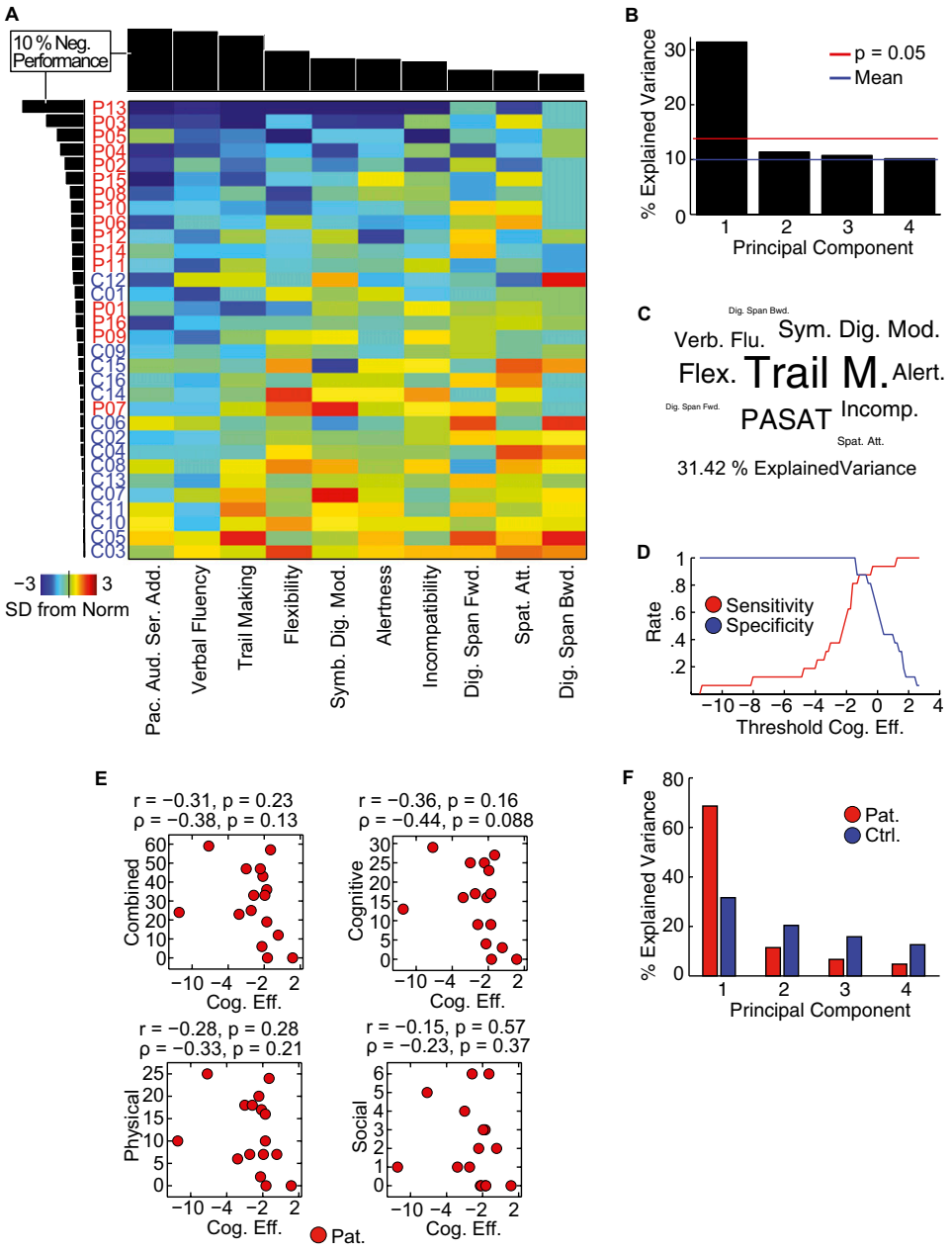

Fig. S1. (*A*) Performance matrix as shown in Fig. 1*A* for the combined patient and control dataset. (*B*) Average explained variance of the first four principal components of the combined patient and control dataset, using a LOOCV procedure (*SI Materials and Methods*). The blue line indicates the average percent explained variance of Gaussian noise weightings, obtained by projecting the data onto random eigenvectors with unit length 1,000×. The red line corresponds to the 95th percentile of this distribution. Crossing this line indicates the component's explained variance to be significantly different from Gaussian noise at an α-level of $P = 0.05$. These results suggest that only the first behavioral component contains meaningful predictive power for further analyses ($P < 10^{-16}$). (*C*) Test name size scaled by the loading of the first principle component derived from the combined dataset using a LOOCV procedure. These loadings correspond to the first component shown in *C* (cf. Fig. 1*B*). Spatial test name positions are arbitrary. (*D*) Sensitivity and specificity for a binary classification between patients and controls based on cognitive efficiency. (*E*) The relation of the level of cognitive efficiency to fatigue. Each scatter plot shows the correlation of cognitive efficiency with a subscale of the Modified Fatigue Impact Scale. (*Left* to *Right*) All subscales combined, cognitive subscale, physical subscale, and social subscale. The results of correlation analysis using Pearson's *r* as well as Spearman's ρ are given above the panels. (*F*) Explained variance of the first four principal components calculated for each study group separately. The control group exhibited a richer pattern of behavioral variability, which led to a wider distribution of components.

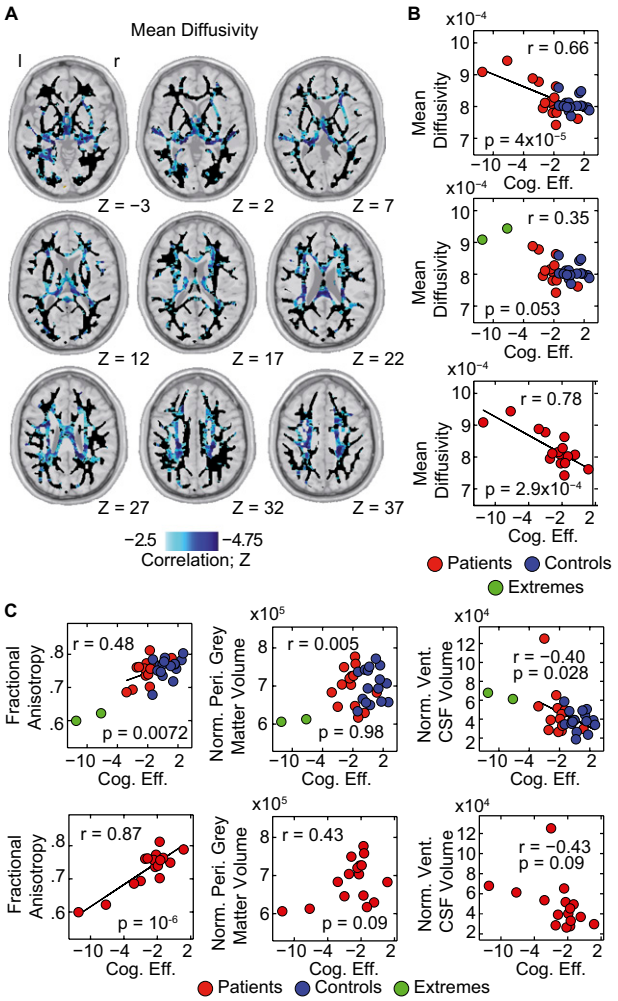

Fig. S2. (*A*) Correlation of cognitive efficiency with voxel-wise mean diffusivity. The analysis was performed within a standard-space white matter mask shown as a black underlay. Correlations are shown as corresponding z-scores and have been thresholded at a false discovery rate-corrected α-level of $P = 0.05$. No positive correlations passing this threshold were observed. (*B*) The relation of the average mean diffusivity within a corpus callosum mask to the level of cognitive efficiency for different compositions of the study participants. (*Top*) All participants; (*Middle*) excluding the two most extreme patients; (*Bottom*) patients only. (*C*) Corresponding figures to *B* for the three anatomical parameters shown in Fig. 2.

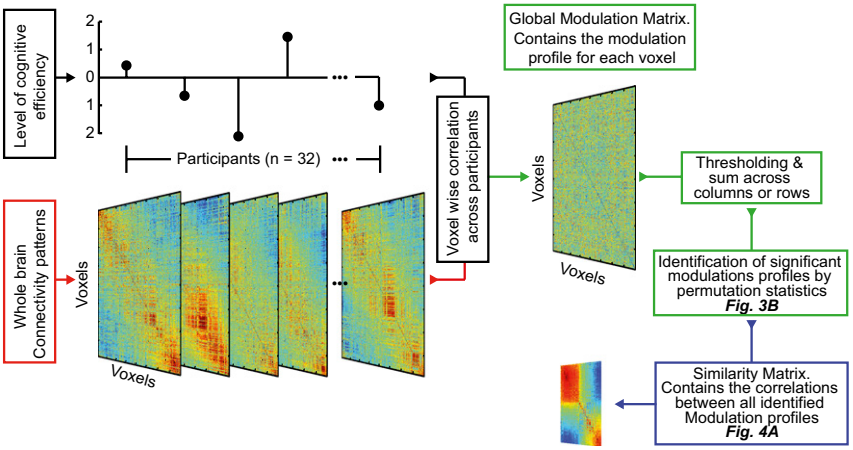

Fig. S3. Schematic depiction of the analysis stream. The colored frames correspond to the three levels of analysis shown in Fig. 3*A*. For each participant, we calculated a whole-brain connectivity graph in a first step. Each entry in this matrix represents the correlation (Pearson's *r*) of two voxels' BOLD time series. To quantify the change of connectivity between two voxels across participants, we calculated the correlation between the connectivity of each voxel pair and the level of cognitive efficiency, which resulted in the global connectivity modulation matrix. The amount of connectivity modulation for each voxel was subsequently calculated as the sum across all columns (or rows) after thresholding. We derived z-scores and *P* values by subtracting the mean and dividing by the SD of an empirical null hypothesis distribution of connectivity modulations at each voxel. This distribution was obtained by randomly permuting the behavioral parameter and repeating the analysis 100×. Based on these results, we constructed the similarity matrix, containing the correlations between all identified modulation profiles.

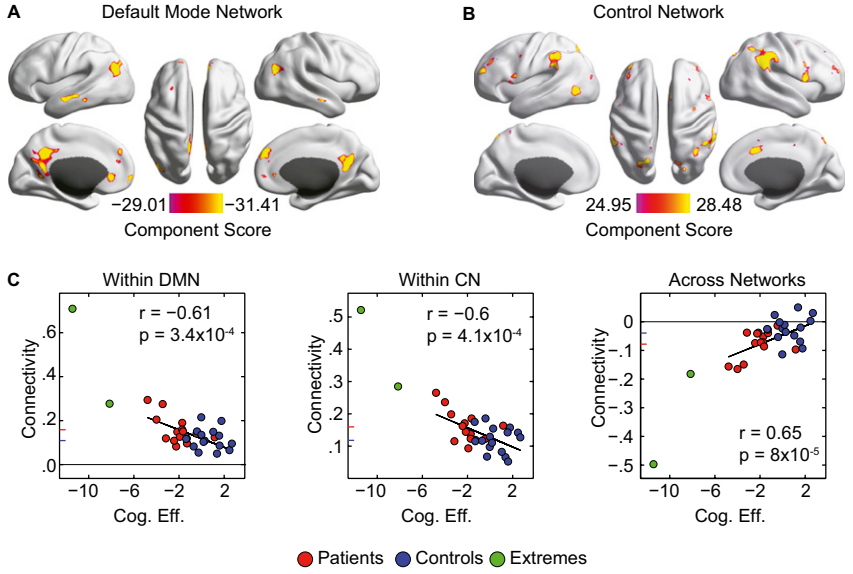

Fig. S4. (*A*) The top 5% of negative values of the dominant spatial pattern of connectivity modulations (shown in Fig. 4*B*). These voxels were used to derive the connectivity to the default mode network. (*B*) The top 5% of positive values of the dominant spatial pattern of connectivity modulations. These voxels were used to derive the connectivity to the control network. (*C*) Relation of the identified connectivity to cognitive efficiency effects when omitting the two most extreme cases of the patient group. The correlation of connectivity with behavior is given in the corresponding panels. The group means of the connectivity are indicated as colored bars at the ordinate. All connectivity measures significantly differed between the groups (*t* test, DMN: $P = 0.028$, CN: $P = 0.012$, across networks: $P = 0.018$).

Table S1. Clinical and demographic information of all patients

Patient no.	Age	Sex	School education, y	Diagnosis	Disease duration, y/mo	EDSS	Medication	HADS depression status	HADS anxiety status
P01	23	Female	10	RRMS	1.75/21	0	Copaxone	Normal	Normal
P02	30	Female	13	CIS	0.5/6	2	—	Normal	Positive
P03	34	Male	10	MS	1.25/15	0	—	Normal	Normal
P04	41	Female	10	RRMS	1.83/22	3	—	Normal	Ambiguous
P05	36	Male	10	RRMS	1.5/18	1.5	—	Normal	Ambiguous
P06	29	Female	10	RRMS	3/36	2	Copaxone	Normal	Normal
P07	45	Female	13	RRMS	2.08/25	2	—	Normal	Normal
P08	36	Female	12	RRMS	2.67/32	1	Copaxone	Normal	Normal
P09	36	Female	13	RRMS	2.17/26	3	Rebif	Normal	Ambiguous
P10	25	Female	10	RRMS	2.33/28	0	Mitoxanthrone	Ambiguous	Positive
P11	39	Female	10	RRMS	3.66/44	2	Copaxone	Normal	Positive
P12	46	Female	12	CIS	2.17/26	2	Copaxone	Normal	Normal
P13	41	Male	10	RRMS	1.16/14	2.5	Avonex	Ambiguous	Normal
P14	43	Female	13	RRMS	1.75/21	3.5	—	Normal	Normal
P15	29	Female	12	MS	3.66/44	0	—	Normal	Normal
P16	32	Female	13	RRMS	1.75/21	0	—	Normal	Ambiguous
Mean	35.3		11.31		2.03/24.93	1.53			
Median	36		11		1.95/23.5	2			
SD	6.9		1.40		0.86/10.29	1.21			

CIS, clinically isolated syndrome; RRMS, relapsing-remitting MS.

Table S2. Average coordinates of the 10 largest clusters exhibiting significant ($P < 0.05$, false discovery rate-corrected) modulation

Cluster size, voxels	Anatomical label	*X*	*Y*	*Z*
53	BA 23	5.83	−53.97	16.44
50	BA 39	−44.1	−70.68	18.72
37	BA 10	−3.4	60.2	0.12
21	BA 39	40.28	−67.5	19.92
18	BA 39	50	−63.83	9.66
18	BA 10	−27.16	57.66	−1
14	BA 40	51.21	−44.57	30.64
13	BA 31	−10.84	−44.88	27.11
13	BA 24	−3.46	29.19	6.8
12	BA 45	38.25	27.75	5.5

Data from Fig. 3*B*.

nature neuroscience

Large-scale cortical correlation structure of spontaneous oscillatory activity

Joerg F Hipp[1,2], David J Hawellek[1], Maurizio Corbetta[3], Markus Siegel[2] & Andreas K Engel[1]

Little is known about the brain-wide correlation of electrophysiological signals. We found that spontaneous oscillatory neuronal activity exhibited frequency-specific spatial correlation structure in the human brain. We developed an analysis approach that discounts spurious correlation of signal power caused by the limited spatial resolution of electrophysiological measures. We applied this approach to source estimates of spontaneous neuronal activity reconstructed from magnetoencephalography. Overall, correlation of power across cortical regions was strongest in the alpha to beta frequency range (8–32 Hz) and correlation patterns depended on the underlying oscillation frequency. Global hubs resided in the medial temporal lobe in the theta frequency range (4–6 Hz), in lateral parietal areas in the alpha to beta frequency range (8–23 Hz) and in sensorimotor areas for higher frequencies (32–45 Hz). Our data suggest that interactions in various large-scale cortical networks may be reflected in frequency-specific power envelope correlations.

As a measure of functional connectivity, the co-variation of spontaneous hemodynamic signals has revealed fundamental insights into the large-scale functional organization of the human brain[1,2]. Blood oxygen level–dependent functional magnetic resonance imaging (BOLD fMRI) has provided consistent evidence for correlated fluctuations of spontaneous neuronal activity in highly structured networks of brain regions[3–9]. The gross spatial correlation structure that constitutes these networks is highly robust and often studied during resting fixation. Furthermore, the correlation structure also reflects task demands[8,10], the subjects' conscious state[11], and psychiatric and neurological disorders[12,13].

However, an important limitation of the available fMRI studies is that hemodynamic signals only provide an indirect measure of neuronal activity[14–16]. In contrast, electroencephalography (EEG) and magnetoencephalography (MEG) directly measure the electrophysiological activity of interest. Furthermore, with their high temporal resolution, these electrophysiological measures sample the rich temporal dynamics of neuronal population activity. These temporal dynamics entail neuronal oscillations that, with their specific frequencies, reflect the biophysical properties of different local and large-scale network interactions[17–19]. Thus, connectivity measures based on specific spectral components of neuronal population activity may provide qualitatively new insights into the circuit mechanisms underlying the large-scale organization of brain activity[19]. However, little is known about the brain-wide correlation of such frequency-specific neuronal population signals. To characterize the brain-wide correlation structure of oscillatory power, we developed a new analysis approach for investigating large-scale functional connectivity that overcomes current methodological limitations in EEG and MEG. We applied this approach to MEG recordings of healthy human subjects during resting fixation.

RESULTS

We recorded MEG from 43 subjects that were instructed to fixate a centrally presented cross (average duration, ~500 s). We applied time-frequency transformation and linear 'beamforming' to the MEG data to derive temporally, spectrally and spatially resolved estimates of neuronal population activity. The temporal evolution of spectral power (power envelope) in different brain regions around a given carrier frequency served as the signal for our correlation analysis[20] (**Fig. 1a**). Notably, the correlation between power envelopes that we investigated should not be confused with measures of the phase relation between the underlying signals, such as coherence[19,21–23].

It is difficult to investigate the relationship between neuronal population signals from EEG and MEG because of notable methodological problems[19,23–25]. As a result of the limited spatial resolution of EEG and MEG, even distant sensors or source estimates can be sensitive to the same neuronal sources. In source space, this translates into a trivial spatial interaction pattern that drops off with distance from any reference location. **Figure 1b** illustrates this problem for the power envelope correlation between a reference location in the left somatosensory cortex and the rest of the brain. The spatial correlation pattern is dominated by an unstructured decay from the reference site that is caused by the fact that source estimates close to the reference location are sensitive to the same true sources as the reference estimate. This spurious correlation pattern is problematic, as it masks the physiological correlation structures of interest. To overcome this problem, we developed a new analysis approach for studying functional connectivity based on power envelope correlations.

Power envelope correlation between orthogonalized signals

Electrical and magnetic neuronal signals are measured virtually instantaneously at different sensors. Thus, signal components that reflect the

[1]Department of Neurophysiology and Pathophysiology, University Medical Center Hamburg-Eppendorf, Hamburg, Germany. [2]Centre for Integrative Neuroscience, University of Tübingen, Tübingen, Germany. [3]Departments of Neurology, Radiology, Anatomy, and Neurobiology, Washington University School of Medicine, St. Louis, Missouri. Correspondence should be addressed to J.F.H. (joerg.hipp@cin.uni-tuebingen.de).

Received 13 February; accepted 4 April; published online 6 May 2012; doi:10.1038/nn.3101

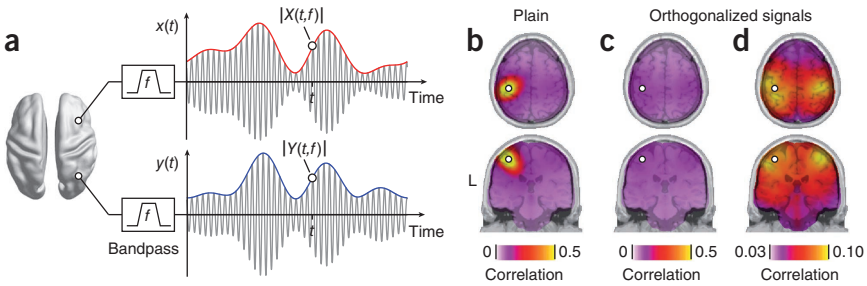

Figure 1 Power envelope correlation. (**a**) Illustration of spectrally resolved power envelopes for one exemplary carrier frequency *f* (that is, center frequency of the bandpass filter). The gray sinusoidal lines represent bandpass-filtered neuronal signals estimated at two source locations. The corresponding blue and red lines, the amplitude envelopes, quantify the evolution of the signal amplitude at a slower timescale. We used the logarithm of the squared amplitude envelopes (power envelopes) for correlation analyses. (**b**) Plain power envelope correlation between the left somatosensory cortex (white circle) and the rest of the brain at a carrier frequency of 16 Hz. The correlation values are overlaid on cortical slices intersecting the seed location. L, left. (**c**) Power envelope correlation between orthogonalized signals from the left somatosensory cortex (white circle) and the rest of the brain at a carrier frequency of 16 Hz. Note that the color scale is identical to that used in **b**. (**d**) Data are presented as in **c**, but scaled to the minimal and maximal correlation value that occurs.

same source at two different sensors (or source estimates) are characterized by an identical phase[24]. In contrast, for many cases, signals from different neuronal populations can be thought of as having a variable phase relation. We exploited this difference to discount the spurious correlation pattern caused by the limited spatial resolution of MEG. For each pair of signals, time window and carrier frequency, we removed the signal components that shared the same phase before computing the signals' power estimates. In other words, we orthogonalized the signals before deriving their power envelopes. As a measure of interaction, we then computed the linear correlation between these power envelopes. This procedure ensures that the signals do not share the trivial correlation in power resulting from the methodological problems described above (see Online Methods, **Supplementary Data** and **Supplementary Figs. 1** and **2**). Applying this approach to the above example had a strong effect. The pattern that dominated the plain correlation vanished, which revealed residual correlation of much smaller magnitude (**Fig. 1c**). This residual spatial correlation pattern was highly structured and extended to distant cortical areas (**Fig. 1d**). Correlation was strongest to the vicinity of the reference and to the homologous somatosensory cortex in the other hemisphere.

We next derived the correlation between all 2,925 locations on a regular three-dimensional grid covering the entire brain. The average correlation was significantly higher than zero for all carrier frequencies from 2 to 128 Hz (*t* test, $P < 0.05$, false discovery rate (FDR) corrected). The average correlation was strongest in the alpha to beta frequency range ($r = 0.069 \pm 0.060$, mean ± s.d. at 16 Hz) with about 90% of positive correlations. To identify spatial structure in the correlation, we statistically tested for correlation higher than the average correlation across the brain. As a starting point, we followed up on the introductory example and analyzed interhemispheric correlation between homologous early sensory areas across different modalities.

Interhemispheric correlation of homologous sensory areas

A fundamental property of human brain anatomy is that most homologous areas in the two hemispheres are anatomically connected. Accordingly, fMRI studies[1,26], intracranial recordings[27] and MEG studies[28,29] have found that homologous sensory areas exhibit correlated spontaneous activity. Consequently, we expected to find a related pattern for power envelope correlations using our new analysis approach.

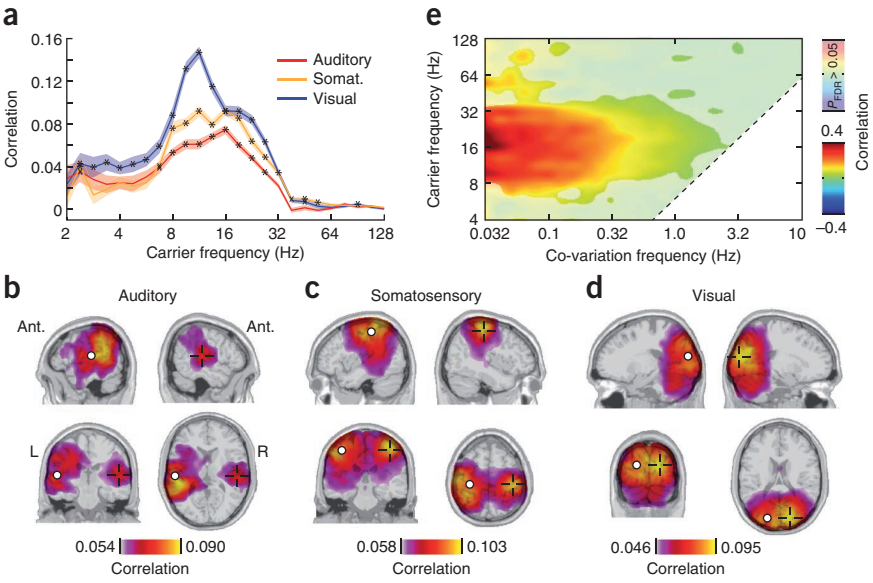

Figure 2 Power envelope correlations between orthogonalized spontaneous signals from homologous early sensory areas. (**a**) Correlation between the auditory cortices (red), the somatosensory cortices (Somat.) (yellow) and the visual cortices (blue) resolved for carrier frequency. Colored bands indicate the s.e.m. across subjects. Spatial specificity is tested by comparison to the average correlation with the rest of the brain (one-tailed *t* test, $^{X}P < 0.05$, $^{*}P < 0.01$; see **Supplementary Fig. 3a**,**b** for a control analyses with different spectral smoothing). (**b**–**d**) Spatial distribution of the correlation between the left auditory (**b**), somatosensory (**c**) and visual (**d**) cortices and the rest of the brain. Correlation values are statistically masked (one-tailed *t* test for correlation > average correlation with the rest of the brain, $P < 0.05$, FDR corrected for number of voxel). White circles indicate the location of the reference site and the crosses indicate the mirrored location in the other hemisphere. Ant., anterior; L, left; R, right. (**e**) Correlation between homologous sensory areas as a function of the carrier frequency and the co-variation frequency (center frequency of the bandpass applied to the power envelopes before computing correlation on the second level). Note that the highest co-variation frequency is limited by the underlying carrier frequency (diagonal dashed line). The values are averaged across sensory modalities and subjects and are statistically masked (one-tailed *t* test for correlation > average correlation to the rest of the brain, $P < 0.05$, FDR corrected for the number of carrier and co-variation frequencies; see **Supplementary Fig. 3c,d** for control analyses with different spectral parameters).

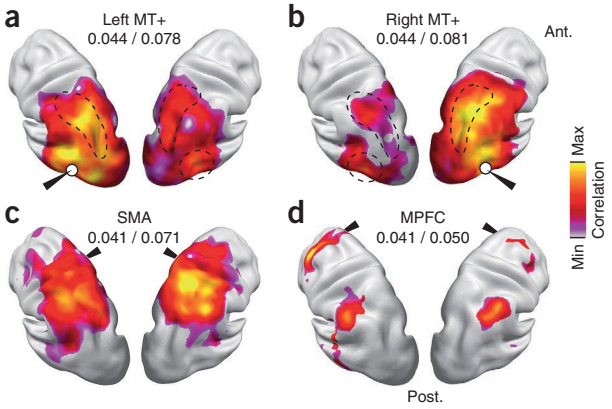

Figure 3 Correlation maps for selected locations at a carrier frequency of 16 Hz. Correlation maps are statistically masked (voxel-wise one-sided *t* test for correlation > average correlation to the rest of the brain, $P < 0.05$, FDR corrected for the number of voxels). The white circles indicate the approximate location of the seeds. The values underneath the seed labels indicate the minimal (min) and maximal (max) correlation in the statistical mask. (**a**,**b**) Left and right MT+. The homologous area in the other hemisphere and the intraparietal sulci are depicted by dashed lines. (**c**) SMA. (**d**) MPFC. Post., posterior.

We focused on bilateral early auditory, visual and somatosensory cortices and investigated a broad range of different carrier frequencies (**Fig. 2a**). In all three sensory systems, we found the strongest correlation in the alpha to beta carrier frequency range (8–32 Hz). The analysis of the brain-wide correlation at 16 Hz, the center of this frequency range, revealed that the correlation between homologous sensory cortices was spatially specific (one-sided *t* test for correlation > average correlation, $P < 0.05$, FDR corrected; **Fig. 2b–d**). The strongest correlations were expressed to areas in direct proximity of the reference locations and to the homologous cortex in the contralateral hemisphere.

We spectrally resolved the power envelope correlation (co-variation frequency; **Fig. 2e**) to assess its temporal scale. The correlation between homologous areas was significantly increased in a broad, low co-variation frequency range from 0.032 Hz (the lowest frequency analyzed) to above 1 Hz (one-sided *t* test for correlation > average correlation, $P < 0.05$, FDR corrected). Thus, modulation of signal power on the timescale of several seconds drove the correlation of spontaneous activity between sensory areas. These findings were insensitive to specific parameters of spectral analyses. We varied the spectral smoothing of the carrier and the co-variation frequencies and obtained similar results (**Supplementary Fig. 3**). In summary, our analysis approach revealed that spontaneous oscillatory population activity in different homologous early sensory cortices was correlated on a slow timescale in a spatially and spectrally specific manner.

Spatially specific correlation of higher order cortices

We next extended our analysis beyond early sensory regions and investigated how functional relations of higher order cortices are reflected in power correlations. We characterized correlation maps of a higher visual area, a higher sensory-motor area and a prefrontal associative area for a 16-Hz carrier frequency. The middle temporal area (MT+) is part of the dorsal visual pathway. Indeed, correlation with left and right MT+ peaked in the homologous area in the contralateral hemisphere and in the dorsal visual pathway along the intraparietal sulcus (one-sided *t* test for correlation > average correlation, $P < 0.05$, FDR corrected; **Fig. 3a**,**b**). Correlation with the supplementary motor area (SMA), which is part of the sensory-motor cortex involved in planning of movements, peaked in frontal regions that are compatible with the frontal eye fields and other regions in the parietal cortex (one-sided *t* test for correlation > average correlation, $P < 0.05$, FDR corrected; **Fig. 3c**). Also the medial prefrontal cortex (MPFC), a higher order associative area, exhibited spatially well-confined and symmetric correlation patterns (one-sided *t* test for correlation > average correlation, $P < 0.05$, FDR corrected; **Fig. 3d**). Correlation with MPFC peaked in bilateral dorsal prefrontal cortex (DPFC) and bilateral lateral parietal cortex (LPC).

The differences between the correlation patterns of these reference sites indicate that power envelope correlations can reveal distinct functional networks. However, the different correlation patterns also shared similar features. In particular, most reference sites showed a high correlation with parietal areas. This raised the question of whether specific areas such as the parietal cortex might have a particularly prominent role in the global patterning of power envelope correlations. We studied the correlation of power envelopes across the full cortico-cortical space to address this question.

Global correlation structure

We derived the full connectivity matrix between 2,925 sources (nodes) that covered the brain in a regular three-dimensional grid. We defined

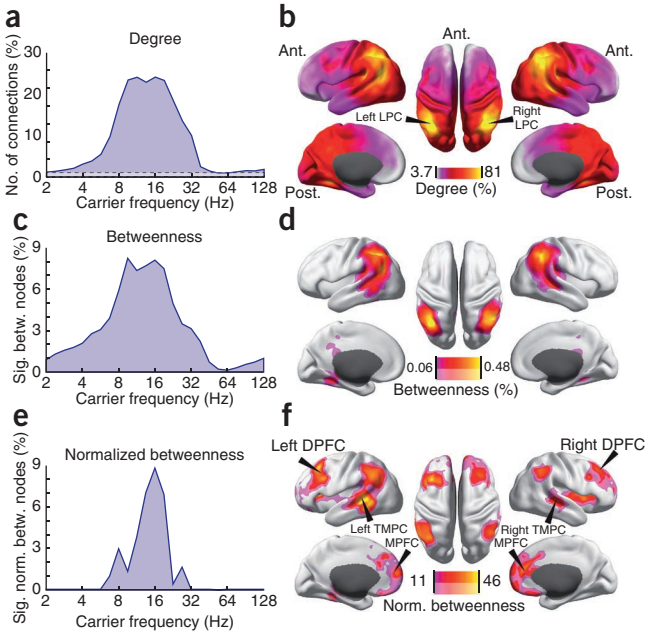

Figure 4 Graph-theoretical analysis of the global correlation structure of band-limited neuronal signals. (**a**) Spectrally resolved degree. The dashed line indicates the significance threshold (1.01%, $P = 0.05$, corrected for the number of nodes). (**b**) Degree at a carrier frequency of 16 Hz resolved in cortical space (LPC). The color scale is adjusted to the maximal and minimal degree that occurred. (**c**) Spectrally resolved number of nodes with significantly increased betweenness compared with the average betweenness value (voxel-wise permutation test for betweenness > average betweenness, corrected for the number of nodes, $P < 0.05$). (**d**) Betweenness at a carrier frequency of 16 Hz resolved in cortical space. Betweenness is statistically masked at two levels (permutation test, corrected for the number of nodes, $P < 0.05$, saturated color scale; permutation test, $P < 0.05$, uncorrected, desaturated color scale). The color scale is adjusted to the maximal and minimal betweenness in the statistical mask. (**e**) Spectrally resolved number of normalized betweenness nodes defined analogously to **c**. (**f**) Normalized betweenness at a carrier frequency of 16 Hz resolved in cortical space analogously to **d**.

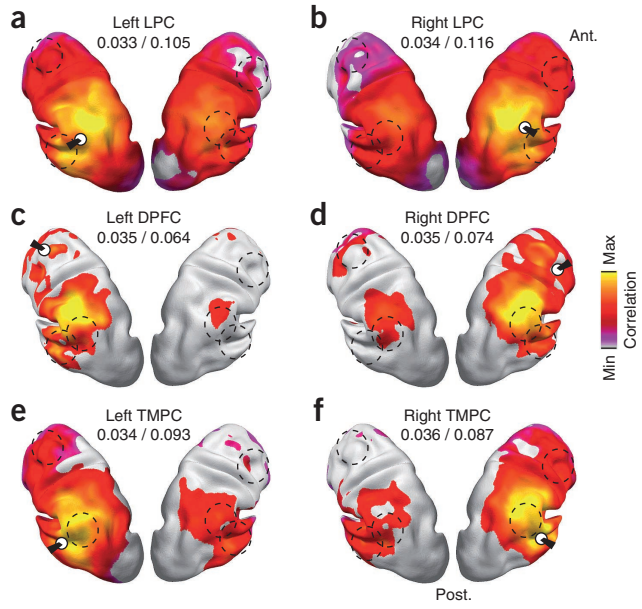

Figure 5 Correlation maps for identified hubs at a carrier frequency of 16 Hz. Correlation maps are statistically masked (voxel-wise one-sided *t* test for correlation > average correlation to the rest of the brain, $P < 0.05$, FDR corrected for the number of voxels). The white circles indicate the approximate location of the hub that was used as reference for the correlation analysis. The dashed lines indicate the locations of the other hubs. The values underneath the seed labels indicate the minimal and maximal correlation in the statistical mask. (**a**,**b**) Left and right LPC. (**c**,**d**) Left and right DPFC. (**e**,**f**) Left and right TMPC.

a connection if the correlation between the orthogonalized signals of two sources was significantly higher than the average correlation of these sources to the rest of the brain (one-sided *t* test, $P < 0.01$). We used graph-theoretical measures to quantify basic properties of the connectivity matrix[30]. The number of connections (termed degree) was highest for the alpha and beta carrier-frequency range (8–32 Hz), where it reached ~25% of all possible connections (**Fig. 4a**). The spatial distribution of the degree for this carrier-frequency range was characterized by a global anterior-to-posterior increase (**Fig. 4b**). Besides this strong gradient, the degree distribution peaked prominently in bilateral LPC with connections to ~85% of all sources (MNI coordinates: left, [−39, −54, 32]; right, [46, −45, 39]).

The prominent role of LPC was further supported by its high level of betweenness. Betweenness quantifies the number of all possible shortest paths in a network a given node participates in. It therefore complements degree as a measure that quantifies a node's importance for mediating connectivity between other nodes, that is, it's 'hubness'. For carrier frequencies in the alpha to beta frequency range (8–32 Hz), the number of significant betweenness nodes (permutation test, $P < 0.05$, corrected) and the spatial betweenness distribution qualitatively resembled the degree (**Fig. 4c**,**d**), with prominent maxima in bilateral LPC.

High degree favors high betweenness. Nodes with many connections are more likely to support the shortest paths between many other nodes. To account for this bias, we computed normalized betweenness, that is, the betweenness corrected for betweenness that occurs in random networks with the same degree. The number of voxels with significant normalized betweenness peaked sharply at 16 Hz (permutation test, $P < 0.05$, corrected; **Fig. 4e**). In addition to LPC, this procedure exposed hubs in medial and bilateral dorsal prefrontal cortex (MNI coordinates: MPFC, [10, 60, 10]; left DPFC, [−40, 30, 50]; right DPFC, [30, 20, 30]) and bilateral temporal cortex (TMPC; MNI coordinates: left, [−50, −40, −10]; right, [60, −20, 0]; **Fig. 4f**).

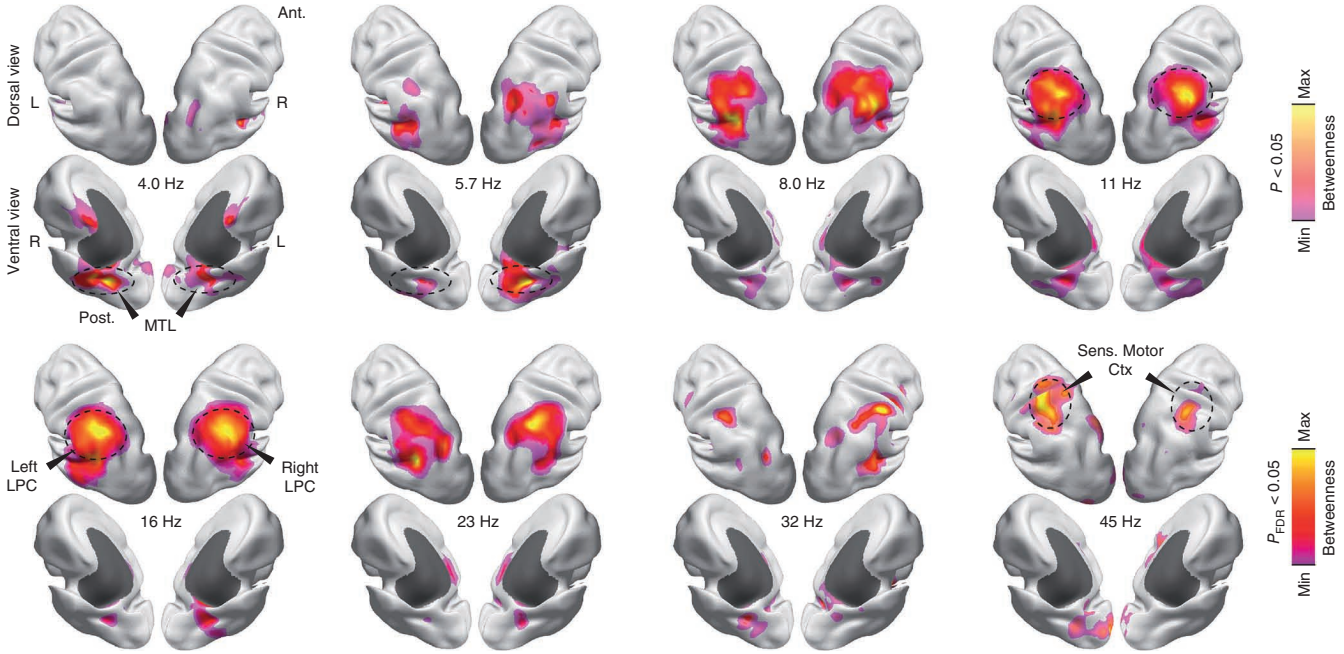

Figure 6 Spatial patterning of betweenness as a function of the carrier frequency. Betweenness values are statistically masked (voxel-wise permutation test for betweenness > average betweenness, corrected for number of nodes, $P < 0.05$, saturated color scale; $P < 0.05$, uncorrected, desaturated color scale). The color scale is adjusted to the minimal and maximal values in the statistical mask. Subcortical areas are masked dark gray (see **Supplementary Fig. 4** for complementary analysis of degree). Sens., sensory; Ctx, cortex.

The pattern of connectivity at 16 Hz differed between the LPC, MPFC, DPFC and TMPC. The high degree of bilateral LPC was driven by a widespread correlation with large parts of the brain (*t* test for correlation > average correlation, $P < 0.05$, FDR corrected; **Fig. 5a**,**b**). The correlation was strongest to the vicinity of the LPC and to the LPC in the other hemisphere. In contrast, the hubs in bilateral MPFC, DPFC and TMPC were characterized by sparser connectivity (**Figs. 3d** and **5c**–**f**). Notably, most of the hub sites showed mutual peaks in the spatial correlation patterns. Thus, the LPC, MPFC, DPFC and TMPC were not diffusely connected, but formed an interconnected network.

Global correlation structure varies with carrier frequency

The above analyses focused on a carrier frequency of 16 Hz. To investigate whether the global correlation structure varies across carrier frequencies, we performed a two-way analysis of variance of the carrier frequency–dependent connectivity (4–45 Hz) with the factors carrier frequency and cortical location. Indeed, degree and betweenness showed significant main and interaction effects (degree: main effect carrier frequency, $F_7 = 4.88 \times 10^4$, $P = 0$; main effect location, $F_{2924} = 102$, $P = 0$; interaction, $F_{7,2924} = 9.88$, $P = 0$; betweenness: main effect carrier frequency, $F_7 = 203$, $P = 5.15 \times 10^{-302}$; main effect location, $F_{2924} = 8.29$, $P = 0$; interaction, $F_{7,2924} = 1.12$, $P = 8.01 \times 10^{-31}$). Thus, degree and betweenness were not only spatially inhomogeneous, but the spatial patterning of connectivity also depended on the underlying carrier frequency.

The frequency-dependent degree revealed three prominent patterns of connectivity (**Fig. 6**). In the theta range (4–6 Hz), we found the highest degree in the medial temporal lobe (MTL, MNI coordinates, left, [−20, −40, −10]; right, [40, −40, 0]). Consistent with the above results, for frequencies in the alpha to beta frequency range (8–23 Hz), LPC showed the highest degree. In the low gamma frequency range (32–45 Hz), we found the highest degree in sensorimotor cortex (MNI coordinates, left, [−40, −40, 60]; right, [40, −30, 50]). These results were consistent with the patterns that we found for the frequency-dependent betweenness (**Supplementary Fig. 4**). In summary, the graph-theoretical analysis of global connectivity revealed spatially symmetric connectivity structure and localized hubs that depended on the underlying carrier frequency.

DISCUSSION

Here we introduce a new analysis approach for characterizing brain-wide functional connectivity based on power envelope correlation that overcomes limitations resulting from the limited spatial resolution of electrophysiological measures. Applying this approach to MEG, we provide a spectrally resolved characterization of the global organization of spontaneous electrophysiological signals in the human brain. The correlation of band-limited neuronal population activity showed prominent hubs that were largely symmetric across hemispheres and depended on the underlying carrier frequency.

Power envelope correlations between orthogonalized signals

Central for our findings was the new analysis approach for estimating power envelope correlations on the basis of orthogonalized signals. We applied this approach to MEG source estimates of spontaneous activity fluctuations of the resting human brain. However, because the underlying physical principles hold for both magnetic and electric fields, this approach should be similarly powerful for the analysis of EEG data. Furthermore, our approach is not limited to the analysis of spontaneous activity, but may also provide new insights into task-related functional connectivity. In general, the approach can be applied to any set of simultaneous electrophysiological signals to derive an index for functional connectivity, which may be relevant for biomedical applications.

The combination of EEG or MEG with our analysis approach complements electrocorticogram (ECoG) recordings, which have a higher spatial resolution and signal-to-noise ratio, but are limited to a few focal sites and studies of the diseased brain[27,31,32]. In fact, our analysis approach may also help in the investigation of correlations between signals from nearby ECoG or microelectrode recordings that may also be affected by spurious correlations resulting from limited spatial resolution.

The applied analysis approach can provide a full connectivity matrix, which allows for studying brain-wide correlation using graph-theoretical methods. It is straightforward to apply this analysis approach to contrasting groups of subjects or experimental conditions. The orthogonalization approach may also be combined with multivariate methods such as independent component analysis (ICA) to identify networks of areas with correlated power envelopes[29]. Furthermore, nonlinear or directed measures of interaction may also be applied to the power envelopes of orthogonalized signals.

The global correlation depends on the carrier frequency

We found that the global correlation of spontaneous activity peaked for carrier frequencies in the alpha to beta range with prominent hubs in the LPC and secondary hubs in PFC and TMPC. These hubs resemble the hub structures reported for spontaneous hemodynamic signals[8]. We found that all of these hubs were not diffusely connected, but were strongly correlated with each other as a global network. This network structure is compatible with the spatial pattern extracted from spontaneous MEG power fluctuations in the alpha to beta band using ICA[29]. The identified network overlaps with two networks in the correlation of hemodynamic signals: the default mode network[2,3,33], which comprises areas typically deactivated during tasks, and the control network[5,7], which has been implicated in executive functions. Besides this global structure, for the same alpha to beta carrier-frequency range, our analysis revealed spatially distinct correlations between functionally related sensory and associative cortices. These results substantiate converging evidence from MEG[28,29,34–36] and EEG[37–39] of the resting brain that suggest a prominent correlation of oscillatory power in particular in the alpha to beta frequency range. Thus, correlation of alpha to beta activity may be a generic signature of intrinsic neuronal interactions.

In addition to the prominent effects in the alpha to beta band, we found spatially specific correlation structure of spontaneous activity for a wide range of carrier frequencies from the theta to the gamma band (4–45 Hz). In the theta frequency range (4–6 Hz), the MTL constituted a global hub. Theta-band oscillations are a prominent feature of neuronal dynamics in the MTL. They seem to be tightly related to memory processes and are phase-coupled to neuronal activity in other cortical regions[40–42]. In addition, studies of fMRI connectivity have identified mnemonic networks that involve the MTL[4,6]. Consistent with these findings, our results suggest that the MTL is central to the brain-wide co-variation of spontaneous theta-band activity.

Timescale of power envelope correlations

Consistent with other MEG[28,35,36] and intracranial recordings[27,43], we found that correlations of oscillatory power were driven by slow co-variations in a broad frequency range below 0.1 Hz. Similarly, hemodynamic correlations are dominated by frequencies below 0.1 Hz[26]. These slow co-fluctuations may arise from intrinsic cortical dynamics[44] and subcortical or neuromodulatory inputs[18,19,43,45]. The slow timescale of power envelope correlations contrasts with the

millisecond timescale of neuronal signaling itself. Power envelope correlations likely reflect the consequence of signaling rather than acting as a mechanism that controls the signaling on a fast timescale.

Relation to local neuronal activity

In the raw EEG or MEG of awake humans, alpha and beta oscillations are the most prominent rhythms. One could speculate that the strong correlations in the alpha and beta frequency range simply reflect the better signal-to-noise ratio of these prominent local signals. However, differences in the spatial characteristics argue against this explanation. Local alpha and beta oscillations appear to be widespread across occipital, parietal and central areas (**Supplementary Fig. 5**). This pattern differs substantially from the global hub structure that we identified in this frequency range based on power envelope correlations (**Fig. 6**). In addition, for other frequencies, the hub structure differs substantially from the spatial distribution of local signal power. Thus, the strength of local oscillatory processes and their brain-wide spatial correlation are dissociated. Consequently, the correlation of signal power may provide complementary information to local signal power that could be exploited in future applications.

Relation to fMRI

EEG and MEG allow for separating neuronal activity into oscillatory components that reflect the biophysical properties of different local and large-scale network processes[17–19]. In contrast, fMRI provides a compound measure of the joint metabolic cost of different network processes and of non-neuronal processes[14–16,18]. This compound nature of the hemodynamic signal is reflected in its correlation with oscillatory neuronal activity across a broad range of frequencies during stimulation[46–48] and at rest[37–39,45,49]. Thus, the correlation structure of electrophysiological and hemodynamic signals should share similarities. Indeed, the patterning and the timescale of electrophysiological signal correlation that we found showed substantial similarities with fMRI connectivity (see above).

However, despite these similarities, the spatial structure of power envelope correlations also exhibited differences to hemodynamic correlation. In particular, hemodynamic correlation is characterized by prominent hubs in the posterior midline[2,8,33], which were largely absent in the electrophysiological connectivity that we observed and in networks extracted from MEG using ICA[29]. This apparent discrepancy may reflect the different nature of electrophysiological and hemodynamic signals. Furthermore, it should be taken into account that source estimates from EEG and MEG may have a spatially inhomogeneous sensitivity, which might result in an attenuation of deep sources.

Power envelope correlation in the gamma frequency range

Neuronal oscillations in the gamma frequency range have been found in various experimental contrasts and may be a generic signature of local cortical activity[18,22]. A growing number of combined electrophysiology and fMRI studies have linked hemodynamic signals to neuronal activity, particularly in the gamma band[45,46,48–50]. These findings suggest that resting state functional connectivity observed using fMRI[2] may manifest in the correlation of oscillatory activity in the gamma frequency range. This notion is supported by invasive ECoG studies that found long-range power correlation in this frequency range[27,31].

In contrast, we did not find prominent global correlation in the gamma frequency range. This seemingly unexpected finding may relate to different issues. First, the source of variance that drives the neuronal signals likely has a profound influence[18]. Sensory stimulation effectively drives cortical gamma-band activity[18,46] that can be measured with EEG and MEG[21,23,48]. In contrast, during rest, gamma-band fluctuations may be much smaller and the global correlation may be dominated by alpha to beta band activity. Second, the spatial sampling of recorded signals is likely to be important. Compared with intracranial electrodes, EEG and MEG average over larger populations of neurons. As a consequence, EEG and MEG may be particularly sensitive to spectral components with a broader spatial coherence, whereas intracranial measures may be more sensitive to locally coherent rhythms. Non-invasive and invasive measures may therefore emphasize signals with different spatial and spectral characteristics.

METHODS

Methods and any associated references are available in the online version of the paper.

Note: Supplementary information is available in the online version of the paper.

ACKNOWLEDGMENTS

We thank C. Hipp for helpful discussions and comments on the manuscript, and the bwGRiD project (http://www.bw-grid.de) for the computational resources. This work was supported by grants from the European Union (NEST-PATH-043457 to A.K.E. and HEALTH-F2-2008-200728 to M.C. and A.K.E.) and the National Institute of Mental Health (R01 MH096482-01 to M.C.).

AUTHOR CONTRIBUTIONS

All of the authors designed the experiment and wrote the paper. J.F.H. and D.J.H. collected the data and performed the data analysis. J.F.H. conceived the orthogonalization approach.

COMPETING FINANCIAL INTERESTS

The authors declare competing financial interests: details accompany the online version of the paper.

Published online at http://www.nature.com/doifinder/10.1038/nn.3101.
Reprints and permissions information is available online at http://www.nature.com/reprints/index.html.

1. Biswal, B., Yetkin, F.Z., Haughton, V.M. & Hyde, J.S. Functional connectivity in the motor cortex of resting human brain using echo-planar MRI. *Magn. Reson. Med.* **34**, 537–541 (1995).
2. Fox, M.D. & Raichle, M.E. Spontaneous fluctuations in brain activity observed with functional magnetic resonance imaging. *Nat. Rev. Neurosci.* **8**, 700–711 (2007).
3. Fox, M.D. *et al.* The human brain is intrinsically organized into dynamic, anticorrelated functional networks. *Proc. Natl. Acad. Sci. USA* **102**, 9673–9678 (2005).
4. Vincent, J.L. *et al.* Coherent spontaneous activity identifies a hippocampal-parietal memory network. *J. Neurophysiol.* **96**, 3517–3531 (2006).
5. Vincent, J.L., Kahn, I., Snyder, A.Z., Raichle, M.E. & Buckner, R.L. Evidence for a frontoparietal control system revealed by intrinsic functional connectivity. *J. Neurophysiol.* **100**, 3328–3342 (2008).
6. Kahn, I., Andrews-Hanna, J.R., Vincent, J.L., Snyder, A.Z. & Buckner, R.L. Distinct cortical anatomy linked to subregions of the medial temporal lobe revealed by intrinsic functional connectivity. *J. Neurophysiol.* **100**, 129–139 (2008).
7. Dosenbach, N.U.F. *et al.* Distinct brain networks for adaptive and stable task control in humans. *Proc. Natl. Acad. Sci. USA* **104**, 11073–11078 (2007).
8. Buckner, R.L. *et al.* Cortical hubs revealed by intrinsic functional connectivity: mapping, assessment of stability, and relation to Alzheimer's disease. *J. Neurosci.* **29**, 1860–1873 (2009).
9. Power, J.D. *et al.* Functional network organization of the human brain. *Neuron* **72**, 665–678 (2011).
10. Lewis, C.M., Baldassarre, A., Committeri, G., Romani, G.L. & Corbetta, M. From the cover: learning sculpts the spontaneous activity of the resting human brain. *Proc. Natl. Acad. Sci. USA* **106**, 17558–17563 (2009).
11. Dehaene, S. & Changeux, J.-P. Experimental and theoretical approaches to conscious processing. *Neuron* **70**, 200–227 (2011).
12. Zhang, D. & Raichle, M.E. Disease and the brain's dark energy. *Nat Rev Neurol.* **6**, 15–28 (2010).
13. Hawellek, D.J., Hipp, J.F., Lewis, C.M., Corbetta, M. & Engel, A.K. Increased functional connectivity indicates the severity of cognitive impairment in multiple sclerosis. *Proc. Natl. Acad. Sci. USA* **108**, 19066–19071 (2011).
14. Logothetis, N.K. What we can do and what we cannot do with fMRI. *Nature* **453**, 869–878 (2008).

15. Sirotin, Y.B. & Das, A. Anticipatory haemodynamic signals in sensory cortex not predicted by local neuronal activity. *Nature* **457**, 475–479 (2009).
16. Heeger, D.J. & Ress, D. What does fMRI tell us about neuronal activity? *Nat. Rev. Neurosci.* **3**, 142–151 (2002).
17. Wang, X.-J. Neurophysiological and computational principles of cortical rhythms in cognition. *Physiol. Rev.* **90**, 1195–1268 (2010).
18. Donner, T.H. & Siegel, M. A framework for local cortical oscillation patterns. *Trends Cogn. Sci.* **15**, 191–199 (2011).
19. Siegel, M., Donner, T.H. & Engel, A.K. Spectral fingerprints of large-scale neuronal interactions. *Nat. Rev. Neurosci.* **13**, 121–134 (2012).
20. Bruns, A., Eckhorn, R., Jokeit, H. & Ebner, A. Amplitude envelope correlation detects coupling among incoherent brain signals. *Neuroreport* **11**, 1509–1514 (2000).
21. Siegel, M., Donner, T.H., Oostenveld, R., Fries, P. & Engel, A.K. Neuronal synchronization along the dorsal visual pathway reflects the focus of spatial attention. *Neuron* **60**, 709–719 (2008).
22. Fries, P. Neuronal gamma-band synchronization as a fundamental process in cortical computation. *Annu. Rev. Neurosci.* **32**, 209–224 (2009).
23. Hipp, J.F., Engel, A.K. & Siegel, M. Oscillatory synchronization in large-scale cortical networks predicts perception. *Neuron* **69**, 387–396 (2011).
24. Nolte, G. *et al.* Identifying true brain interaction from EEG data using the imaginary part of coherency. *Clin. Neurophysiol.* **115**, 2292–2307 (2004).
25. Schoffelen, J.-M. & Gross, J. Source connectivity analysis with MEG and EEG. *Hum. Brain Mapp.* **30**, 1857–1865 (2009).
26. Cordes, D. *et al.* Frequencies contributing to functional connectivity in the cerebral cortex in 'resting-state' data. *AJNR Am. J. Neuroradiol.* **22**, 1326–1333 (2001).
27. Nir, Y. *et al.* Interhemispheric correlations of slow spontaneous neuronal fluctuations revealed in human sensory cortex. *Nat. Neurosci.* **11**, 1100–1108 (2008).
28. Brookes, M.J. *et al.* Measuring functional connectivity using MEG: methodology and comparison with fcMRI. *Neuroimage* **56**, 1082–1104 (2011).
29. Brookes, M.J. *et al.* Investigating the electrophysiological basis of resting state networks using magnetoencephalography. *Proc. Natl. Acad. Sci. USA* **108**, 16783–16788 (2011).
30. Rubinov, M. & Sporns, O. Complex network measures of brain connectivity: uses and interpretations. *Neuroimage* **52**, 1059–1069 (2010).
31. He, B.J., Snyder, A.Z., Zempel, J.M., Smyth, M.D. & Raichle, M.E. Electrophysiological correlates of the brain's intrinsic large-scale functional architecture. *Proc. Natl. Acad. Sci. USA* **105**, 16039–16044 (2008).
32. Miller, K.J., Weaver, K.E. & Ojemann, J.G. Direct electrophysiological measurement of human default network areas. *Proc. Natl. Acad. Sci. USA* **106**, 12174–12177 (2009).
33. Greicius, M.D., Krasnow, B., Reiss, A.L. & Menon, V. Functional connectivity in the resting brain: a network analysis of the default mode hypothesis. *Proc. Natl. Acad. Sci. USA* **100**, 253–258 (2003).
34. Bassett, D.S., Meyer-Lindenberg, A., Achard, S., Duke, T. & Bullmore, E. Adaptive reconfiguration of fractal small-world human brain functional networks. *Proc. Natl. Acad. Sci. USA* **103**, 19518–19523 (2006).
35. Liu, Z., Fukunaga, M., de Zwart, J.A. & Duyn, J.H. Large-scale spontaneous fluctuations and correlations in brain electrical activity observed with magnetoencephalography. *Neuroimage* **51**, 102–111 (2010).
36. de Pasquale, F. *et al.* Temporal dynamics of spontaneous MEG activity in brain networks. *Proc. Natl. Acad. Sci. USA* **107**, 6040–6045 (2010).
37. Laufs, H. *et al.* Electroencephalographic signatures of attentional and cognitive default modes in spontaneous brain activity fluctuations at rest. *Proc. Natl. Acad. Sci. USA* **100**, 11053–11058 (2003).
38. Mantini, D., Perrucci, M.G., Del Gratta, C., Romani, G.L. & Corbetta, M. Electrophysiological signatures of resting state networks in the human brain. *Proc. Natl. Acad. Sci. USA* **104**, 13170–13175 (2007).
39. Jann, K., Kottlow, M., Dierks, T., Boesch, C. & Koenig, T. Topographic electrophysiological signatures of FMRI resting state networks. *PLoS ONE* **5**, e12945 (2010).
40. Buzsáki, G. Theta oscillations in the hippocampus. *Neuron* **33**, 325–340 (2002).
41. Fell, J. & Axmacher, N. The role of phase synchronization in memory processes. *Nat. Rev. Neurosci.* **12**, 105–118 (2011).
42. Battaglia, F.P., Benchenane, K., Sirota, A., Pennartz, C.M.A. & Wiener, S.I. The hippocampus: hub of brain network communication for memory. *Trends Cogn. Sci.* **15**, 310–318 (2011).
43. Leopold, D.A., Murayama, Y. & Logothetis, N.K. Very slow activity fluctuations in monkey visual cortex: implications for functional brain imaging. *Cereb. Cortex* **13**, 422–433 (2003).
44. Deco, G., Jirsa, V.K. & McIntosh, A.R. Emerging concepts for the dynamical organization of resting-state activity in the brain. *Nat. Rev. Neurosci.* **12**, 43–56 (2011).
45. Schölvinck, M.L., Maier, A., Ye, F.Q., Duyn, J.H. & Leopold, D.A. Neural basis of global resting-state fMRI activity. *Proc. Natl. Acad. Sci. USA* **107**, 10238–10243 (2010).
46. Logothetis, N.K., Pauls, J., Augath, M., Trinath, T. & Oeltermann, A. Neurophysiological investigation of the basis of the fMRI signal. *Nature* **412**, 150–157 (2001).
47. Goense, J.B.M. & Logothetis, N.K. Neurophysiology of the BOLD fMRI signal in awake monkeys. *Curr. Biol.* **18**, 631–640 (2008).
48. Scheeringa, R. *et al.* Neuronal dynamics underlying high- and low-frequency EEG oscillations contribute independently to the human BOLD signal. *Neuron* **69**, 572–583 (2011).
49. Magri, C., Schridde, U., Murayama, Y., Panzeri, S. & Logothetis, N.K. The amplitude and timing of the BOLD signal reflects the relationship between local field potential power at different frequencies. *J. Neurosci.* **32**, 1395–1407 (2012).
50. Mukamel, R. *et al.* Coupling between neuronal firing, field potentials, and FMRI in human auditory cortex. *Science* **309**, 951–954 (2005).

ONLINE METHODS

MEG recording. MEG was continuously recorded with a 275-channel whole-head system (Omega 2000, CTF Systems) in a magnetically shielded room. The electro-oculogram was recorded simultaneously for off-line artifact rejection. The head position relative to the MEG sensors was measured continuously using a set of head localization coils (nasion, left and right ears). MEG signals were low-pass filtered online (cutoff = 300 Hz) and recorded with a sampling rate of 1,200 Hz.

Subjects and experimental procedure. Subjects (n = 43, age = 25.5 ± 3.5 years, mean ± s.d., 21 females) fixated a cross projected centrally onto a back projection screen with an LCD projector (Sanyo Pro Xtrax PLC-XP51) from outside the magnetically shielded room. Subjects were instructed to continuously maintain fixation (duration = 505 ± 115 s, mean ± s.d., range = 360–620 s). The study was conducted in accordance with the Declaration of Helsinki and informed consent was obtained from all participants before the recordings.

Preprocessing and artifact rejection. The data were high-pass filtered offline (cut-off = 0.5 Hz, Butterworth, fourth order) and artifactual data (eye movements, strong muscle activity) were rejected on the basis of visual inspection (13.4 ± 7.6%, mean ± s.d.; range = 2.1–39.5%). For the analysis of spectral components above 32 Hz, we performed additional cleaning to account for muscular artifacts. The data were high-pass filtered (30 Hz, Butterworth, fourth order), ICA was computed and artifactual components related to muscular activity were rejected from the data (7 ± 3.8, mean ± s.d.; range = 1–16).

Analysis software. All data analyses were performed in Matlab (MathWorks) using custom scripts and open source toolboxes: Fieldtrip[51] (http://www.ru.nl/fcdonders/fieldtrip/), SPM2 (http://www.fil.ion.ucl.ac.uk/spm/), Brain Connectivity Toolbox[30] (http://www.brain-connectivity-toolbox.net/).

Spectral analysis. We derived spectral estimates using Morlet's wavelets[52] $w(t,f)$

$$w(t,f) = (\sigma_t\sqrt{\pi})^{-1/2} e^{-t^2/2\sigma_t^2} e^{-i2\pi ft}$$

Here, f is the center frequency (carrier frequency) and σ_t is the temporal s.d. The time-frequency estimate $X(t,f)$ of a signal $x(t)$ was then computed by convolution with $w(t,f)$

$$X(t,f) = x(t) * w(t,f)$$

We chose a spectral band-width of 1/2 octave (corresponding to f/σ_f ~5.83; σ_f, spectral s.d.) and spaced the center frequencies logarithmically according to the exponentiation of the base 2 with exponents ranging from 1 to 7 in steps of 1/4. We derived spectral estimates in successive half-overlapping temporal windows that covered $\pm 3\sigma_t$. For time points at which the convolution kernel overlapped with sections marked as artifacts (see preprocessing), the data were discarded.

Source locations and physical forward model. For source analyses, we used three different source configurations defined in MNI space. For correlation maps of selected reference locations, spatial normalization of correlation values for statistical testing (see below) and the all-to-all analysis, we used a regular three-dimensional grid that covered the whole brain (1-cm spacing, 2,925 source locations; for co-variation frequency analyses we used 2-cm spacing, 369 source locations). For the correlation analysis between homologous sensory areas, we defined bilateral sensory locations in MNI space. The coordinates of the sensory regions were identified by a meta-analysis of fMRI literature using the BrainMap.org resources[53] (auditory cortex ([−54, −22, 10], [52, −24, 12]), somatosensory cortex ([−42, −26, 54], [38, −32, 48]), visual cortex ([−20, −86, 18], [16, −80, 26]). Locations of interest derived from fMRI correlation literature[3] for seed correlation analyses: l/r MT+ ([−47, −69, −3], [54, −63, −8]), MPFC ([−3, 39, −2]) and SMA ([−2, 1, 51]).

For source analysis, we constructed individual physical forward models (leadfields). We affine-transformed source locations into individual head space using the participants' individual T1-weighted structural MRI and aligned the MEG sensors to the head geometry on the basis of three fiducial points (nasion, and left and right ear, registered during the MEG acquisition by three head localization coils). To derive the physical relation between sources and sensors, we employed a single-shell model[54].

Source analysis. We used adaptive linear spatial filtering (beamforming)[23,55,56] to estimate the spectral amplitude and phase of neuronal signals at the source level. For each frequency f and source location r, three orthogonal filters ($\hat{A} = [A_1, A_2, A_3]$; one for each spatial dimension) were computed that pass activity from location r with unit gain while maximally suppressing activity from all other sources

$$\hat{A}(r,f) = \left[L^T(r)C_{\text{real}}(f)^{-1}L(r)\right]^{-1} L^T(r)C_{\text{real}}(f)^{-1}$$

Here, $L(r)$ is a matrix whose columns are the leadfields of three orthogonal dipoles at source location r, C_{real} denotes the real part of the complex cross-spectral-density matrix for the sensor level data at frequency f and T indicates the matrix transpose. We linearly combined the three filters to a single filter pointing in the direction of maximal variance, that is, the dominant dipole orientation. To this end, the filters were weighted with the first eigenvectors' elements (the eigenvector with the largest eigenvalue of the real part of the cross-spectral-density matrix at the source location r)

$$v(r,f) = [v_1(r,f), v_2(r,f), v_3(r,f)] = Eig_1\left(\hat{A}(r,f)C_{\text{real}}(f)\hat{A}(r,f)^{*T}\right)$$

$$A(r,f) = v_1(r,f)A_1(r,f) + v_2(r,f)A_2(r,f) + v_3(r,f)A_3(r,f)$$

To derive the complex source estimates, the complex frequency domain data were then multiplied with the real-valued filter

$$X_{\text{source}}(r,t,f) = A(r,f)X_{\text{sensor}}(t,f)$$

Here, $X_{\text{sensor}}(t,f)$ is the frequency domain representation of the sensor level data at time t and frequency f, and $X_{\text{source}}(r,t,f)$ is the corresponding source signal at location r. To account for the spatial bias of the beamforming solution when investigating signal power (**Supplementary Fig. 5**), we jointly normalized the three leadfields for each source location by division with the sum of all squared values.

Power envelope correlation between orthogonalized signals. Here we provide a brief account of the applied method. Please see **Supplementary Data** and **Supplementary Figures 1** and **2** for additional information and numerical simulations on this approach.

We assessed neuronal interactions by quantifying correlations between power envelopes[19,20,57,58]. To this end, we squared the absolute values of the complex spectral estimates and applied a logarithmic transform to render the power statistics more normal. We then computed Pearson's linear correlation between the resulting power envelopes from two different locations.

To discount spurious correlations caused by the limited spatial resolution of source estimates, we orthogonalized any two time series of band-limited activity before computing their power envelopes. We performed this operation in the frequency domain. We defined the complex signal $Y(t,f)$ orthogonalized to the complex signal $X(t,f)$ (see **Supplementary Fig. 1**)

$$Y_{\perp X}(t,f) = \text{imag}\left(Y(t,f)\frac{X(t,f)^*}{|X(t,f)|}\right)$$

The orthogonalization can be done in two directions (X to Y, Y to X). We computed power envelope correlations for both directions of orthogonalized time-series and averaged the values for subsequent analysis. We performed the orthogonalization time point by time point, which requires no assumption about stationarity of the signals' relation beyond the length of the carrier-frequency dependent analysis window. Discounting the non-orthogonal signal components leads to an underestimation of true correlation by a factor of ~0.577. This factor was accounted for when reporting correlation values between orthogonalized signals.

Spectrally resolved correlation of power envelopes (second level analysis). To resolve the correlation between two orthogonalized signals in frequency

(co-variation frequency), we applied spectral analysis to the power envelopes with an approach equivalent to using Morlet's wavelets. We chose a spectral bandwidth of 0.95 octaves ($f/\sigma_f \sim 3.15$) and spaced the center frequencies logarithmically according to the exponentiation of the base 10 with exponents ranging from −1.5 in steps of 0.1 to 1/6 of the carrier frequency. We derived spectral estimates in successive half-overlapping temporal windows that covered $\pm 3\sigma_t$. From these complex numbers, we derived the coherency between power envelopes and took the real part of coherency as the frequency-specific measure of correlation.

Power envelopes were interrupted by periods of missing data resulting from artifacts such as eye blinks or strong muscle activity. Thus, the convolution with Morlet's wavelets as described above was not feasible and we employed a spectral estimate approach that could cope with missing data. For discrete signals, time domain and frequency domain representations are linearly related

$$x = BX, \quad X = \mathrm{inv}(B)x$$

Here, x is the time domain representation, X is the frequency domain representation and B is the Fourier basis (that is, family of orthogonal complex sinusoids). For data with invalid temporal sections, B is rank deficient. In this case, we derived the spectral estimate employing the pseudo inverse.

$$X = \mathrm{pinv}(B)x$$

As a windowing function, we used a Gaussian taper such that if no data was missing, the approach was identical to using Morlet's wavelets. Data sections with more than 50% missing data were discarded from the analysis.

Statistical analysis of correlation structure and definition of connections. Across a broad range of frequencies, power envelope correlations between orthogonalized signals had a positive offset, that is, the brain-wide correlation was consistently larger than zero. To focus on the spatial correlation structure, we used Student's t-tests and identified correlation higher than the average correlation to all locations on a three-dimensional grid covering the brain. We corrected for multiple comparisons by controlling the FDR. Please note that this statistic depends on the sources across which the average correlation is estimated.

For the analysis of the global correlation structure, no particular reference location exists. For this case, the correlation between any two sites can statistically be compared to the brain-wide correlation of either one of the two sites. We established a symmetric connectivity measure by defining a connection to be present if statistics for either one of the two possible normalizations reached significance (we accounted for two tests by Bonferroni correction, $P_{\mathrm{threshold}} = 0.01/2$). This resulted in a symmetric connection matrix that was used for subsequent graph-theoretical analyses. The symmetrization allowed for fully connected nodes; in other words, there could be more than 50% connections (for example, see **Fig. 4b**).

Graph-theoretical analysis. We used graph-theoretical measures[30] to quantify basic properties of global connectivity. We employed three measures highlighting different aspects of the global correlation

Degree is represented as

$$D_i = \frac{1}{N-1}\sum_j a_{ij}$$

Here, D_i is the degree at location i, and a_{ij} is the connection (0 for no connection, 1 for a connection) between locations i and j, and N is the total number of connections. The total degree is the average of the degree at all locations.

Betweenness is represented as

$$B_i = \frac{1}{(N-1)(N-2)} \sum_{\substack{h,j \\ h\neq j, h\neq i, j\neq i}} \frac{\rho_{hj}(i)}{\rho_{hj}}$$

Here, B_i is the betweenness at location i, ρ_{hj} is the number of shortest paths between h and j, and $\rho_{hj}(i)$ is the number of shortest paths between h and j that passes through i.

The normalized betweenness is represented as

$$BN_i = \frac{B_i - \mathrm{mean}(B_i^{\mathrm{rand}})}{\mathrm{sd}(B_i^{\mathrm{rand}})}$$

Here, BN_i is the normalized betweenness at location i derived from the betweenness B_i and the mean and s.d. of a set of betweenness values B_i^{rand} (20 resamples) from connection matrices with identical degree but randomized connectivity[59]. Thus, normalized betweenness accounts for the betweenness that occurs in a random network with identical degree.

Statistical analysis of graph-theoretical measures. We performed random effects statistics to assess the modulation of graph-theoretical measures. We first derived single subject estimates of graph-theoretical measures using a jackknifing procedure. For each subject i of N subjects, we derived a robust jackknife resample R_i by averaging graph-theoretical measures from connectivity matrices based on all, but this subject and one other subject at a time. From these jackknife resamples, we computed single subject estimates G_i

$$G_i = \sum_{j=1}^{N} R_j - (N-1)R_i$$

This corresponds to pseudo-values without bias correction. Based on these estimates, we performed the following random-effects statistics.

To assess the spatial patterning of graph-theoretical measures, we employed random permutation statistics. We generated an empirical null hypothesis distribution for no spatial patterns by randomly permuting source locations for each subject and then computing the average across subjects (10,000 resamples). We selected only the largest value across the entire space of each resample to account for multiple testing. To assess the modulation of graph-theoretical measures with the factors carrier frequency and spatial location and their interaction, we performed a two-way analysis of variance.

Illustration of results. To illustrate the spatial distribution of correlation and graph-theoretical measures, we projected the quantities onto the cortical surface from the population-average, landmark- and surface-based atlas[60], or alternatively as an overlay on brain slices of the SPM99/2 template brain. We used different statistical masks as explained in the corresponding figure legends.

51. Oostenveld, R., Fries, P., Maris, E. & Schoffelen, J.-M. FieldTrip: open source software for advanced analysis of MEG, EEG, and invasive electrophysiological data. *Comput. Intell. Neurosci.* **2011**, 156869 (2011).
52. Tallon-Baudry, C., Bertrand, O., Delpuech, C. & Pernier, J. Stimulus specificity of phase-locked and non-phase-locked 40 Hz visual responses in human. *J. Neurosci.* **16**, 4240–4249 (1996).
53. Laird, A.R. *et al.* ALE meta-analysis workflows via the brainmap database: progress towards a probabilistic functional brain atlas. *Front. Neuroinform.* **3**, 23 (2009).
54. Nolte, G. The magnetic lead field theorem in the quasi-static approximation and its use for magnetoencephalography forward calculation in realistic volume conductors. *Phys. Med. Biol.* **48**, 3637–3652 (2003).
55. Van Veen, B.D., van Drongelen, W., Yuchtman, M. & Suzuki, A. Localization of brain electrical activity via linearly constrained minimum variance spatial filtering. *IEEE Trans. Biomed. Eng.* **44**, 867–880 (1997).
56. Gross, J. *et al.* Dynamic imaging of coherent sources: studying neural interactions in the human brain. *Proc. Natl. Acad. Sci. USA* **98**, 694–699 (2001).
57. Schepers, I.M., Hipp, J.F., Schneider, T.R., Röder, B. & Engel, A.K. Functionally specific oscillatory activity correlates between visual and auditory cortex in the blind. *Brain* **135**, 922–934 (2012).
58. Donner, T.H., Siegel, M., Fries, P. & Engel, A.K. Buildup of choice-predictive activity in human motor cortex during perceptual decision making. *Curr. Biol.* **19**, 1581–1585 (2009).
59. Maslov, S. & Sneppen, K. Specificity and stability in topology of protein networks. *Science* **296**, 910–913 (2002).
60. Van Essen, D.C.A. Population-average, landmark- and surface-based (PALS) atlas of human cerebral cortex. *Neuroimage* **28**, 635–662 (2005).

doi:10.1038/nn.3101

Supplementary Information

Large-scale cortical correlation structure of spontaneous oscillatory activity

Joerg F. Hipp[1,2], David J. Hawellek[1], Maurizio Corbetta[3], Markus Siegel[2] & Andreas K. Engel[1]

[1] Department of Neurophysiology and Pathophysiology, University Medical Center Hamburg-Eppendorf, 20246 Hamburg, Germany

[2] Centre for Integrative Neuroscience, University of Tübingen, 72076 Tübingen, Germany

[3] Departments of Neurology, Radiology, Anatomy, and Neurobiology, Washington University School of Medicine, 63110, St. Louis, MO

Correspondence should be addressed to:

Joerg F. Hipp (joerg.hipp@cin.uni-tuebingen.de)

Nature Neuroscience: doi:10.1038/nn.3101

Supplementary Data

Here, we provide additional information on how to estimate power-envelope correlations between orthogonalized signals. First, we elaborate on the core part of our analysis approach, the orthogonalization of signals. Then, we provide numerical simulations that illustrate properties of the approach.

Orthogonalization

The key step of the analysis approach is to orthogonalize two signals before deriving their power envelopes for correlation analysis. This procedure ensures that the signals do not share the trivial co-variability in power due to measuring the same sources while preserving co-variation related to measuring different sources.

Using ordinary least squares, the instantaneous linear relation between two signals in the frequency domain can be derived as follows: Let $X(t,f)$ and $Y(t,f)$ be the frequency domain representation of two time series x and y, where t and t' are the time points of the center of the windows for spectral analysis and f is the frequency of interest (see Spectral Analysis in the **Online Methods**). Then, the part of a complex time series Y that can instantaneous and linearly be predicted from X, i.e. $Y_{||X}$, is:

$$Y_{||X}(t,f) = a_{X,Y}(f,T)X(t,f) = real\left(\frac{\sum_{t'\in T} X(t',f)Y(t',f)^*}{\sum_{t'\in T} X(t',f)X(t',f)^*}\right)X(t,f)$$

Where $a_{X,Y}$ is the regression coefficient that describes the instantaneous linear relation between X and Y that is estimated from data in the time interval T, * is the complex conjugate, and $real(\,)$ is the real part of a complex number. The signal Y orthogonalized to the signal X, i.e. $Y_{\perp X}(t,f)$, can be derived by subtracting the parallel signal component:

$$Y_{\perp X}(t,f) = Y(t,f) - Y_{||X}(t,f)$$

The orthogonalization can similarly be performed in the time domain where it generalizes to broadband signals.

Of practical importance is the selection of the time interval T to derive the regression coefficient. The interval can range from the entire dataset to just a single time window. Within this time interval, the signals' relation should be constant. If such stationarity is fulfilled, longer time intervals provide more robust estimates and may lead to a superior sensitivity of the method. However without stationarity, the orthogonalization may be incomplete. The dynamics of the

Nature Neuroscience: doi:10.1038/nn.3101

instantaneous relation between EEG and MEG signals is influenced by various factors. Neuronal interaction may vary over time. Artifactual signals like muscle activity are waxing and waning in time. In the MEG system, the subjects' head can move relative to the sensors, which changes the statistical relation between signals. Since the time-constants of these non-stationarities are unknown, we chose the shortest time interval possible, i.e. a single window around time t. In other words, we performed the orthogonalization independently for each analysis window. In this case, the sum over t' in the above formula for $Y_{\perp X}(t,f)$ vanishes:

$$Y_{\perp X}(t,f) = Y(t,f) - real\left(\frac{X(t,f)Y(t,f)^*}{|X(t,f)|^2}\right)X(t,f) = Y(t,f) - real\left(\frac{X(t,f)}{|X(t,f)|}Y(t,f)^*\right)\frac{X(t,f)}{|X(t,f)|}$$

Thus, $Y_{\perp X}(t,f)$ is the difference between $Y(t,f)$ and the part of $Y(t,f)$ that points into the direction of $X(t,f)$ (see **Supplementary Fig. 1b**). Transformation yields the form presented in the **Online Methods**:

$$Y_{\perp X}(t,f) = imag\left(Y(t,f)\frac{X(t,f)^*}{|X(t,f)|}\right)\hat{e}_{\perp X}(t,f)$$

$$\hat{e}_{\perp X}(t,f) = \frac{iX(t,f)}{|X(t,f)|}$$

Where * is the complex conjugate, $imag(\,)$ is the imaginary part of a complex number, and $\hat{e}_{\perp X}(t,f)$ is a complex number of unit length pointing orthogonal to the direction of X in clock-vise direction. In other words, $\hat{e}_{\perp X}(t,f)$ describes the orientation in the complex plane. Since $\hat{e}_{\perp X}(t,f)$ does not contribute to the power envelope, we ignored it in the **Online Methods** for simplicity.

Nature Neuroscience: doi:10.1038/nn.3101

Properties of Power-Envelope Correlation Between Orthogonalized Signals

We used numerical simulations to quantitatively study the properties of power-envelope correlation between orthogonalized signals. In particular, we addressed the following questions: (1) Does the power-envelope correlation between orthogonalized signals vanish if no 'true' correlation exists? (2) Does the power-envelope correlation between orthogonalized signals detect 'true' correlations between sources, and if so, is the magnitude of the estimate affected by the orthogonalization? (3) Does the presence of coherence, i.e. of a systematic relation between the signals on the fine temporal scale, influence power-envelope correlation estimates between orthogonalized signals?

Signals for Numerical Simulations. As a model of frequency transformed physiological signals, we generated complex random numbers with Rayleigh distributed amplitude and random phase. This corresponds to the frequency transform of Gaussian noise in the time-domain. Although this signal model is very general, the conclusions drawn from the present simulations are limited to this model.

We constructed two signals with correlated power envelopes: The first signal was defined as a series of random complex numbers (see above). The second signal was constructed as a weighted sum of the first signal and another series of random complex numbers (weight signal 1 = c; weight random = $\sqrt{1-c^2}$; c, coherence). This resulted in two complex time-series with coherence c. The power-envelope correlation between two signals generated this way is monotonically related to their coherence (see **Supplementary Fig. 2f**, inlay). Thus, we adjusted coherence to specify the power-envelope correlation. To create signals with anti-correlated power envelopes, we constructed the second time series as a weighted sum of a modified version of the first signal and another series of random complex numbers. The modification was to map the amplitude values into the range of 0 to 1 using the cumulative Rayleigh distribution, subtract the remapped values from 1, and back-transform the values to amplitude space. In other words, we 'mirrored' the envelope of the signal. This operation resulted in negative power-envelope correlations between the constructed signals. Analogous to the case of positive correlation, the strength of correlation was specified by adjusting the coherence parameter. For the simulations we either took the generated signal pairs, or randomized the phase of one of the signals.

Insensitivity to Spurious Correlation. We performed three simulations with different numbers and spatial configurations of independent (and thus uncorrelated) sources (number of sources:

Nature Neuroscience: doi:10.1038/nn.3101

3, 5, and 15) to investigate how the orthogonalization approach discounts spurious correlations. For each simulation, we derived measurements at two sensors that were defined as mixtures of the true sources (the sensors can also be thought of as reconstructed sources). The mixing simulated the limited spatial resolution of EEG and MEG, where several 'true' sources contribute to the signal of a given sensor (or reconstructed source). For the sensors, we computed plain power-envelope correlations and power-envelope correlation between orthogonalized signals.

We started with a simple configuration of 3 uncorrelated sources. Two sources contributed strongly to one of the sensors, while not influencing the other sensor. Additionally, there was a central uncorrelated source, influencing both sensors (mixing matrix: w = [1, 1, 0; 0, 1, 1]). We repeatedly estimated the plain and orthogonalized power-envelope correlations (number of samples: 200, number of resamples: 1000). The plain correlation was systematically increased although none of the underlying sources was correlated (**Supplementary Fig. 2a**, blue, r = 0.165 ± 0.069, mean ± s.d., t-test, $P < 10^{-14}$). This correlation reflects the two sensors measuring the same central source. The magnitude of this spurious correlation depends on the sensors' sensitivity to the same sources. In contrast, the orthogonalized power-envelope correlation did not differ significantly from 0 (**Supplementary Fig. 2a**, red, r = 0.001 ± 0.060, mean ± s.d., t-test, P > 0.05). We repeated the simulation for two other source arrangements of increasing complexity (**Supplementary Fig. 2b**; mixing matrix w = [1, 1, 0, 1.25, 0.75; 0, 1, 1, 0.75, 1.25]; plain correlation, r = 0.345 ± 0.065, mean ± s.d., t-test, $P < 10^{-14}$; orthogonalized correlation, r = –0.001 ± 0.061, mean ± s.d., t-test, P > 0.05; **Supplementary Fig. 2c**; mixing matrix 15 x 2 random numbers; plain correlation, r = 0.231 ± 0.068, mean ± s.d., t-test, $P < 10^{-14}$; orthogonalized correlation, r = 0.000 ± 0.060, mean ± s.d., t-test, P > 0.05). For all source configurations, the orthogonalization approach rendered power-envelope correlations insensitive to spurious correlations.

Sensitivity to true correlation. To investigate the sensitivity of the orthogonalization approach to true correlations, we simulated signals with a defined correlation of 0.5 and derived power-envelope correlation estimates for plain and orthogonalized signals for different sample sizes (**Supplementary Fig. 2d**, sample sizes: 50, 100, 200, 400; 10,000 repetitions). The orthogonalized power-envelope correlations had approximately half the size of the plain correlation values, while the variance of the estimate was comparable to the plain correlation and became smaller for larger sample sizes. To quantify the reduction in correlation estimate, we varied the strength of correlation between amplitudes. The relation between the defined (true) correlation coefficient and the orthogonalized correlation was linear with a slope of 0.577

Nature Neuroscience: doi:10.1038/nn.3101

(**Supplementary Fig. 2e**). Consequently, the true correlation coefficient could be recovered by multiplication of the orthogonalized correlation value with 1.73.

The Influence of Systematic Phase Relations. The above simulations were performed with random phase relations between sources. What happens if this assumption is violated? The effect depends on the strength of phase synchronization and on the phase lag between the signals. If the phase lag of the carrier oscillations is 0, the estimated power-power correlation will be reduced. If the phase lag is 90 degree, the power-power correlation estimate will be identical to the true correlation, but higher compared to signals with random phase relation. The effect size depends on the strength of phase synchronization. This effect is illustrated in **Supplementary Figure 2f** that shows simulations with signals of different degrees of coherence (and corresponding levels of correlation, see inset) and different phase lags. Thus, phase-coherence between signals can modulate the power-envelope correlation estimate of orthogonalized signals, but importantly, phase-coherence cannot induce spurious measures of power-envelope correlations.

In summary, simulations confirm the viability of the approach to estimate power-envelope correlations between orthogonalized signals. In the absence of phase-coherence and for normal amplitude distributions, the approach provides a measure that is insensitive to spurious correlation and allows for estimating the true correlation. Strong phase-coherence may modulate the estimate but will not introduce spurious correlation if no true power correlation exists.

Nature Neuroscience: doi:10.1038/nn.3101

Supplementary Figures

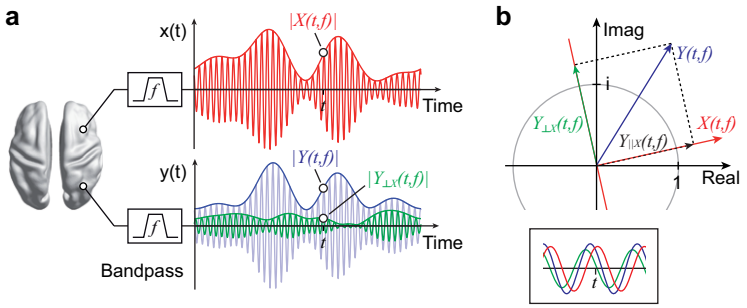

Supplementary Figure 1. Correlation between power envelopes of orthogonalized signals. (**a**) Illustration of power envelopes for one exemplary carrier frequency f (i.e. center frequency of the band-pass filter). The red and blue sinusoidal lines represent band-pass filtered neuronal signals estimated at two source locations. The corresponding blue and red lines – the power envelopes – quantify the evolution of the amplitudes at a slower time-scale. The green sinusoidal line depicts to the blue signal orthogonalized with respect to the red signal. The red power envelope and the green power envelope of the orthogonalized signal are then used for correlation analysis. (**b**) Graphical illustration of the orthogonalization of two complex signals as shown in **a**. The inset depicts the two band-pass filtered signals $y(t)$ and $x(t)$ around time t that are analyzed in the complex domain: The signal $Y(t,f)$ is orthogonalized in the complex plane with respect to $X(t,f)$. This results in a positive number $|Y_{\perp X}(t,f)|$ which is then squared and log-transformed, and correlated with $|X(t,f)|$.

Nature Neuroscience: doi:10.1038/nn.3101

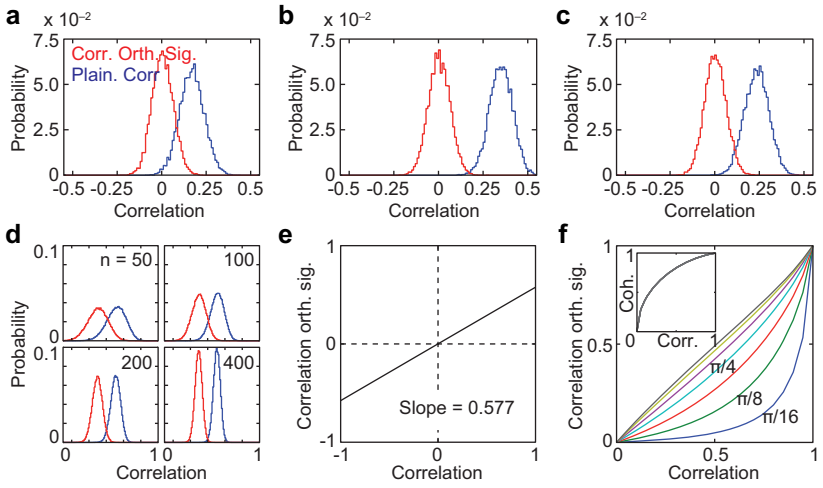

Supplementary Figure 2. Properties of power-envelope correlation between orthogonalized signals. See **Supplementary Data** for a detailed description. (**a–c**) Simulations of independent sources with different spatial configurations and two sensors that measure a mixture of the sources' activities. **a**: w = [1, 1, 0; 0, 1, 1], **b**: w = [1, 1, 0, 1.25, 0.75; 0, 1, 1, 0.75, 1.25], **c**: 15 random weights for each measurement. The figures show the distribution of correlation values of 1000 random resamples (red: power-envelope correlation of orthogonalized signals, blue: plain power-envelope correlation; 200 samples). (**d**) Simulation of two signals with random phase relation and a defined power-envelope correlation of 0.5. Distribution of estimated correlation values for different samples sizes (50, 100, 200, and 400; red: power-envelope correlation or orthogonalized signals; blue: plain power-envelope correlation). (**e**) Relation of 'true' correlation and orthogonalized power-envelope correlation for signals with random phase relation. (**f**) Power-envelope correlations between two orthogonalized signals with varying degrees of coherence and different phase lags (phase lags: [1:7]/16π). Inset: relation between coherence and power envelope correlation that was used for this simulation.

Nature Neuroscience: doi:10.1038/nn.3101

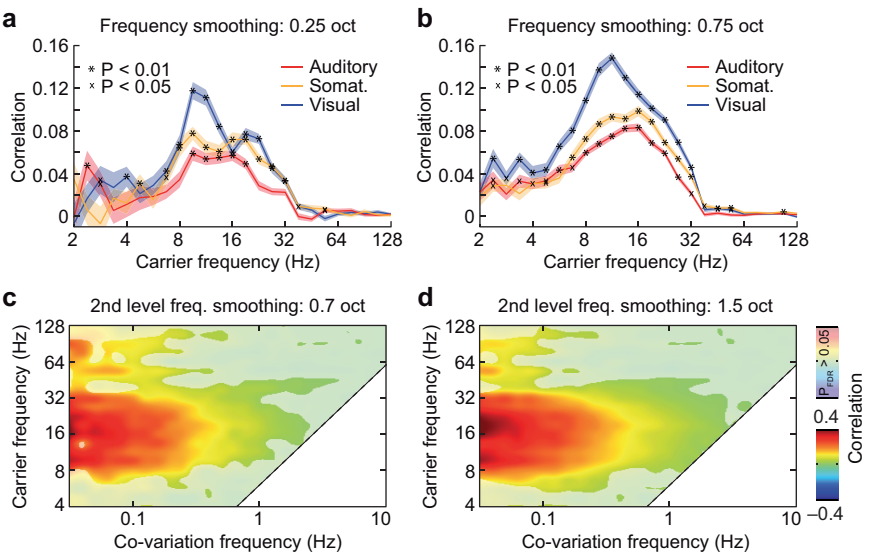

Supplementary Figure 3. Variation of parameters for spectral analyses. (**a**,**b**) Correlation between the auditory cortices (red), the somatosensory cortices (yellow), and the visual cortices (blue) resolved for carrier frequency. The analyses are identical to the one reported in **Figure 2a**, but with different carrier-frequency smoothing (**a**, σ_f = 0.25 oct, σ_f/f ~ 11.6; **b**, σ_f = 0.75 oct, σ_f/f ~ 3.93; as opposed to σ_f = 0.5 oct, σ_f/f ~ 5.83 in the main text). The results are largely invariant to the variation of the carrier frequency smoothing parameter. Less frequency smoothing revealed more distinct correlation structure but at the cost of reduced effect strength. For less frequency smoothing, the correlation between visual areas showed distinct peaks for alpha and beta carrier frequencies. (**c**,**d**) Correlation between homologous sensory areas as a function of the carrier- and the co-variation frequencies. The analyses are identical to the analysis reported in **Figure 2e,** but with different co-variation frequency smoothing (**c**, σ_f = 0.7 oct, σ_f/f ~ 4.20; **d**, σ_f = 1.5 oct, σ_f/f ~ 2.09; as opposed to σ_f = 0.95 oct, σ_f/f ~ 3.15). The correlation for increased and decreased frequency smoothing is very similar to the results reported in **Figure 2e**. The effect strength increased with increased frequency smoothing.

Nature Neuroscience: doi:10.1038/nn.3101

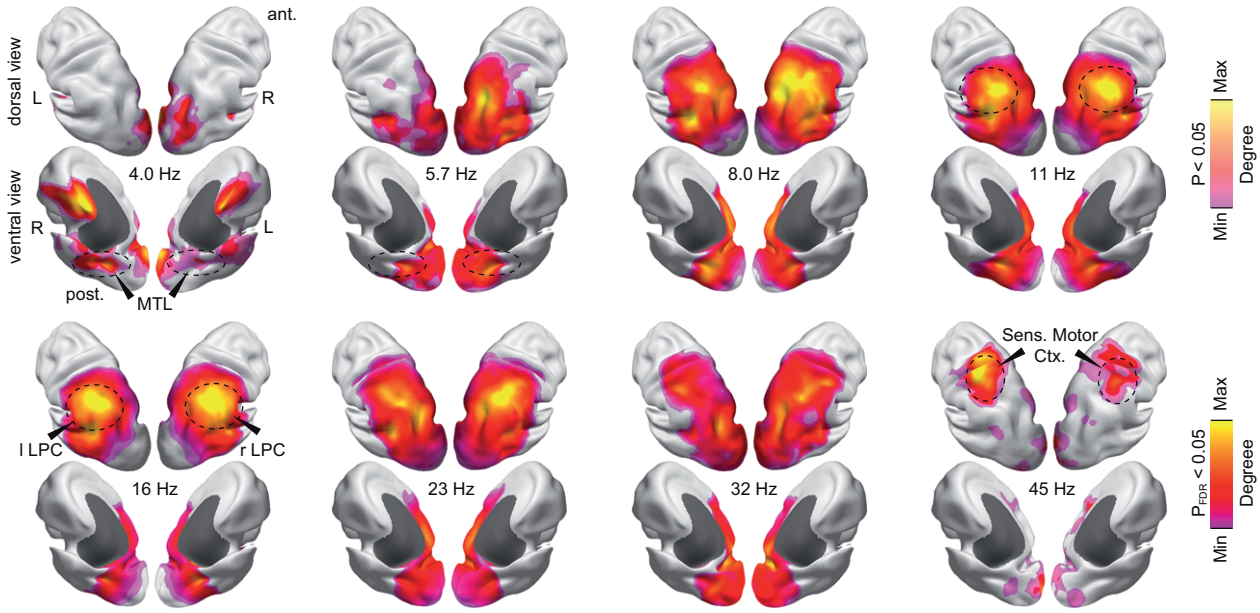

Supplementary Figure 4. Spatial patterning of degree as a function of the carrier frequency. Degree values are statistically masked (voxel-wise permutation test for betweenness > average betweenness, corrected for number of nodes, $P < 0.05$, saturated color scale; $P < 0.05$, uncorrected, desaturated color scale). The color scale is adjusted to the minimal and maximal values within the statistical mask. Subcortical areas are masked dark gray.

Nature Neuroscience: doi:10.1038/nn.3101

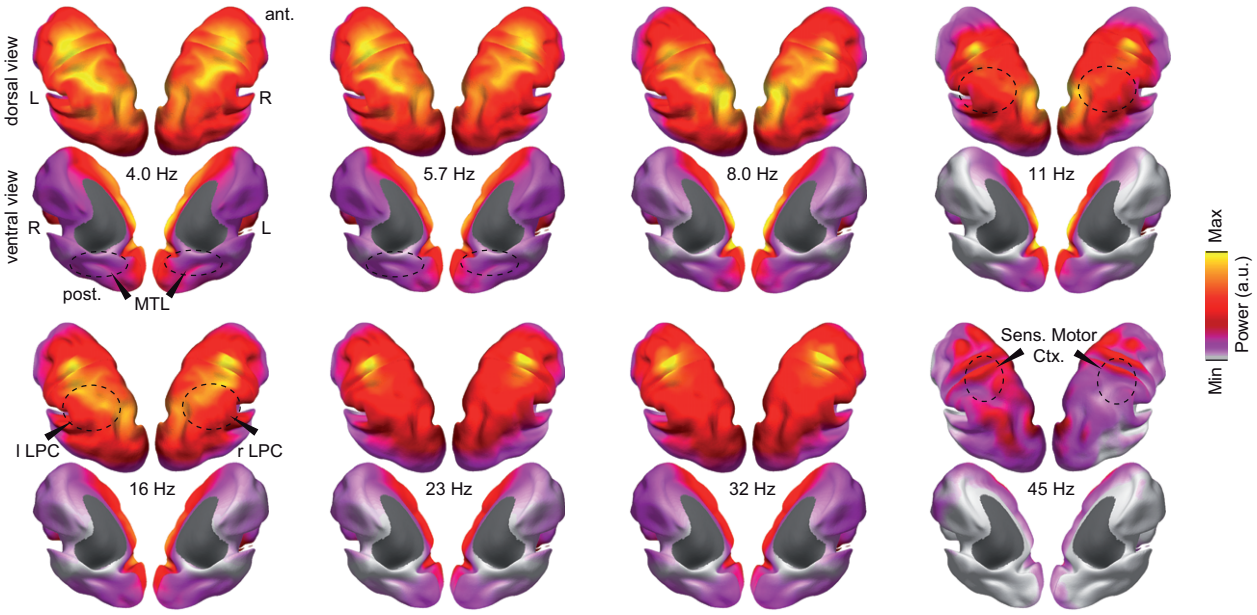

Supplementary Figure 5. Spatial patterning of local signal power as a function of the carrier frequency. Subcortical areas are masked dark gray. Local signal power and the hubs in the global correlation as quantified by graph theoretical measures differ substantially. The dashed lines depict sites with high betweenness (see **Fig. 6**).

Nature Neuroscience: doi:10.1038/nn.3101

Intrinsic local and long-range couplings in oscillatory activity of blind visual cortex

Abbreviated title: Reorganized spontaneous oscillations in the blind

David J. Hawellek [a1], Inga M. Schepers [a], Andreas K. Engel [a], Markus Siegel [b*], Joerg F. Hipp [ab1*]

a: Department of Neurophysiology and Pathophysiology, University Medical Center Hamburg-Eppendorf, 20246 Hamburg, Germany

b: Centre for Integrative Neuroscience, University of Tübingen, 72076 Tübingen, Germany

[1] To whom correspondence should be addressed:

David J. Hawellek, Department of Neurophysiology and Pathophysiology, University Medical Center Hamburg-Eppendorf, Martinistrasse 52, 20246 Hamburg, Germany, E-mail: d.hawellek@uke.de

Joerg F. Hipp, Centre for Integrative Neuroscience, University of Tübingen, 72076 Tübingen, Germany, E-mail: joerg.hipp@cin.uni-tuebingen.de

* These authors contributed equally

Number of pages: n, Number of figures: 3, Number of words: Abstract (245), Introduction (498), Discussion (979)

The authors declare no conflict of interest

Abstract

As a consequence of severe sensory deprivation in congenital blindness the brain undergoes dramatic plastic changes. Areas, which predominantly process visual information in the sighted, are recruited for non-visual tasks in the blind. Here we studied changes in neuronal dynamics that reflect these plastic processes in MEG recordings during rest. In a group of congenitally blind participants, we found visual cortical areas to exhibit power-power correlations in the delta (~2 Hz) and gamma (~90 Hz) range that were absent in matched, sighted controls. These two rhythms were related to one another: The phase of the delta oscillation predicted the amplitude of the gamma oscillation. Phase-amplitude relations the alpha (~10 Hz) to low gamma (~ 40 Hz) range along with the strong alpha power over occipital sites that emerged as dominating features of the sighted controls were strongly reduced in the blind. Furthermore we identified an extended network of prefrontal regions whose intrinsic signal power correlated with visual areas in the beta frequency range (~25 Hz).

In summary, we show oscillatory neuronal signatures in the visual cortex of the blind during rest that resemble activity in the visual cortex of sighted individuals during visual processing. Additionally, we identify specific prefrontal areas to exhibit beta range functional connectivity with occipital regions in the blind. These findings may suggest that the visual cortex of the blind serves non-visual processing in unconstrained mental activity and that a prefrontal pathway may underlie the reintegration of these resources into cortical processing.

Introduction

In congenital blindness brain areas, which usually develop to process visual information, undergo a remodeling of their structural and functional properties to gain an entirely different response profile and processing characteristic (Bavelier and Neville, 2002; Merabet and Pascual-Leone, 2010). While the structural extent of occipital brain regions appears to be reduced in terms of their volume and surface (Noppeney et al., 2005; Jiang et al., 2009; Park et al., 2009; Leporé et al., 2010) as well as their thalamic embedding (Shimony et al., 2006), these areas exhibit elevated levels of metabolic demands as measured with PET (Veraart et al., 1990). Furtermore, the activity level of blind visual cortex exhibits striking modulation upon stimulation of other sensory modalities as well as cognitive demands (Schepers et al., in press; Rösler et al., 1993; Sadato et al., 1996; Büchel et al., 1998; Röder et al., 1999, 2002; Amedi et al., 2003; Gougoux et al., 2005; Collignon et al., 2009, 2011; Bedny et al., 2011), often occurring in a functionally specific manner and even following subtle cognitive manipulations such as priming. This, together with the observation that the interference with occipital activity may cause a loss of performance in specific tasks in the blind (Cohen et al., 1997; Amedi et al., 2004), suggests that the computational resources of the formerly visual areas are newly integrated into an intact but functionally reorganized cortical processing.

Here we investigated changes of spontaneous, oscillatory neuronal activity in the congenitally blind. Oscillatory activity is a ubiquitous phenomenon in the dynamics of neuronal populations (Buzsáki and Draguhn, 2004; Donner and Siegel, 2011) and is intimately linked to a range of cognitive phenomena and fundamental aspects of the physiology of nervous computations (Buzsaki, 2006). Yet, the information that these signals hold about the reorganization of the circuitry in the blind remains largely unexplored. We used task free, resting MEG data and source analysis to study couplings in intrinsic oscillatory activity on a local (visual cortex) as well as global (whole brain) level. In the blind, visual areas exhibited power-power correlations in the

delta (~2 Hz) and gamma (~90 Hz) range where the phase of the delta oscillations predicted the gamma amplitude. These relations were absent in the sighted, where visual areas instead exhibited alpha range dominated processes, with a ~10 Hz oscillation predicting the amplitude of slow gamma (~40 Hz). In addition, we employed a data driven procedure based on power correlations to identify specific correlation patterns that dissociated the blind from the sighted. A pattern of functional connectivity emerged in the beta (~25 Hz) range showing visual areas to be embedded into a network with prefrontal regions. Overall our results provide novel evidence for an association of visual areas with specific prefrontal sites in the blind together with signatures of active visual processing during rest. These results suggest that the processing resources of occipital areas are used for non-visual functions during unconstrained mental activity and may be integrated into functional cortical processing an via specific prefrontal brain regions.

Materials & Methods

Participants

Eleven congenitally blind participants (6 female; age 35.5 ± 9.5 years, mean ± SD, range 23 - 48 years) and eleven control participants matched in age, gender, handedness and education (age 34.4 ± 7.4 years, mean ± SD) participated in this study and received monetary compensation for their participation. The causes of blindness included retinopathy of prematurity (6), genetic defects (2), oxygen deficiency at birth (1), a distorted optic nerve (1) and retinoblastoma (1). Four of the congenitally blind participants had very weak residual light perception. All participants had normal hearing and had no history of neurological or psychiatric illness. Approval of the local ethics committee for this study was obtained and the study was conducted in accordance with the Declaration of Helsinki. Informed consent was obtained from all participants prior to the recordings.

Data acquisition & preprocessing

MEG (275 channel, Omega 2000, CTF Systems Inc., Port Coquitlam, Canada) was recorded continuously for 5 min during silent wakefulness before the start of another experiment (Schepers et al., in press). The electro-oculogram (EOG) and electro-cardiogram (ECG) were recorded simultaneously and the head position relative to the MEG sensors was measured continuously using a set of head localization coils (nasion, left and right ears). The blind and sighted participants were blindfolded during the recording period. For three sighted controls no such resting recordings were made. Corresponding data of matching controls was taken from a different experiment and these recordings were done during silent fixation without blindfold. One MEG sensor was deactivated for all recordings (MLF21), while during the three replaced control recordings one additional channel was deactivated (2xMRO11 and 1xMRP44). The MEG signals were low-pass filtered online (cuttoff: 300 Hz) and recorded with 1200 Hz. Offline, the data were high-pass filtered (cuttoff: 0.5 Hz, Butterworth filter, filter order of 4) and resampled to 600 Hz.

Line noise was removed by subtracting the 50, 100, 150 and 200 Hz Fourier components. To suppress artifacts, the whole recording period was decomposed using independent component analysis (Hyvärinen, 1999). Selection of artifactual components was based on careful visual inspection of the 100 components explaining most signal variance. A component was only treated as artifact (e.g. eye related, muscle, heart) when the conjunction of the topography, power spectrum and time course was clearly conclusive. The data was then remixed, not retaining artifacutal components.

Data analysis

All analyses were done in Matlab (MathWorks, Natick, MA) using custom scripts as well as the open source toolboxes Fieldtrip (http://www.ru.nl/fcdonders/fieldtrip (Oostenveld et al., 2011)) and SPM (http://www.fil.ion.ucl.ac.uk/spm). For displaying results on the cortical surface we projected the data onto the data on the inflated surface of the Population-Average, Landmark and Surface-based (PALS) Atlas (Van Essen, 2005). We corrected the whole brain maps for multiple comparisons by controlling the false discovery rate (FDR) (Benjamini and Hochberg, 1995).

The sensor level power spectra were derived using fast Fourier transforms of hanning windowed 10s time windows, which were shifted half overlapping through the data. The spectra were averaged across all data points and channels, which were available for all recordings and then interpolated to a logarithmic scale.

All bivariate measures (power to power and phase to amplitude couplings) were calculated after source projecting the MEG data with adaptive, linear, spatial filters (Van Veen et al., 1997; Gross et al., 2001) to predefined source locations. Individual physical forward models were constructed by applying an affine transform (based on individual T1 MRI scans) to source locations defined in MNI space (Colin27), bringing them into individual head space and aligning the MEG sensors to the head geometry based on 3 fiducial points (nasion, left and right ear, defined in the MEG

by the 3 head localization coils). The physical relation between the sources and sensors was then derived employing a single shell model (Nolte, 2003). For the global analysis a regular grid (1 cm spacing, 2925 source locations) spanning the entire MNI brain volume was used. Based on this grid we retained locations within a functional V1 mask (Nielsen, 2003) to obtain 171 sources for the local analysis of early visual cortex. The implementation details of the beamformers were as follows: For each source location, 3 orthogonal filters ($\hat{A} = [A_x, A_y, A_z]$; one for each spatial dimension) were computed that pass activity from a given location with unit gain, while maximally suppressing activity from all other sources: $\hat{A} = [L \cdot C^{-1} \cdot L]^{-1} \cdot L \cdot C^{-1}$. Here, L is a matrix whose columns are the leadfields of three orthogonal dipoles at a given source location, and C denotes either the real part of the complex cross-spectral-density matrix (frequency domain beamformer for the power correlation analyses, see below) or the covariance matrix (time domain beamformer, cross frequency coupling analyses) for the data and ^{T} indicates the matrix transpose. We then linearly combined the 3 filters to a single filter pointing in the direction of maximal variance, i.e. the dominant dipole orientation. To this end, the filters were weighted with the first eigenvectors' elements (the eigenvector with the largest eigenvalue of the real part of the cross-spectral-density (covariance) matrix at the source location). To project the sensor data to source estimates, the data was then multiplied with the filter: $X_{source} = A \cdot X_{sensor}$.

The power correlation analyses were done using methods described in fill detail elsewhere (Hipp et al., in press). In short, complex time series spanning the entire recordings were derived using Morlet's wavelets. These spectral estimates were used to calculate the cross-spectral density for calculating the beamformer. The kernels were chosen to achieve a logarithmic frequency spacing and smoothing (1/2 octave). A phase orthogonalization approach was applied to remove power components common to the time series before computing the correlations. Linear correlations were then calculated between the squared absolutes of the complex spectral estimates after a source projection and a logarithmic transform that rendered the signals more normal. For deriving the connectivity within the early visual areas the correlations of each

location were spatially normalized (subtraction of the mean correlation to the rest of the brain and division by the standard deviation) and all connections within the visual grid exceeding a value of 1.64 were counted as existing within each participant. Changing this threshold in a broad range of values (0.5 to 5) did not alter the results qualitatively. The global analysis was based on all connections present in the entire grid of 2925 source locations (Hawellek et al., 2011). For each frequency paired t-tests for all connections (raw correlation values) were calculated between the blind and sighted and the number of differences exceeding an uncorrected threshold of $p = 0.01$ were counted (across the entire grid, Figure 2. For each source location, Figure 3). Changing the level of this threshold within reasonable ranges ($p = 0.05$ to $p = 0.001$) did yield highly similar results. To assign significance to the global connectivity differences a permutation procedure was applied in which the analysis was repeated 1000x while randomly shuffling the group assignments between blind and sighted. This yielded an empirical distribution for the null hypothesis of no differences in connectivity between the groups. A normal distribution was fit to these resamples and the raw scores were normalized (subtraction of the mean, division by the standard deviation) to derive Z-scores and p values. The dominant difference maps were then derived as the first principal component of the average global difference patterns for all voxels identified as being significant in the procedure described above at $p < 0.05$, FDR corrected.

The cross-frequency coupling between phase and amplitude was computed based on the Hilbert transform of band pass filtered signals (Canolty et al., 2006). The sensor level data were bandpass filtered into slow (1 to 15 Hz in steps of 1 Hz, bandwidth of 3 Hz) and fast (24 to 144 Hz, bandwidth of 9 Hz) signals using 4th order Butterworth filters. Based on these filtered data time domain beamformers were calculated and applied to derive band-limited signals from the early visual areas. After Hilbert transform of the source projected data, the phase of the slower frequency bands was used as the imaginary part and the amplitude of the faster frequency bands as the real part of a new synthetic complex signal resolved in time (Canolty et al., 2006).

The raw coupling score was then calculated as the absolute of the average complex value across the entire recording session and normalized to the coupling score reported here with a permutation distribution (subtraction of the mean, division by the standard deviation). This distribution was obtained by randomly shuffling the phase and amplitude relation 100x. This normalization removes the positive bias due to the finite recordings and renders random effect statistic sensitive. After normalization the coupling scores were averaged across the visual source locations.

Results

Intrinsic oscillations in visual cortex. We studied intrinsic oscillatory activity of visual areas in 11 blind and matched sighted participants. The most direct indication of a reorganization of oscillatory activity in the blind was a drop in the level of alpha (~10 Hz, t-test between groups for average power 8-12 Hz: $p = 0.016$) and beta range (~20 Hz, t-test between groups for average power 19-24 Hz: $p = 0.033$) oscillations over occipital MEG sensors (**Fig. 1A**), suggesting a loss or restructuring of the circuitry giving rise to these classical signatures of the resting human M/EEG (Kriegseis et al., 2006). However, beyond the mere strength with which these oscillations may be picked up from the scalp (signal power), the spatial patterns in which they occur well as the temporal dependencies between the different oscillations may reveal important additional aspects about the rewiring of visual areas in the blind. We thus further analyzed power-power correlations as a measure of spatial properties and phase-amplitude couplings as a measure of temporal relations of oscillatory activity within early visual areas.

We computed power correlations within a grid of 171 voxels spanning the early visual cortex, employing a novel method that allows for assessing such functional connectivity from noninvasive electrophysiological data while being insensitive to the problem of sources seeing the same signal (Hipp et al., in press). Before computing the power correlations we removed from the signals those parts that shared a common phase. This procedure ensured, that any power components that would lead to spurious interactions between two locations did not contribute to the correlation.

This analysis revealed that both, the blind and sighted exhibited comparable levels of alpha and beta range power correlations in visual cortex (**Fig. 1B**). However, the visual areas in the blind exhibited coordinated power fluctuations across visual areas in the delta (~2 Hz) and gamma (~90 Hz) range, which were absent in the sighted controls (t-tests between groups, average connectivity 1-3 Hz: $p = 0.008$; average connectivity 70-120 Hz: $p = 0.032$). In a next step we

tested whether there existed temporal relations among the oscillations in terms of cross-frequency phase to amplitude relationships. The co-fluctuations of delta and gamma power in the visual areas of the blind coincided with an increased cross frequency coupling in these frequency ranges (**Fig 1C**), where the delta phase predicted the gamma amplitude in the blind but not the sighted (t-test between groups average cross-frequency coupling for 1-3 Hz phases and 70-120 Hz amplitudes: $p = 0.0047$). This increase in delta-gamma coupling was followed by a marked loss in coupling between alpha frequency phases (~10 Hz) and low gamma (~40 Hz) amplitude, which was a dominant feature in the sighted (t-test between groups average cross-frequency coupling for 8-12 Hz phases and 24-54 Hz amplitudes: $p = 0.023$).

Overall we found specific alterations in the intrinsic oscillations of blind visual areas. The absolute power of alpha and beta range processes was reduced. Along with the loss of alpha power went the loss of a cross frequency relation between alpha phase and low gamma amplitude. The blind visual areas instead exhibited co-fluctuations of delta and gamma oscillations for which the phase of the delta oscillation was predictive of the amplitude of the gamma oscillations.

The global oscillatory architecture. We then receded from the visual focus and analyzed the organization of brain wide oscillatory activity with a data driven procedure based on power correlations. In a grid of 2925 source locations spanning the whole brain we quantified for each frequency the percent of all global connections, which differed between the groups at an uncorrected alpha level of $p < 0.01$ (changing the threshold to $p = 0.05$ or $p = 0.001$ yielded highly similar results). For assessing the statistical significance of this measure of group dissociation at each frequency we created a permutation distribution for the null hypothesis of no effect by repeating the analysis while shuffling the group labels. This procedure revealed the delta (~1-3 Hz) and beta (~20-34 Hz) range connectivity to dissociate between the groups on the global level (**Fig. 2**). The permutation distribution revealed highly non-uniform noise across the

different frequencies, which followed the overall amount of connectivity present at a given frequency (Hipp et al., in press), suggesting that the presence of strong physiological connectivity drives random differences to also occur more often. In a subsequent step we then further analyzed the patterns underlying the dissociation of connectivity between blind and sighted in the beta and delta ranges.

Breaking down the change in global connectivity in the beta effect to the individual voxel level revealed an extended set of frontal regions with a large cluster of medial premotor areas as well as smaller clusters in temporal and occipital areas (**Fig 3A.**, 551 voxels, $p < 0.05$ FDR corrected). The connectivity of these brain regions in the beta range could thus dissociate between the groups. However, this analysis did not reveal how these regions changed their connectivity. The detected brain regions may either show an individual pattern of global connectivity differences or instead one underlying pattern may dominate the effect. To assess the nature of the connectivity modulation within these areas we subjected the global patterns of all detected voxels to a principal component analysis (PCA). One global pattern of connectivity differences explained 54.3% of the variance in connectivity differences with a steep drop to subsequent components forming a flat plateau and explaining less than 5% of connectivity differences. Thus, the beta effect was dominated by a single pattern of connectivity differences (**Fig. 3B**). This pattern revealed a similar set of brain regions as those identified by the initial procedure that identified the effect (**Fig. 3A**) but extending to medial visual areas, posterior cingulate cortex and left lateralized frontal areas. In addition, the dominant pattern of connectivity differences exhibited a single sign, indicating that the nature of the effect was that this pattern of connectivity was present in one group and not in the other. For investigating how this pattern of connectivity differences related to the groups we calculated in a last step the average, raw orthogonalized correlations between the voxels found in the initial procedure (**Fig. 3A**) and those composing the dominant difference map (**Fig. 3B**, excluding self connections) for each participant (**Fig 3C**). Both groups exhibited significant connectivity (t-tests, blind: $p = 2.3 \times 10^{-4}$,

sighted: $p = 4.3 \times 10^{-4}$) with the congenitally blind exhibiting stronger connectivity (paired t-test: $p = 0.011$). Thus, visual deprivation led to stronger beta range connectivity across a distributed set of frontal, temporal and occipital regions.

An analogous analysis revealed the delta range connectivity be informative about the group affiliation mainly in occipital areas as well as some smaller clusters in right parietal, somatomotor and frontal regions (**Fig 3D**, 115 voxels, $p < 0.05$). Likewise the effect was dominated by one major pattern of global connectivity differences, explaining 15.9% of the total variance in connectivity differences (**Fig 3E**), with the other components forming a flat plateau of less than 4% explained variance. Similar brain regions as indicated by the effect were contained in the dominant map of connectivity differences, extending largely to medial and ventral visual areas and posterior cingulate cortex. As for the beta effect the dominant map of connectivity differences exhibited a single sign. The average raw correlations between the identified regions and the dominant map revealed the connectivity to be present in the blind (t-test: $p = 2.7 \times 10^{-8}$) and absent in the sighted (t-test: $p = 0.52$, paired t-test between the groups: $p = 0.1 \times 10^{-5}$).

Overall we found that the global structuring of delta and beta range power fluctuations is different between the blind and sighted. In both frequency ranges correlation structures existed in the blind, which were either absent or markedly weaker in the sighted. In the beta range an extended network of frontal and temporal regions exhibited stronger connectivity with early visual areas in the blind compared to the sighted. Additionally, the blind exhibited increased connectivity in the delta range among occipital and ventral visual as well as somato-motor and frontal areas.

Discussion

We found intrinsic oscillatory neuronal population activity to exhibit characteristic differences between the blind and sighted.

In the blind, alpha related processes (~10 Hz) in occipital areas were diminished in both, power and their phase-amplitude relation to a faster rhythm (~40Hz). These findings suggest a remodeling of the circuitry of alpha generators and associated processes and functions and may especially reflect the altered thalamocortical associations of occipital areas (Kriegseis et al., 2006; Shimony et al., 2006; Osipova et al., 2008). Alpha range activity has been linked to processes of functional inhibition (Jensen and Colgin, 2007; Klimesch et al., 2007). Decreased inhibitory processes are well in line with an increased level of baseline activity for blind visual areas (Veraart et al., 1990). This view is further supported by the increased delta (~2 Hz) to gamma (~90 Hz) couplings in the blind. We found the co-occurence of both, local visual delta and gamma power co-fluctuations and a phase-amplitude relation in which the slower delta phase modulated the faster gamma amplitude. Recent reports highlighted the significance of these frequency ranges and their interaction in active visual processing, both in humans (Händel and Haarmeier, 2009) as well as non-human primates (Lakatos et al., 2008; Whittingstall and Logothetis, 2009). Thus, our observations coherently point to a shift in intrinsic oscillations in visual cortex from a domination of inhibitory processes to signatures that occur during active processing.

Notably, the drop in power over posterior sensors for both the alpha and beta range was not associated to an obvious alteration in the spatial structuring within visual cortex, as the connectivity indexed by power co-fluctuations was on a comparable level in the blind and sighted. Vice versa, the increased delta and gamma range power connectivity was not represented by an increased power for these frequencies over posterior sensors. This double dissociation power and power correlation effects suggests that the bivariate measure reveals

additional information about circuit organization, which cannot be resolved from the mere signal strength (Hipp et al., in press). Similarly, the phase-amplitude couplings revealed also novel yet complementary insights into the organization of the blind visual cortex, such as the presence of the alpha to low gamma phase-amplitude relationship in the sighted. Our results, thus, suggest that incorporating measures of the spatiotemporal structuring of oscillatory neuronal activity (as e.g. power-power or phase-amplitude relations) enables a more detailed, largely non-redundant characterization of the organization of oscillatory neuronal activity.

With a data driven procedure we identified global correlation structures in power fluctuations in the delta (~ 2Hz) and beta (~25 Hz) range, which dissociated the blind from the sighted. Two common themes to these correlations structures were the involvement of the visual cortex as well as the marked presence of the patterns only in the blind. While for the delta range especially the occipital cortex exhibited the increased connectivity, the increase in beta connectivity became most apparent in an extended set of frontal areas. The global delta effect further corroborates the analysis of the local connectivity analysis within visual areas and suggests that slow (~2 Hz) excitability fluctuations prevail in occipital brain regions during periods of unconstrained mental activity in the blind. A gamma range effect could not be resolved globally, which may relate to a very confined, local nature of the gamma power fluctuations and the presence of a stronger noise regime (**Fig. 2**). The connectivity between frontal and visual areas is in line with a functional magnetic resonance imaging (fMRI) investigation of the intrinsic connectivity of visual areas in the blind, reporting increased frontal associations (Liu et al., 2007). Interestingly, next to medial premotor structures there was a set of left lateralized lateral frontal regions exhibiting the increased beta connectivity. This finding is in accord with fMRI studies showing an involvement and connectivity of blind visual areas with language processing networks (Noppeney et al., 2003; Bedny et al., 2011). The beta frequency range of the connectivity may suggest especially integrative functions to underlie the nature of the connectivity (Engel et al., 2001; Engel and Fries, 2010; Donner and Siegel, 2011). Beta range

phase synchrony has been identified as a potential mechanism of long-range cortico-cortical interaction in large-scale cortical networks (Buschman and Miller, 2007; Saalmann et al., 2007; Pesaran et al., 2008; Hipp et al., 2011). Thus, this long-range functional connectivity pattern may be an indication of the pathway with which visual brain areas are reintegrated into functional cortical processing in the blind.

The task free data enabled us to study rearrangements of oscillatory neuronal activity in the blind without the biases of a specific cognitive task. This approach allows for an identification of physiologically meaningful patterns, which are inherent to the way that the blind access and use occipital resources and which may otherwise be obscured by the constraints and contexts of highly specific paradigms and task structures. While this is a great benefit of studying intrinsic oscillatory activity, the lack of associations with behavioral measures puts into question whether the correlation structures truly are of any functional significance. Future studies need to address this issue and test the link between the frontal to visual connectivity as well as their impact on behavior of the blind in detail.

Overall we found the structuring of spontaneous oscillatory neuronal activity to be highly informative about the reorganization of the brain circuitry in the blind. Visual areas exhibited oscillatory signatures of active processing during rest as well beta range functional connectivity with prefrontal areas. These findings imply occipital processing resources to be used for non-visual demands in unconstrained mental activity in the blind and further suggest specific frontal sites to be involved in the integration of these resources into the reorganized but functionally intact processing in the blind. Our results demonstrate that the rich spectral content of ongoing brain activity may offer a novel handle onto an important but otherwise not accessible level of description for the reorganization and plasticity of processing in cortical networks.

References

Amedi A, Floel A, Knecht S, Zohary E, Cohen LG (2004) Transcranial magnetic stimulation of the occipital pole interferes with verbal processing in blind subjects. Nat Neurosci 7:1266–1270.

Amedi A, Raz N, Pianka P, Malach R, Zohary E (2003) Early “visual” cortex activation correlates with superior verbal memory performance in the blind. Nat Neurosci 6:758–766.

Bavelier D, Neville HJ (2002) Cross-modal plasticity: where and how? Nat Rev Neurosci 3:443–452.

Bedny M, Pascual-Leone A, Dodell-Feder D, Fedorenko E, Saxe R (2011) Language processing in the occipital cortex of congenitally blind adults. Proc Natl Acad Sci USA 108:4429–4434.

Benjamini Y, Hochberg Y (1995) Controlling the False Discovery Rate: A Practical and Powerful Approach to Multiple Testing. Journal of the Royal Statistical Society Series B (Methodological) 57:289–300.

Büchel C, Price C, Frackowiak RS, Friston K (1998) Different activation patterns in the visual cortex of late and congenitally blind subjects. Brain 121 (Pt 3):409–419.

Buschman TJ, Miller EK (2007) Top-down versus bottom-up control of attention in the prefrontal and posterior parietal cortices. Science 315:1860–1862.

Buzsaki G (2006) Rhythms of the Brain, 1st ed. Oxford University Press, USA.

Buzsáki G, Draguhn A (2004) Neuronal oscillations in cortical networks. Science 304:1926–1929.

Canolty RT, Edwards E, Dalal SS, Soltani M, Nagarajan SS, Kirsch HE, Berger MS, Barbaro NM, Knight RT (2006) High gamma power is phase-locked to theta oscillations in human neocortex. Science 313:1626–1628.

Cohen LG, Celnik P, Pascual-Leone A, Corwell B, Falz L, Dambrosia J, Honda M, Sadato N, Gerloff C, Catalá MD, Hallett M (1997) Functional relevance of cross-modal plasticity in blind humans. Nature 389:180–183.

Collignon O, Vandewalle G, Voss P, Albouy G, Charbonneau G, Lassonde M, Lepore F (2011) Functional specialization for auditory-spatial processing in the occipital cortex of congenitally blind humans. Proc Natl Acad Sci USA 108:4435–4440.

Collignon O, Voss P, Lassonde M, Lepore F (2009) Cross-modal plasticity for the spatial processing of sounds in visually deprived subjects. Exp Brain Res 192:343–358.

Donner TH, Siegel M (2011) A framework for local cortical oscillation patterns. Trends Cogn Sci (Regul Ed) 15:191–199.

Engel AK, Fries P (2010) Beta-band oscillations--signalling the status quo? Curr Opin Neurobiol 20:156–165.

Engel AK, Fries P, Singer W (2001) Dynamic predictions: oscillations and synchrony in top-down processing. Nat Rev Neurosci 2:704–716.

Van Essen DC (2005) A Population-Average, Landmark- and Surface-based (PALS) atlas of

human cerebral cortex. Neuroimage 28:635–662.

Gougoux F, Zatorre RJ, Lassonde M, Voss P, Lepore F (2005) A functional neuroimaging study of sound localization: visual cortex activity predicts performance in early-blind individuals. PLoS Biol 3:e27.

Gross J, Kujala J, Hamalainen M, Timmermann L, Schnitzler A, Salmelin R (2001) Dynamic imaging of coherent sources: Studying neural interactions in the human brain. Proc Natl Acad Sci USA 98:694–699.

Händel B, Haarmeier T (2009) Cross-frequency coupling of brain oscillations indicates the success in visual motion discrimination. Neuroimage 45:1040–1046.

Hawellek DJ, Hipp JF, Lewis CM, Corbetta M, Engel AK (2011) Increased functional connectivity indicates the severity of cognitive impairment in multiple sclerosis. Proc Natl Acad Sci USA 108:19066–19071.

Hipp JF, Engel AK, Siegel M (2011) Oscillatory synchronization in large-scale cortical networks predicts perception. Neuron 69:387–396.

Hipp JF, Hawellek DJ, Siegel M, Corbetta M, Engel AK (in press) The large-scale organization of spontaneous oscillatory neuronal activity. Nature Neuroscience.

Hyvärinen A (1999) Fast and robust fixed-point algorithms for independent component analysis. IEEE Trans Neural Netw 10:626–634.

Jensen O, Colgin LL (2007) Cross-frequency coupling between neuronal oscillations. Trends Cogn Sci (Regul Ed) 11:267–269.

Jiang J, Zhu W, Shi F, Liu Y, Li J, Qin W, Li K, Yu C, Jiang T (2009) Thick visual cortex in the early blind. J Neurosci 29:2205–2211.

Klimesch W, Sauseng P, Hanslmayr S (2007) EEG alpha oscillations: the inhibition-timing hypothesis. Brain Res Rev 53:63–88.

Kriegseis A, Hennighausen E, Rösler F, Röder B (2006) Reduced EEG alpha activity over parieto-occipital brain areas in congenitally blind adults. Clin Neurophysiol 117:1560–1573.

Lakatos P, Karmos G, Mehta AD, Ulbert I, Schroeder CE (2008) Entrainment of neuronal oscillations as a mechanism of attentional selection. Science 320:110–113.

Leporé N, Voss P, Lepore F, Chou Y-Y, Fortin M, Gougoux F, Lee AD, Brun C, Lassonde M, Madsen SK, Toga AW, Thompson PM (2010) Brain structure changes visualized in early- and late-onset blind subjects. Neuroimage 49:134–140.

Liu Y, Yu C, Liang M, Li J, Tian L, Zhou Y, Qin W, Li K, Jiang T (2007) Whole brain functional connectivity in the early blind. Brain 130:2085–2096.

Merabet LB, Pascual-Leone A (2010) Neural reorganization following sensory loss: the opportunity of change. Nat Rev Neurosci 11:44–52.

Nielsen FA (2003) The Brede database: a small database for functional neuroimaging. NeuroImage 19 Available at: http://www.imm.dtu.dk/~fn/Nielsen2003Brede_abstract/Nielsen2003Brede_abstract.html.

Nolte G (2003) The magnetic lead field theorem in the quasi-static approximation and its use for

magnetoencephalography forward calculation in realistic volume conductors. Phys Med Biol 48:3637–3652.

Noppeney U, Friston KJ, Ashburner J, Frackowiak R, Price CJ (2005) Early visual deprivation induces structural plasticity in gray and white matter. Curr Biol 15:R488–R490.

Noppeney U, Friston KJ, Price CJ (2003) Effects of visual deprivation on the organization of the semantic system. Brain 126:1620–1627.

Oostenveld R, Fries P, Maris E, Schoffelen J-M (2011) FieldTrip: Open source software for advanced analysis of MEG, EEG, and invasive electrophysiological data. Comput Intell Neurosci 2011:156869.

Osipova D, Hermes D, Jensen O (2008) Gamma power is phase-locked to posterior alpha activity. PLoS ONE 3:e3990.

Park H-J, Lee JD, Kim EY, Park B, Oh M-K, Lee S, Kim J-J (2009) Morphological alterations in the congenital blind based on the analysis of cortical thickness and surface area. Neuroimage 47:98–106.

Pesaran B, Nelson MJ, Andersen RA (2008) Free choice activates a decision circuit between frontal and parietal cortex. Nature 453:406–409.

Röder B, Stock O, Bien S, Neville H, Rösler F (2002) Speech processing activates visual cortex in congenitally blind humans. Eur J Neurosci 16:930–936.

Röder B, Teder-Sälejärvi W, Sterr A, Rösler F, Hillyard SA, Neville HJ (1999) Improved auditory spatial tuning in blind humans. Nature 400:162–166.

Rösler F, Röder B, Heil M, Hennighausen E (1993) Topographic differences of slow event-related brain potentials in blind and sighted adult human subjects during haptic mental rotation. Brain Res Cogn Brain Res 1:145–159.

Saalmann YB, Pigarev IN, Vidyasagar TR (2007) Neural mechanisms of visual attention: how top-down feedback highlights relevant locations. Science 316:1612–1615.

Sadato N, Pascual-Leone A, Grafman J, Ibañez V, Deiber MP, Dold G, Hallett M (1996) Activation of the primary visual cortex by Braille reading in blind subjects. Nature 380:526–528.

Schepers IM, Hipp JF, Schneider TR, Röder B, Engel AK (in press) Functionally specific oscillatory activity correlates between visual and auditory cortex in the blind. Brain.

Shimony JS, Burton H, Epstein AA, McLaren DG, Sun SW, Snyder AZ (2006) Diffusion tensor imaging reveals white matter reorganization in early blind humans. Cereb Cortex 16:1653–1661.

Van Veen BD, van Drongelen W, Yuchtman M, Suzuki A (1997) Localization of brain electrical activity via linearly constrained minimum variance spatial filtering. IEEE Trans Biomed Eng 44:867–880.

Veraart C, De Volder AG, Wanet-Defalque MC, Bol A, Michel C, Goffinet AM (1990) Glucose utilization in human visual cortex is abnormally elevated in blindness of early onset but decreased in blindness of late onset. Brain Res 510:115–121.

Whittingstall K, Logothetis NK (2009) Frequency-band coupling in surface EEG reflects spiking activity in monkey visual cortex. Neuron 64:281–289.

Legends

Figure 1. The intrinsic oscillatory profile of visual cortex. A Power spectra over occipital MEG sensors (inset) for blind (red line) and sighted controls (blue line). The shadings depict the standard error. The line noise frequency was sparred for display purposes. The bars at the x-axis mark frequencies for which the groups significantly differed. B Connectivity as indexed by power-power correlations within a grid of voxels in early visual areas. Connections were derived within the individual subjects and are shown as percent of all connections maximally possible. The shadings depict the standard error. C Cross-frequency couplings between the phase of slower oscillations and the amplitude of faster oscillations within early visual cortex. The average coupling scores within the groups and the average difference of the coupling scores are shown along with the difference statistic between the groups.

Figure 2. The global oscillatory architecture differentiates the blind from sighted. The number of group differences (paired t-tests, $p < 0.01$) across frequencies, which occur in all connections of a grid spanning the whole brain with 2925 source locations. The raw number of is given in percent of all connections possible and shown in black. A permutation distribution for the hypothesis of no difference between the groups is shown as grey line with the shading depicting one standard deviation. The bars at the x-axis mark frequencies for which the connectivity significantly deviates from this distribution at the alpha levels indicated.

Figure 3. Increased beta and delta connectivity in the blind. A Source locations exhibiting a significant ($p = 0.05$, FDR corrected) global beta range connectivity difference between the blind and the sighted. B First principal component of the average global difference maps of all voxels shown in A. This dominant difference map in connectivity explained 54.3% of the total variance in connectivity differences. C Raw orthogonalized correlation values between the voxels shown in A and all voxels of the difference map shown in B. D-F Same as A-C but shown for the delta range. The dominant difference map explained 15.9% of the overall variance.

Illustrations

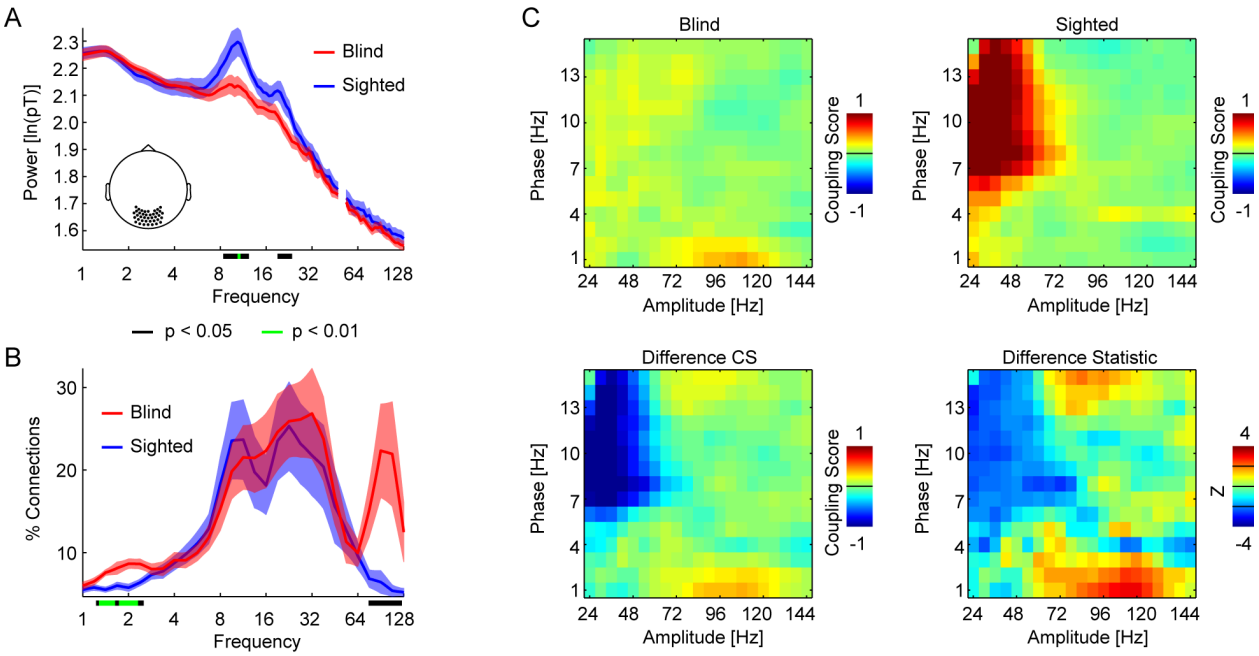

Figure 1

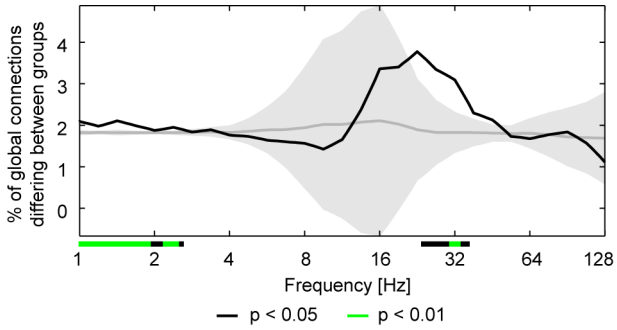
% of global connections differing between groups
0
1
2
3
4
1
2
4
8
16
32
64
128
Frequency [Hz]
p < 0.05
p < 0.01

Figure 2

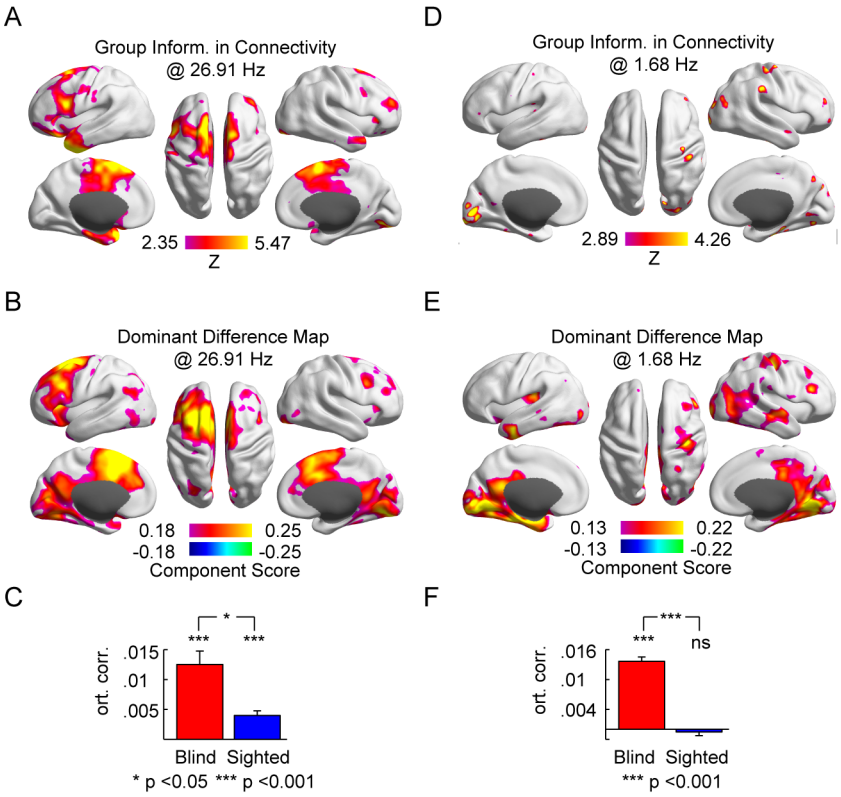
A
Group Inform. in Connectivity
@ 26.91 Hz
2.35
5.47
Z
D
Group Inform. in Connectivity
@ 1.68 Hz
2.89
4.26
Z
B
Dominant Difference Map
@ 26.91 Hz
0.18
0.25
-0.18
-0.25
Component Score
E
Dominant Difference Map
@ 1.68 Hz
0.13
0.22
-0.13
-0.22
Component Score
C
ort. corr.
.015
.01
.005
*
***
***
Blind
Sighted
* p <0.05 *** p <0.001
F
ort. corr.
.016
.01
.004
***
***
ns
Blind
Sighted
*** p <0.001

Figure 3